ARISTOTLE UNIVERSITY OF THESSALONIKI

FACULTY OF SCIENCES

SCHOOL OF GEOLOGY

VASILIKI KAFIRA

GEOLOGIST

CONTEMPORARY COASTLINE CHANGES AND FLOOD SUSCEPTIBILITY ASSESSMENT OF KASSANDRA PENINSULA, HALKIDIKI, USING REMOTE SENSING AND GIS

MASTER THESIS

THESSALONIKI 2015

VASILIKI KAFIRA

GEOLOGIST

CONTEMPORARY COASTLINE CHANGES AND FLOOD SUSCEPTIBILITY ASSESSMENT OF KASSANDRA PENINSULA, HALKIDIKI, USING REMOTE SENSING AND GIS

Submitted in fulfillment of the requirements for the degree of Master of Science in Geology and Geoenvironment
in the Aristotle University of Thessaloniki, Greece.

DATE OF ORAL EXAMINATION: 05/06/2015

THESIS COMMITTEE:

Associate Professor Dr. Kostantinos Albanakis, Supervisor

Lecturer Dr. Dimitrios Oikonomidis, Advisory Committee

Associate Professor Dr. Kostantinos Voudouris, Advisory Committee

ΑΡΙΣΤΟΤΕΛΕΙΟ ΠΑΝΕΠΙΣΤΗΜΙΟ ΘΕΣΣΑΛΟΝΙΚΗΣ
ΣΧΟΛΗ ΘΕΤΙΚΩΝ ΕΠΙΣΤΗΜΩΝ
ΤΜΗΜΑ ΓΕΩΛΟΓΙΑΣ

ΒΑΣΙΛΙΚΗ ΚΑΦΗΡΑ

ΠΤΥΧΙΟΥΧΟΣ ΓΕΩΛΟΓΟΣ

ΠΡΟΣΦΑΤΕΣ ΜΕΤΑΒΟΛΕΣ ΤΗΣ ΑΚΤΟΓΡΑΜΗΣ ΚΑΙ ΕΚΤΙΜΗΣΗ ΤΗΣ ΠΛΗΜΜΥΡΙΚΗΣ ΕΠΙΔΕΚΤΙΚΟΤΗΤΑΣ ΤΗΣ ΧΕΡΣΟΝΗΣΟΥ ΚΑΣΣΑΝΔΡΑΣ, ΧΑΛΚΙΔΙΚΗΣ, ΜΕ ΧΡΗΣΗ ΤΗΛΕΠΙΣΚΟΠΗΣΗΣ ΚΑΙ GIS

ΜΕΤΑΠΤΥΧΙΑΚΗ ΔΙΑΤΡΙΒΗ ΕΙΔΙΚΕΥΣΗΣ

ΘΕΣΣΑΛΟΝΙΚΗ 2015

ΒΑΣΙΛΙΚΗ ΚΑΦΗΡΑ

Πτυχιούχος Γεωλόγος

ΠΡΟΣΦΑΤΕΣ ΜΕΤΑΒΟΛΕΣ ΤΗΣ ΑΚΤΟΓΡΑΜΗΣ ΚΑΙ ΕΚΤΙΜΗΣΗ ΤΗΣ ΠΛΗΜΜΥΡΙΚΗΣ ΕΠΙΔΕΚΤΙΚΟΤΗΤΑΣ ΤΗΣ ΧΕΡΣΟΝΗΣΟΥ ΚΑΣΣΑΝΔΡΑΣ, ΧΑΛΚΙΔΙΚΗΣ, ΜΕ ΧΡΗΣΗ ΤΗΛΕΠΙΣΚΟΠΗΣΗΣ ΚΑΙ GIS

Υποβλήθηκε στο Τμήμα Γεωλογίας, στο πλαίσιο του Μεταπτυχιακού Προγράμματος Σπουδών 'Γεωλογία και Γεωπεριβάλλον'

Τομέας Φυσικής και Περιβαλλοντικής Γεωγραφίας.

Ημερομηνία Προφορικής Εξέτασης: 05/06/2015

ΤΡΙΜΕΛΗΣ ΣΥΜΒΟΥΛΕΥΤΙΚΗ ΕΠΙΤΡΟΠΗ:

Αναπληρωτής Καθηγητής Αλμπανάκης Κωνσταντίνος, Επιβλέπων

Λέκτορας Οικονομίδης Δημήτριος, Μέλος Τριμελούς Συμβουλευτικής Επιτροπής

Αναπληρωτής Καθηγητής Βουδούρης Κωνσταντίνος, Μέλος Τριμελούς Συμβουλευτικής Επιτροπής

Citation: Kafira V. 2015. Contemporary coastline changes and flood susceptibility assessment of Kassandra peninsula, Halkidiki, using Remote Sensing and GIS. Master Thesis, School of Geology, Aristotle University of Thessaloniki, pp. 1-151.

ΚΑΦΗΡΑ Β. 2015. ΠΡΟΣΦΑΤΕΣ ΜΕΤΑΒΟΛΕΣ ΤΗΣ ΑΚΤΟΓΡΑΜΗΣ ΚΑΙ ΕΚΤΙΜΗΣΗ ΤΗΣ ΠΛΗΜΜΥΡΙΚΗΣ ΕΠΙΔΕΚΤΙΚΟΤΗΤΑΣ ΤΗΣ ΧΕΡΣΟΝΗΣΟΥ ΚΑΣΣΑΝΔΡΑΣ, ΧΑΛΚΙΔΙΚΗΣ, ΜΕ ΧΡΗΣΗ ΤΗΛΕΠΙΣΚΟΠΗΣΗΣ ΚΑΙ GIS. ΔΙΑΤΡΙΒΗ ΕΙΔΙΚΕΥΣΗΣ, ΤΜΗΜΑ ΓΕΩΛΟΓΙΑΣ ΑΠΘ, ΣΕΛ. 1-151.

To my Family and Nala

ACKNOWLEDGMENTS

I am using this opportunity to express my gratitude to everyone who supported me throughout the course of this master thesis. I am thankful for their inspiring guidance, invaluably constructive criticism and friendly advice during the project's work. I am sincerely grateful to them for sharing their truthful and illuminating views on a number of issues related to the project.

I would like to express my special appreciation and thanks to my advisor Associate Professor Dr. Kostantinos Albanakis. You have been a tremendous mentor for me. I would like to thank you for encouraging my research and for allowing me to grow as a research scientist. I would also like to thank my committee members, lecturer Dr. Dimitrios Oikonomidis and Associate Professor Dr. Kostantinos Voudouris for serving as my committee members even during hardships. I also want to thank you for letting my defense be an enjoyable moment, and for your brilliant comments and suggestions.

I would like to express my gratitude to Associate Professor Evangelia Tsoukala, Lecturer Dr. Antonios Mouratidis, Dr. Kalliopi Koliadimou and PhD candidate Christos Domakinis for the useful comments, remarks and engagement through the learning process of this master thesis.

I am also grateful to Rob Thieler, Ph.D. from U.S. Geological Survey Coastal and Marine Geology Program and his team for the permission to use the ArcGIS extension: Digital Shoreline Analysis System (DSAS) version 4.0 and the user guide.

A special thanks to my family. Words cannot express how grateful I am to my mother and father for all of the sacrifices that you've made on my behalf. Your prayers for me were what has sustained me thus far. I would also like to thank all of my friends who supported me during writing, and incented me to strive towards my goal. Finally I would like express my appreciation of my beloved dog Nala who spent sleepless nights with me and was always my support in the moments when there was no one to answer my queries.

ABSTRACT

This study concentrates, on the first part, on the construction of a flood susceptibility map, of the study area, by combining vulnerability elements, using the Analytical Hierarchy Process/ AHP (Saaty, 1980). After processing of a digital elevation model (DEM), important secondary data were extracted, such as the slope map, the flow direction and the flow accumulation. Together with additional thematic information (e.g. geological maps, land cover etc.), these led to the final four major factors for creating the flood susceptibility map, i.e. the Topographic wetness index, Lithology, Roughness - Land cover and Vegetation cover index (NDVI). These factors were co-evaluated, in order to produce the final map, which categorizes the area into zones of higher to lower flood susceptibility, in GIS environment.

The second part of the thesis detects and examines the changes of the coastlines in Kassandra peninsula, using remote sensing and GIS. Kassandra peninsula comprises a very energetic and diversified coast. The study focused on the analysis of the coastal dynamics and the spatio-temporal changes of coastal morphology for the years 1977, 1985, 2007 and 2011, using the digital shoreline analysis system (DSAS) extension. This part's main goal is to estimate whether there is erosion or accretion and the size of it. One of the purposes of this thesis is to implement this new methodology in the Department of Geology AUTH, therefore it has been decided to use parts of the guide (Digital Shoreline Analysis System (DSAS) version 4.0— An ArcGIS extension for calculating shoreline change: U.S. Geological Survey Open-File Report 2008-1278. Available online at http://woodshole.er.usgs.gov/project-pages/DSAS in agreement with Robert Thieler, Ph.D. from U.S. Geological Survey Coastal and Marine Geology Program, in order to guide future users in a more helpful way.

ΠΕΡΙΛΗΨΗ

Η μελέτη αυτή επικεντρώνεται, στο πρώτο μέρος, στην κατασκευή χάρτη πλημμυρικής επιδεκτικότητας, της περιοχής μελέτης, συνδυάζοντας στοιχεία τρωτότητας, και χρησιμοποιώντας την Διαδικασία Αναλυτικής Ιεραρχίας / AHP (Saaty, 1980). Με την επεξεργασία των κατάλληλων δεδομένων σε συνδυασμό με πρόσθετες θεματικές πληροφορίες (π.χ. γεωλογικούς χάρτες, κάλυψη γης κλπ), υπολογίστηκαν οι τέσσερις βασικοί παράγοντες για τη δημιουργία του χάρτη πλημμυρικής επιδεκτικότητας, δηλαδή ο τοπογραφικός δείκτης υγρασίας, η λιθολογία, η τραχύτητα και ο δείκτης φυτοκάλυψης (NDVI). Αυτοί οι παράγοντες συν-αξιολογούνται, προκειμένου να παραχθεί ο τελικός χάρτης, ο οποίος κατηγοριοποιεί την περιοχή σε ζώνες από υψηλότερη σε χαμηλότερη επιδεκτικότητα στην εμφάνιση πλημμυρών.

Το δεύτερο μέρος της διατριβής εντοπίζει και εξετάζει τις αλλαγές των ακτών της χερσονήσου Κασσάνδρας, με τη χρήση τηλεπισκόπησης και των GIS. Η Κασσάνδρα περιλαμβάνει μια πολύ δυναμική και ποικιλόμορφη ακτογραμμή. Η μελέτη επικεντρώθηκε στην ανάλυση των παράκτιων μεταβολών για τα έτη 1977, 1985, 2007 και το 2011, χρησιμοποιώντας το σύστημα ψηφιακής ανάλυσης ακτογραμμών (DSAS). Ο κύριος στόχος αυτού του τμήματος είναι να εκτιμηθεί αν υπάρχει διάβρωση ή απόθεση, καθώς επίσης ο ρυθμός και το μέγεθός τους. Ένας από τους σκοπούς αυτής της εργασίας είναι η εφαρμογή αυτής της νέας μεθοδολογίας στο Τμήμα Γεωλογίας του ΑΠΘ, ως εκ τούτου, έχει αποφασιστεί να χρησιμοποιούν τμήματα του οδηγού (*Digital Shoreline Analysis System (DSAS)* σε συμφωνία με τον Robert Thieler, Ph.D. από το US Geological Survey Coastal and Marine Geology Program, με σκοπό να καθοδηγήσει τους μελλοντικές τους χρήστες.

TABLE OF CONTENTS

INTRODUCTION

Floods are natural phenomena as well as an integral part of the water cycle. The majority of them are the result of climatic conditions, but floods are also affected by the geology and geomorphology of the area, by topography and hydrology, by the water permeability of the soil and the vegetation cover, as well as by all kinds of human activities and structures. However, from the moment that human lives are at risk and significant economic impact is recorded, this natural phenomenon becomes a natural disaster. Flood management is now a key issue at regional and local level around the world, affecting human lives and activities .

The majority of floods are unlikely to be fully predicted, but it is feasible to reduce their risks through appropriate management plans and constructions. This study was carried out due to the repeated catastrophic floods that have occurred in Kassandra peninsula, Halkidiki, Greece and more specifically in the area of Fourka, causing numerous damages. The main purpose of this study is to evaluate the contribution of remote sensing technology and Geographic Information Systems (GIS) in assessing the susceptibility of this region to flood events.

Kassandra is facing "anthropogenic" floods; human interventions on streams, the beds of which have been trampled to build houses and hotels or have been converted into roads, are causing flooding after every heavy rainfall. The streams crossing settlements and areas with high touristic development have been intensively modified by humans, as the pressure for real estate development land is growing.

In particular, several areas in Kassandra are facing a high risk of extensive flood occurrence, since fires happened in the past and flood protection infrastructure has been seriously damaged.. Such examples are the catastrophic fires in August 2006, which destroyed 60 % of the forested area of Kassandra and the dramatic floods that followed in September 2007.

The assessment of cliffs and rocky coasts, beach dynamics and coastal processes is fundamental for a monitoring of littoral areas (Trenhaile, 1987, 1997; Carter, 1988; Woodroffe, 2003; Green and King, 2003; Fookes et al. , 2007; Bird, 2008). As coastal

populations continue to grow and community infra- structures are threatened by erosion, there has been an increase in demand for accurate information regarding cliff retreat or shoreline movement. Thus, one of the more important aspects of coastal management and planning programs that merits further investigation is shoreline dynamics (Crous et al. , 2004; Hapke and Reid, 2007; Hapke et al. , 2009; Morton and Miller, 2005; Morton et al. , 2004; Rogers et al. , 2008, 2010).

1. ENVIRONMENT OF THE STUDY AREA

1.1 CHAPTER'S CONTENTS

This chapter is devoted to a detailed description of the environment of the study area, starting with basic geographic data, meteorological data, land cover, vegetation, geology, geomorphology and hydrology of the study area. Initially, there are some general data and then the particular data on the area of interest.

1.2 GENERAL INFORMATION

The Halkidiki prefecture is one of the 51 prefectures of Greece. It is one of the prefectures of the geographical region of Macedonia, which belongs to the Authority of the region Central Macedonia (www.ypes.gr). The county of Halkidiki borders the prefecture of Thessaloniki to the North - Northwest and Mount Athos to the south-east, while the rest of it is surrounded by the Aegean Sea. The county of Halkidiki extends to 2.918km^2. 729 km^2 are lowlands (25%), the 1,464 km^2 hilly (50%) and the 725 km^2 mountainous area (25%). The vegetation covers 1.450km^2, that is 50% of its total extension.

Halkidiki has varied terrain. The northeast and central Halkidiki is mountainous (Mt Cholomontas 1165m, Mt Athos 2033m). The western part of the county, which is also our study area, is hilly with mild relief, formed by smooth undulating surfaces, separated from each other by seasonal streams and torrents.

Halkidiki is geographically located between parallels N.G.P. 39^o 50 'and 40^o 45' and between the meridians E.G.M. 22th 45 and 24th 30 '. (Syrides, 1990)

The Halkidiki prefecture geographically consists of the peninsula of Halkidiki with the characteristic shape of the three peninsulas ('legs of Halkidiki'), except the easternmost peninsula of Mount Athos, which is administratively independent.

Halkidiki consists of a main body (the north part) which is separated, to the south, into three elongated and parallel to each other peninsulas, Kassandra, Sithonia, Athos

(Mount Athos) (South part). To the north the basin of Mygdonia separates it from the main terrestrial trunk of Macedonia. (Syrides, 1990)

The peninsulas show main mountainous morphology with a dense network of deep narrow valleys. The coastline on the west Halkidiki and Kassandra peninsula rise steeply with obvious strong coastal erosion. Between them stretch out low sandy beaches with pleasing landscapes of high touristic value. The coasts of N.E. Halkidiki and Sithonia peninsula are steep, and are composed of crystalline rocks and granites. (Veranis, 1994)

1.3 CLIMATIC-WEATHER FEATURES

Generally, the study area's climate is characterized as a transition between the continental climate of Central Europe and the Mediterranean climate (Katafioti, 2008). From Table 1 with the climatological data presented below, it emerges that the average climate of the study area is characterized by relatively mild summer temperatures of around 25 ° C and cold winter temperatures close to 10 ° C.

The assessment of climate characteristics made use of data from the meteorological station of Kassandria:

Table 1 ***Climatological Reports for the year 2014***

(source: http://penteli.meteo.gr/stations/kassandreia/NOAAPRYR.TXT)

ANNUAL CLIMATOLOGICAL SUMMARY 2014

NAME: kassandreia CITY: STATE:

ELEV: 29 m LAT: 40° 06' 00" N LONG: 23° 24' 00" E

TEMPERATURE (°C),

HEAT BASE 18.3, COOL BASE 18.3

YR	MO	MEAN MAX	MEAN MIN	MEAN	DEP. FROM NORM	HEAT DEG DAYS	COOL DEG DAYS	MAX HI	MAX DATE	MIN LOW	MIN DATE	MAX >=32	MAX <=0	MIN <=0	MIN <=-18
14	1	14.0	6.2	10.1	0.0	256	0	19.3	20	2.0	27	0	0	3	0
14	2	14.1	6.9	10.5	0.0	219	0	19.7	10	3.6	26	0	0	2	0
14	3	16.7	6.7	11.8	0.0	204	3	23.8	18	2.9	13	0	0	2	0
14	4	19.0	9.7	14.5	0.0	120	5	23.4	15	4.4	12	0	0	0	0
14	5	24.8	12.7	18.9	0.0	50	69	30.9	28	8.3	8	0	0	0	0
14	6	29.2	17.5	23.4	0.0	8	160	37.0	26	12.9	3	4	0	0	0
14	7	30.9	19.9	25.6	0.0	0	227	34.1	10	16.5	5	7	0	0	0
14	8	32.0	20.7	26.3	0.0	0	248	35.3	13	17.9	20	17	0	0	0
14	9	25.7	16.7	21.2	0.0	15	100	29.2	1	11.6	24	0	0	0	0
14	10	20.9	12.6	16.8	0.0	80	33	28.6	17	7.9	24	0	0	0	0
14	11	16.1	10.6	13.5	0.0	146	0	19.6	19	4.8	25	0	0	0	0
14	12	13.5	6.6	10.1	0.0	257	0	17.9	6	-1.7	30	0	0	3	0
		21.5	12.3	16.9	0.0	1354	846	37.0	JUN	-1.7	DEC	28	0	3	0

PRECIPITATION (mm)

DEP. FROM YR	MO	MAX OBS. TOTAL	NORM	DAYS OF RAIN OVER DAY	DATE	.2	2	20
14	1	46.7	0.0	13.6	28	21	5	0
14	2	21.8	0.0	8.8	23	11	3	0
14	3	71.4	0.0	39.6	3	12	5	1
14	4	28.4	0.0	7.8	18	14	5	0
14	5	17.6	0.0	8.4	29	8	3	0
14	6	60.0	0.0	13.8	3	8	5	0
14	7	47.6	0.0	42.2	15	3	2	1
14	8	37.6	0.0	23.2	7	4	4	1
14	9	78.2	0.0	28.0	2	15	6	1
14	10	112.8	0.0	42.2	24	16	7	2
14	11	91.8	0.0	41.0	9	16	5	2
14	12	144.8	0.0	67.0	8	20	8	2
758.8			0.0	67.0	DEC 148	58		10

WIND SPEED (km/hr)

DOM

YR	MO	AVG.	HI	DATE	DIR
14	1	4.9	45.1	21	ENE
14	2	5.8	45.1	4	ENE
14	3	5.9	54.7	20	E
14	4	5.6	48.3	10	E
14	5	5.9	64.4	14	E
14	6	5.4	78.9	19	ENE
14	7	5.5	69.2	15	ENE
14	8	4.9	49.9	17	ENE
14	9	4.2	53.1	7	ENE
14	10	6.0	64.4	24	ENE
14	11	4.8	75.6	13	E
14	12	6.8	64.4	21	NW
5.5		78.9	JUN	ENE	

According to Figure 1 in the region of the West part of Kassandra, mainly strong Northwest winds prevail.

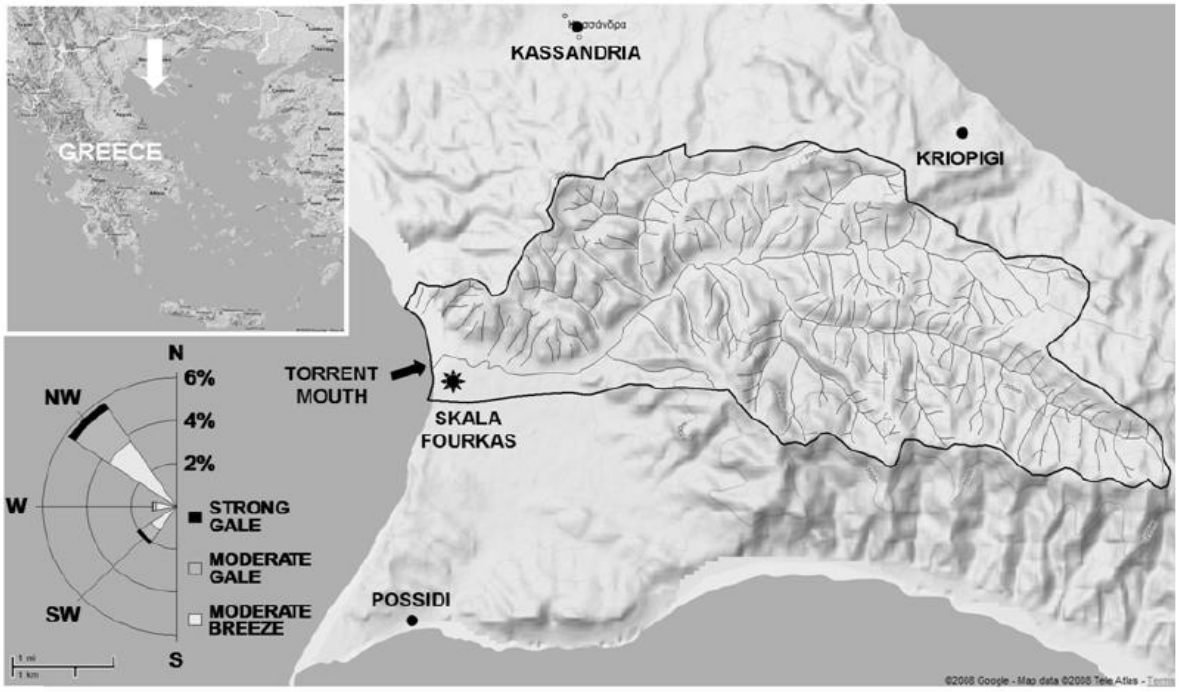

Figure 1 Direction of winds (Samaras, A., Koutitas, C., 2009).

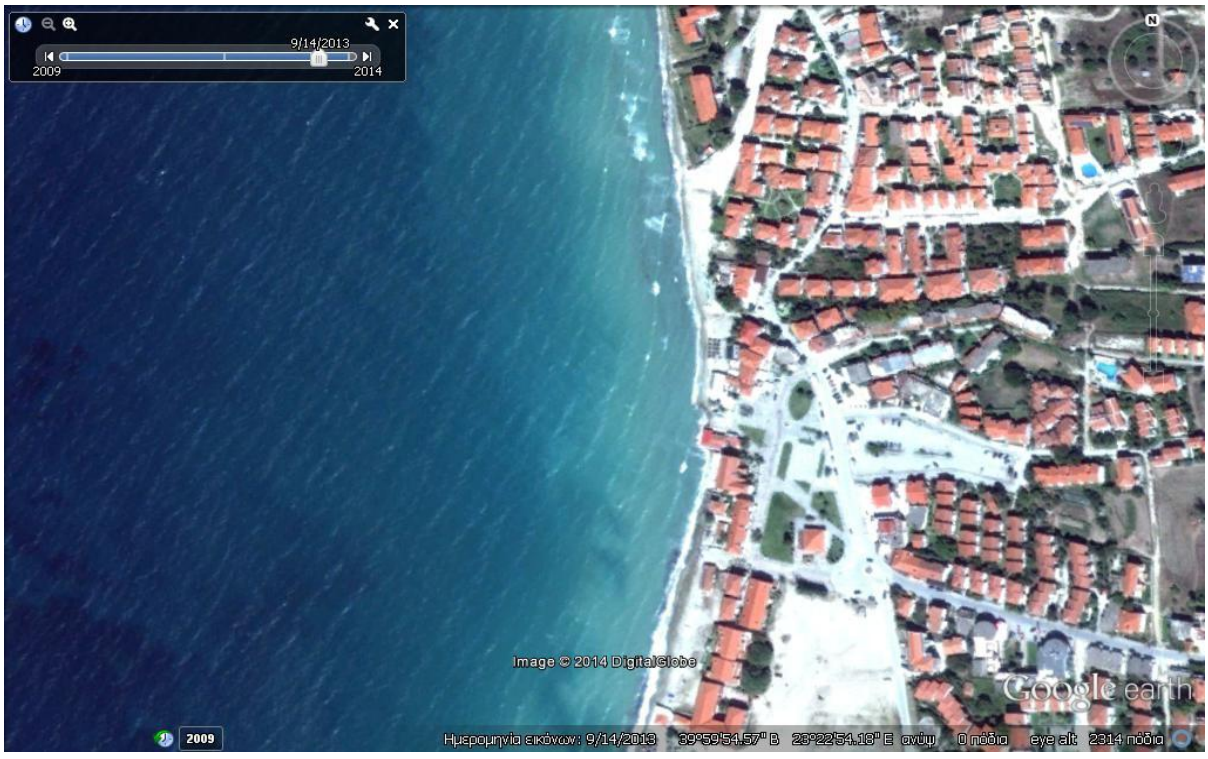

Figure 2 Fourka area, where we can see the direction if the wind blowing from North West. (Google earth picture 14/09/2013).

1.4 CORINE LAND COVER 2000

The land cover of the study area is given by the CORINE LAND COVER 2000. This program, using common methodology, provides the first standardized study on land cover for the year 2000 and the changes which have occurred during the decades that followed since the conducting of the first program CORINE LAND COVER in the late ‘90s. According to the program, land uses found in the study area are the following:

• **112: Artificial surfaces** / Urban fabric / Discontinuous urban fabric

• **121: Artificial surfaces** / Industrial, commercial and transport units / Industrial or commercial units

• **142: Artificial surfaces** / Artificial, non-agricultural vegetated areas / Sport and leisure facilities

• **211: Agricultural areas** / Arable land / Non-irrigated arable land.

• **223: Agricultural areas** / Permanent crops / olive groves

• **242: Agricultural areas** / Heterogeneous agricultural areas / Complex cultivation patterns

• **243: Agricultural areas** / Heterogeneous agricultural areas / Land principally occupied by agriculture, with significant areas of natural vegetation

• **312: Forest and semi natural areas** / Forest / Coniferous forest

• **313: Forest and semi natural areas** / Forest / Mixed Forest

• **321: Forest and semi natural areas** / Scrub and/or herbaceous vegetation associations / Natural grasslands

• **323: Forest and semi natural areas** / Scrub and/or herbaceous vegetation associations / Sclerophyllous vegetation

• **324: Forest and semi natural areas** / Scrub and/or herbaceous vegetation associations / Transitional woodland-shrub

• **421: Wetlands** / Marine wetlands / Salt marshes

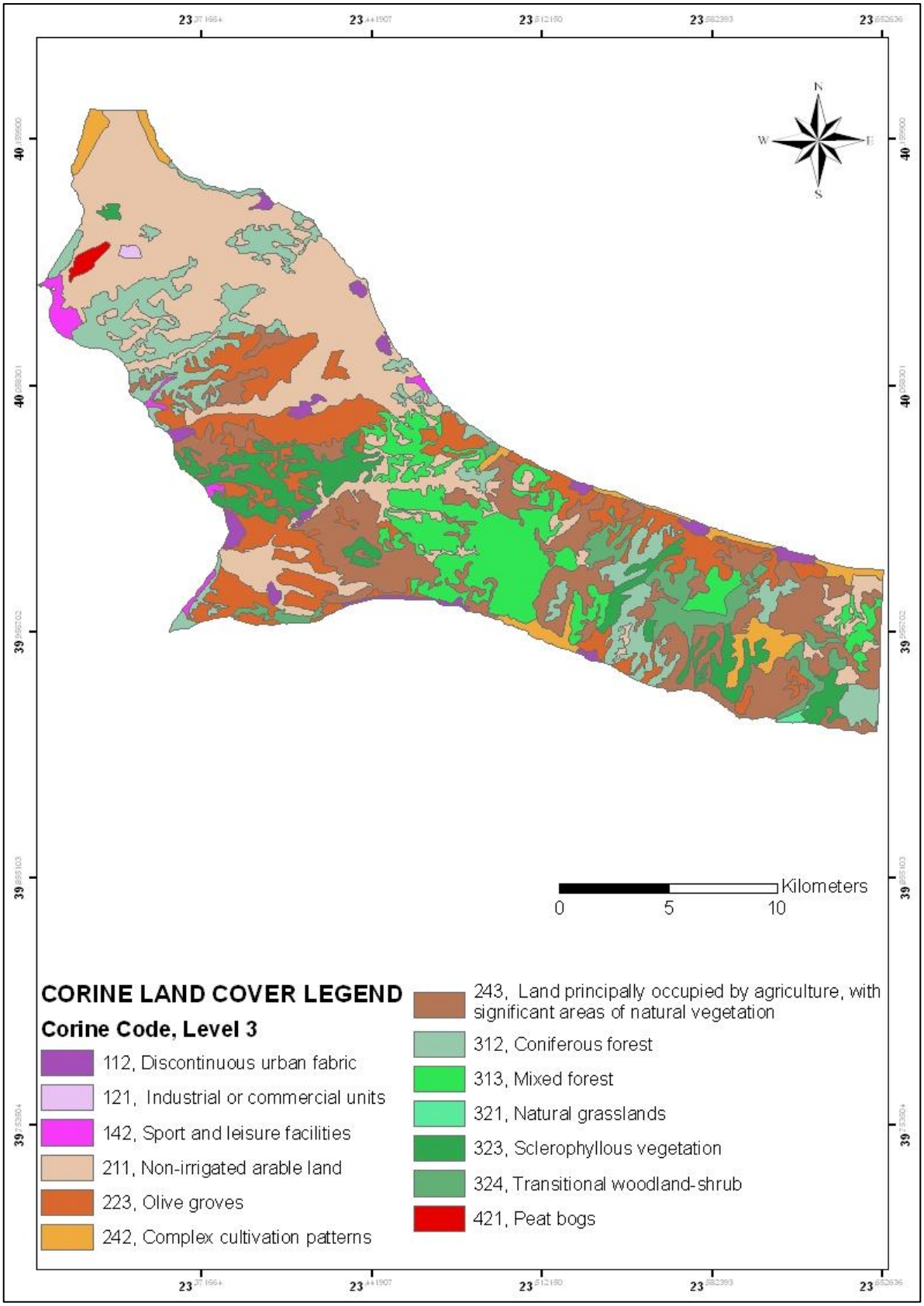

Figure 3 Land cover map of the study area (by CLC 2000 / for an explanation of the codes see. above).

Table 2 Type of land use covering the study area and the area it occupies.

Land Cover Codes	Label Level 3	Area (km^2)	Percentage (%)
112	Discontinuous urban fabric	6,6	1,73
121	Industrial or commercial units	0,39	0,09
142	Sport and leisure facilities	3,04	0,86
211	Non-irrigated arable land	98,76	28,19
223	Olive groves	48,58	13,81
242	Complex cultivation patterns	12,66	3,45
243	Land principally occupied by agriculture, with significant areas of natural vegetation	65,17	18,70
312	Coniferous forest	42,13	12,08
313	Mixed forest	34,93	9,78
321	Natural grasslands	0,36	0,09
323	Sclerophyllous vegetation	23,10	6,62
324	Transitional woodland-shrub	12,23	3,45
421	Salt marshes	1,02	0,29

1.5 GEOMORPHOLOGY OF THE STUDY AREA

As characteristically stated by Verstappen (1977), the form of the relief is the main point of interest in almost every interpretation of remote sensing images, because this is what constitutes the "face of the Earth", as seen from above (Mouratidis, 2010).

According to Dikau (1989), the relief can be classified into 4 categories according to the altitudes: flat, hilly, semi-mountainous and mountainous.

Table 3 Classification of the relief according to altitude from sea level (Dikau, 1989).

Altitude (m)	Classification
<150	Lowlands
150-600	Hilly areas
600-900	Semi-mountainous areas
>900	Mountainous areas

The map of Altitudes was constructed, according to the classification of Dikau, 1989, based on the digital elevation model (DEM), with the help of the program ArcGIS 9.3.

Table 4 Terrain Classification of the study area by Dikau, 1989.

Topography	Area (km^2)	Percentage (%)
Lowlands (<150m)	297	84,38
Hilly Areas (150-327m)	55	15,63

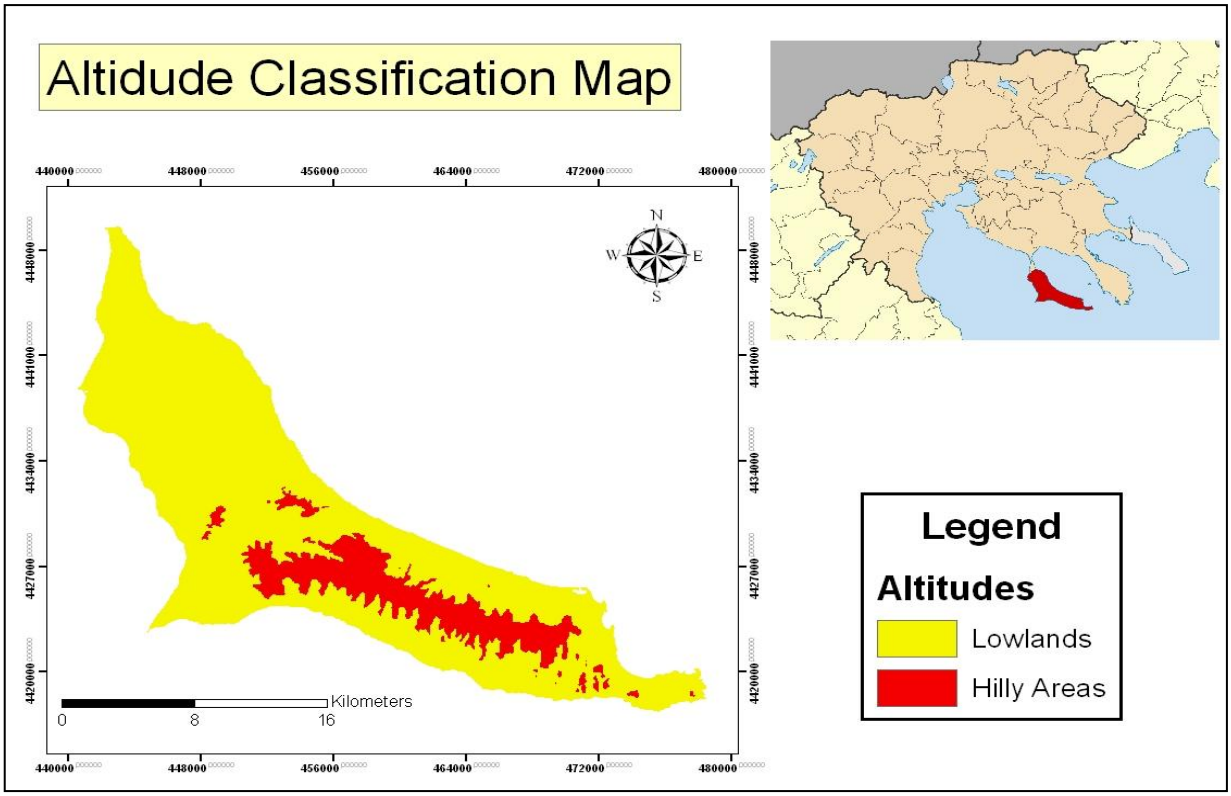

Figure 4 Altitude classification map by Dikau.

1.6 GEOLOGY OF THE STUDY AREA

1.6.1 GEOTECTONIC VIEW OF THE STUDY AREA

From a geotectonic view Halkidiki is placed between the Greek mainland (Rodopi and Serbomacedonian Masses) and the internal Ellinides. (Moudrakis, 1985). Three geotectonic zones of the Greek site meet in the area of Halkidiki:

1. Serbomacedonian mass in the eastern part

2. Perirodopiki zone in the central part

3. The subzone of Paionia in the western part

The study area belongs to the geotectonic zone of Paionia, which consists of the easternmost of the three zones where the zone formerly known as the Axios zone was divided. (Mercier 1966, Moudrakis 1985, Syridis 1990).

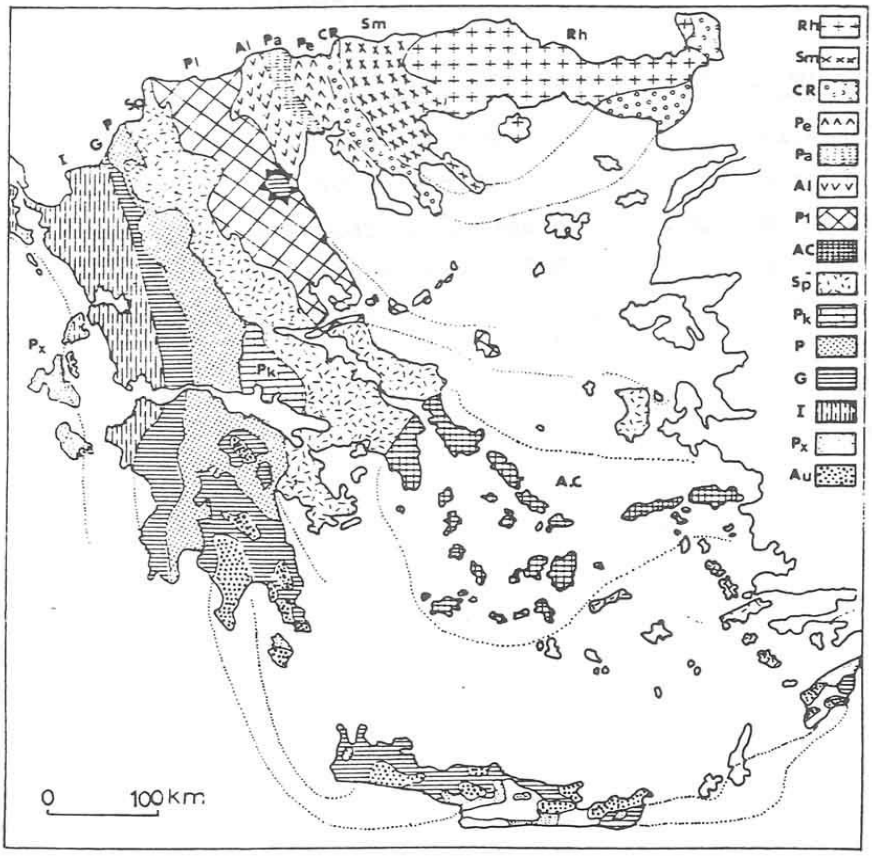

Figure 5 Sketch of geotectonic structure of central Macedonia. PL: Pelagonian zone, AL: sub Almopia, PA: sub Paiko, PE: sub Paeonia (the AL, PA and PE are the Axios zone). CR: Perirodopiki zone, SM: Serbomacedonian mass, RH: Mass Rodopi.

The Axios zone has NNW-SSE direction. It starts from the area of Skopje, crosses the Thermaikos Gulf and the islands of the N. Sporades and then turns east to Asia Minor. A key feature of the Axios zone is the presence of ophiolites as this specific zone consists the inner ophiolithic strip of Greek site (IRO). The view that the Axios zone became part of the ocean of Tethys in the Greek area was based on this. Of course along with ophiolites we also meet the accompanying deep sea sediments (Mesozoic). The Axios zone is divided into three sections, from east to west:

1. Section of Paionia

2. Section of Paiko and

3. Section of Almopia.

Paleogeographicaly, the Section of Paiko was a shallow water platform between trenches (deep sea), between the Sections of Paeonia and Almopia. The basic criterion (certainly not the only one) for this distinction is the existence of a thick neritic limestone series in the Section of Paiko, contrary to clay-chertic sediments (sedimentation of deep sea) occurring in the Paeonia and Almopia Sections.

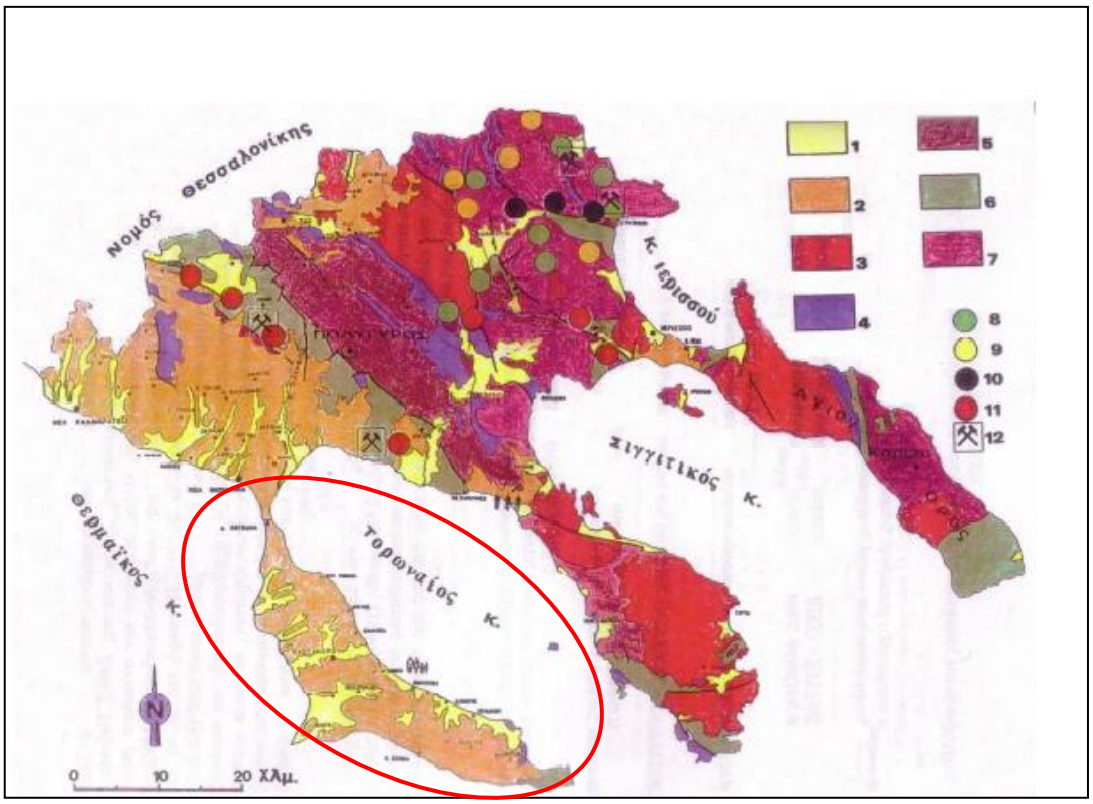

Figure 6 Geological map of municipality of Halkidiki (IGME, 1999)

1. Lake, land and recent deposits: clays, sands, conglomerates, red clay, loam, side scree, scree cones and coastal deposits (Pleistocene-Holocene).
2. Lacustrine and terrestrial deposits: conglomerates, sands, loam, red soil, margaikoi limestones and clays (down-Pliocene).
3. Granites: granites, granodiorites and monzonites (Jurassic - Tertiary).
4. Carbonate rocks: limestones and marbles (Triassic - Jurassic).
5. Metaklastika rocks: shales, sandstones, quartzites, phyllites, intersections, ammouches loam and hornstones (Triassic - Jurassic).
6. Prasinopetromata: spilites gabbros, peridotites, dunites, Olivenite, pyroxenites, chloritikoi schists and amphibolites (Palaiozoiko- Triassic).
7. Gnefsioschistolithoi: gneisses, schists, migmatites and amphibolites (Paleozoic - Triassic).
8. Views and deposits Pb -Zn
9. Views and deposits Fe - Cu
10. Views and deposits Mn

11. Views and deposits Cr
12. Mines

In brief, in the Paeonia Section, we come across various rocks such as shales, mudstones, sandstones, dolerites, limestones, marbles, conglomerates etc. Also tectonically the Paeonia zone is characterized by flaky tectonic scales of the Tertiary. Obviously not all scales are visible as many of these are covered by Quaternary sediments. The section of Paiko is generally characterized by metamorphic rocks and faults of NW and NE direction. Finally the Almopia zone is formed of ophiolites and deep sea sediments from Upper Cretaceous sediments and from pre-ophiolite metamorphic rocks. The contact area of Almopia with the Section of Paiko is tectonic with reversed faults of NW-SE direction; Furthermore the Zone of Almopia rides westward the Pelagonian zone (Moudrakis, 1985).

1.6.3 QUATERNARY SEDIMENTS

At the low relief part of the W. Halkidiki and Kassandra peninsula the Pre-Neogene background is covered in a thick layer of younger, mainly loose sediments. It consists of terrestrial-fluvial, fluvial-deltaic, lake-deltaic, lacustrine and terrestrial deposits formed during the development of the trench of the wider area of Axios - Thermaikos (Psilovikos al, 1988).

These deposits include a wide variety of lithological types, such as conglomerates, terra rossa, sands, sandstones, clays, marls, marly limestones, biogenic limestone and travertines. The sedimentary layers are shown slightly inclined towards the NNW in the Kassandra peninsula and control greatly the recent morphology (Syrides 1990).

1.7 HYDROLOGY OF THE STUDY AREA

The total amount of surface water streams (rivers, streams, etc.) connected together in a specific way and draining one basin is defined as drainage network (Sotiriades, 1984, Nikolaidou, 2009).

The drainage network of the region, that is all the streams draining in the basins, consists of streams up to the 5th order, according to the classification method of Strahler (Strahler, 1952).

At W. Halkidiki and Kassandra peninsula the existence of a thick sediment cover allowed the development of a drainage network with branches extremely elongated and parallel to each other. At Kassandra the entire northern part drains to the west; Meanwhile the eastwards runoff is almost nonexistent, and as a result the eastern shores play the role of the watershed. On the contrary, in the southern part the watershed is located in the axis of the peninsula and the drainage network consists of parallel valleys developed evenly on both sides of the watershed. (Syrides 1990).

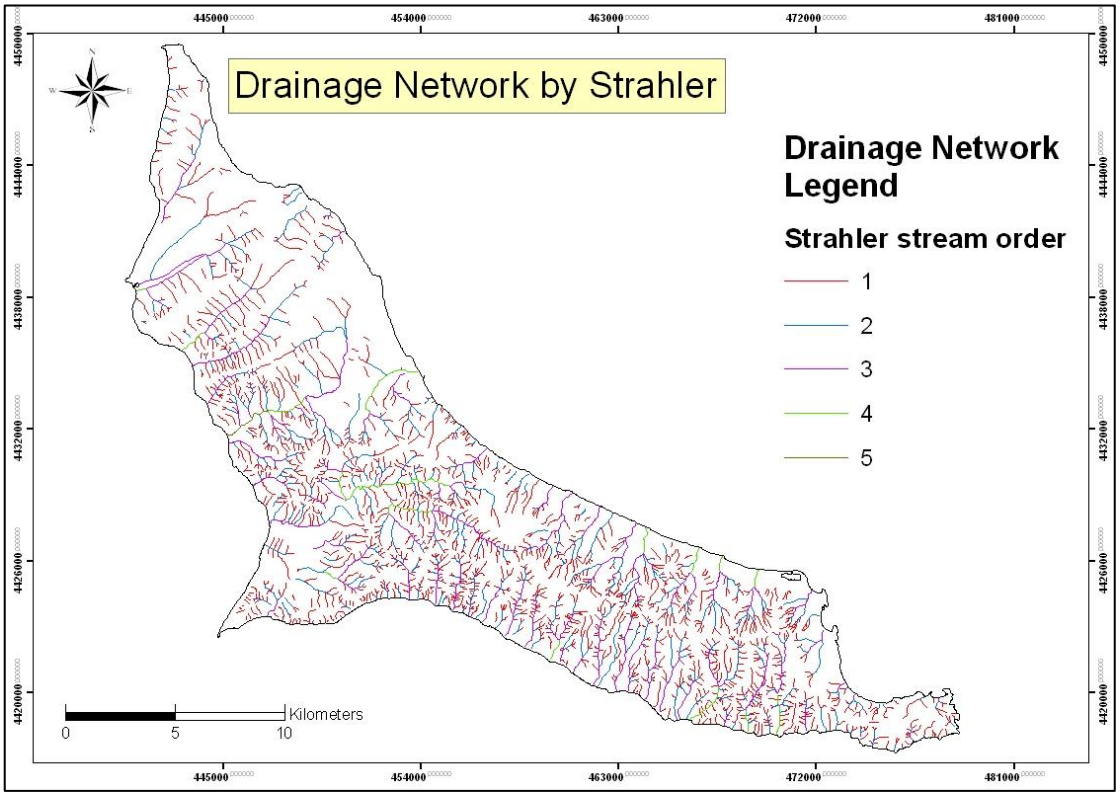

Figure 7 Drainage network of Kassandra peninsula according to Strahler.

The region of West Halkidiki and the part of North Kassandra display mature, old relief, with little morphological gradient 2-5^{o} / S-SW and elongated open "U" shaped valleys. These valleys are either dry or flowed by small torrents, to which this great

widening cannot be attributed. The terrain is probably inherited by the former cycle progression as evidenced by the sudden termination of the old morphological surface on the shores of the tectonic and coastal erosion (Marinos et al. 1970, Syrides, 1990). Thus almost the entire length of the W. coast's coastal terraces and hanging dry valleys were formed, alternating with small coastal plains. These areas were formed by filling older valleys' mouths. Also clear characteristics of renewal of the valleys and the beginning of a new cycle of erosion are distinguished by creating new valleys within the old ones and the erosion of the loose sediments (Psilovikos, 1988).

PART A’

2. FLOOD SUSCEPTIBILITY MODEL

2.1 INTRODUCTION

The science of remote sensing in combination with Geographic Information Systems has introduced new methods in the management of natural ecosystems. The possibility of longitudinal monitoring of the Earth's surface quickly and at a relatively low cost, allows the recording of changes that occur in the natural environment and thus facilitates treatment or anticipation of potential problems.

The purpose of the study is to evaluate the contribution of Remote Sensing and GIS technologies flood management in the study area, by the construction of flood susceptibility maps.

2.2. NATURAL DISASTERS

According to UNDRO (United Nations Disaster Relief Organization), a destruction can be defined, mostly quantitatively, as: "*An event, set in space and time, during which a community faces a serious hazard and its members face such losses that the social structure is ruptured and the completion of all or most of its basic functions is hindered* "(Lekkas, 2000, Pappa, 2012).

A natural disaster can cause loss of life or property damage (U.S. Billion-Dollar Weather and Climate Disasters), and typically leaves some economic damage in its wake, the severity of which depends on the affected population's resilience, or ability to recover (Bankoff et al. 2003). An adverse event will not rise to the level of a disaster if it occurs in an area without vulnerable population (Luis Flores Ballesteros, 2008; Alexander, 2002; Wisner, 2004).

2.2.1. FLOODS

Flood is the overflow of water onto lands that are normally dry and is the most commonly experienced natural hazard (Keller and Blodgett, 2006). The EU directive defines a flood as ground which normally is not covered from water being covered from water (Directive 2007/60/EC Chapter 1 Article 2). Floods were always thought of as the hazard influencing the most people and bringing on greater economic pressures than any other. This happens because they are the most common hazard, given the extensive geographical diaspora of the fluvial systems on the surface of the earth. This has also been proved by Parker (2000), who cites facts that render floods as the most common starting points for disasters, during the second half of the twentieth century. In the current paper we deal with ***fluvial floods,*** therefore a (fluvial) flood is the situation during which the discharge of a river's water body (or part of it) cannot be achieved through its normal river bed, and as a result the water body overflows the latter and spreads to the neighboring soils (Strahler, 2003; Lekkas 2000). Most fluvial floods are a result of **(i)** the total amount and rainfall distribution, **(ii)** the rock's permeability **(iii)** the topography. Some floods are the result of the melting of ice and snow during the spring or, in rare occasions, the destruction of a dam. Finally, the use of land in small drainage catchment, could influence the flood phenomenon significantly (Lekkas, 2000).

2.2.2. TYPES OF FLOODS

In general, there are two kinds of floods:

- **Upstream floods/ flash floods**: upstream floods occur at the highest parts of drainage and are generally the result of intense rainfalls of small duration over a relatively small area. Although floods can be mostly intense over this area, they are not, generally, caused by the greater streams to which they connect. Because upstream floods occur without warning, are the most dangerous for humans (Jha et al. 2012). Greece mostly suffers from flash floods.

- **Downstream floods:** Downstream floods cover a wider area. Usually, they are the result of long duration storms that permeate the ground and have increased runoff flow (Lekkas, 1996).

2.3. FLOOD SUSCEPTIBILITY

Susceptibility is more commonly obtained indirectly by measuring those intrinsic properties which are believed to govern the occurrence of an event. Geomorphological mapping techniques may be used here, since depiction of landforms and associated processes may permit the experienced researcher to estimate susceptibility (Hansen, 1984; Boardman et al., 2003). The technique is both rapid and cost effective and was particularly popular in the 1970s and 1980s (Brunsden et al., 1975, Kienholz et al., 1983; Boardman et al., 2003). Heuristic approaches may also be used. Here, a priori knowledge is used to rank and/or weight those factors which influence susceptibility. However, this approach entails a high degree of subjectivity, particularly with respect to each factor's assumed a priori importance (Gupta and Joshi, 1989; Boardman et al., 2003).

According to Boardman, 2013 flood susceptibility is an important step in calculating hazard mapping and risk assessment. Where on one hand hazard maps include the extend of flooding for a given flood recurrence interval, and other fundamental hydraulic information such as flood depth, velocity and frequency of inundation (Wolman, 1971; Alcantara et al. 2010). While on the other hand, risk maps express the indicative number of the inhabitants and the type of economic activity of the area potentially affected, information about the transported sediments and other significant sources of pollution (Directive 2007/60/EC).

2.4. REMOTE SENSING AND GIS IN ASSESSMENT OF FLOOD SUSCEPTIBILITY

A GIS can be used to construct a map of susceptibility to flooding, which indicates the areas where flood is most likely to occur. GIS functions and database management systems allow for the storing, recall, management and combination of various thematic data layers which has been recorded for a specific area. These data may be derived from Remote Sensing from various thematic maps, ground gauges and observations but also from historical records. These varied data layers can be combined, exploited and applied to the prevention of flood events, to their prediction and to the effect of their impact. (Tholey et al., 1997; Nikolaidou, 2009). The effective management of emergency situations demands the merging of disaster management plans, historical records and real time information. The information must be relayed and understood as soon as possible. The combination of GIS technology and special Remote Sensing sensors enables immediate reactions providing the personnel with the most exact information whenever needed, giving the professional crisis managers the ability to gather a great amount of information relevant to the area in crisis and, after analysis, use this information in an efficient and clever way (Nikolaidou, 2009; Risk-EOS Geo)

2.5. MATERIAL AND METHODOLOGY

2.5.1 AVAILABLE DATA

For the purposes of the current study the following software was used:

- **ArcGIS (ArcInfo 9,3 edition),** with its subprograms **(ArcMap, ArcCatalog, ArcToolbox)** and **extensions** such as **Spatial Analyst™**
- **ENVI™ 4.7+IDL 4.7 (**Evaluation license)
- **Microsoft Office™ (Access, Word, Excel, Power-point)**

In the current master thesis the ASTER (Global Digital Elevation Model,G-DEM) was used, pixel size about 30m x 30 m. Then, out of the digital elevation model of the study area came the contours, the drainage network, the flow direction map, the flow accumulation map, the shaded relief map, the slope angle map and the slope aspect map. Out of the geological map (Kassandra sheet I.G.M.E.) the lithological formations of the study area were digitized. Finally the topographic wetness index was calculated with the aid of the Raster Calculator. All the above data were integrated in a GIS with the aid of ArcMap. The digital processing of the Landsat satellite image followed and the NDVI (Normalized Difference Vegetation Index) routine was followed with the aid of the Remote Sensing software ENVI. Thus the data layer of vegetation was derived for the study area and integrated into GIS.
The aforementioned data layers were properly combined and various thematic maps were compiled. From the factors mentioned above, the following levels of information were produced:

- map depicting moisture distribution, based on the topography
- map depicting the permeability of the geological formations
- surface roughness map
- vegetation map

Ratings were assigned to the above levels, based on their importance to the occurrence of flooding. These rating were calculated with the help of the "Analytic Hierarchy Process" (Saaty, 1980) (From Domakinis, 2005). Subsequently, these levels were combined and co-evaluated for the classification of the region into zones according to susceptibility to floods. The factors that affect flooding, as well as the information derived from them, are presented henceforth.

2.5.2 DIGITAL ELEVATION MODEL

The most common and widespread way of depicting earth's relied is the Digital Elevation Model/ DEM. The representation of earth's relief with numerical positions and elevation of specific ground points (digital data) which are properly used for the creation of a mathematical function (model) that satisfactorily expresses the continuous ground relief is the definition of the Digital Elevation model (DEM) (Soulakelis, 1994; Aleksaki, 2003; Nikolaidou, 2009). The relief is depicted by a network of equidistant points and each of them has a specific value that corresponds to the elevation. For the calculation of the elevation between two known points, the interpolation method is used, that the elevation is calculated according to the elevations of the neighboring points. This method is judged to be much more effective than the one in which the elevation is calculated without interference and is considered equal to the elevation of the nearest point. (Badellas, et al.. 1996; ESRI 2001; Fourniadis, 2002; Nikolaidou, 2009).

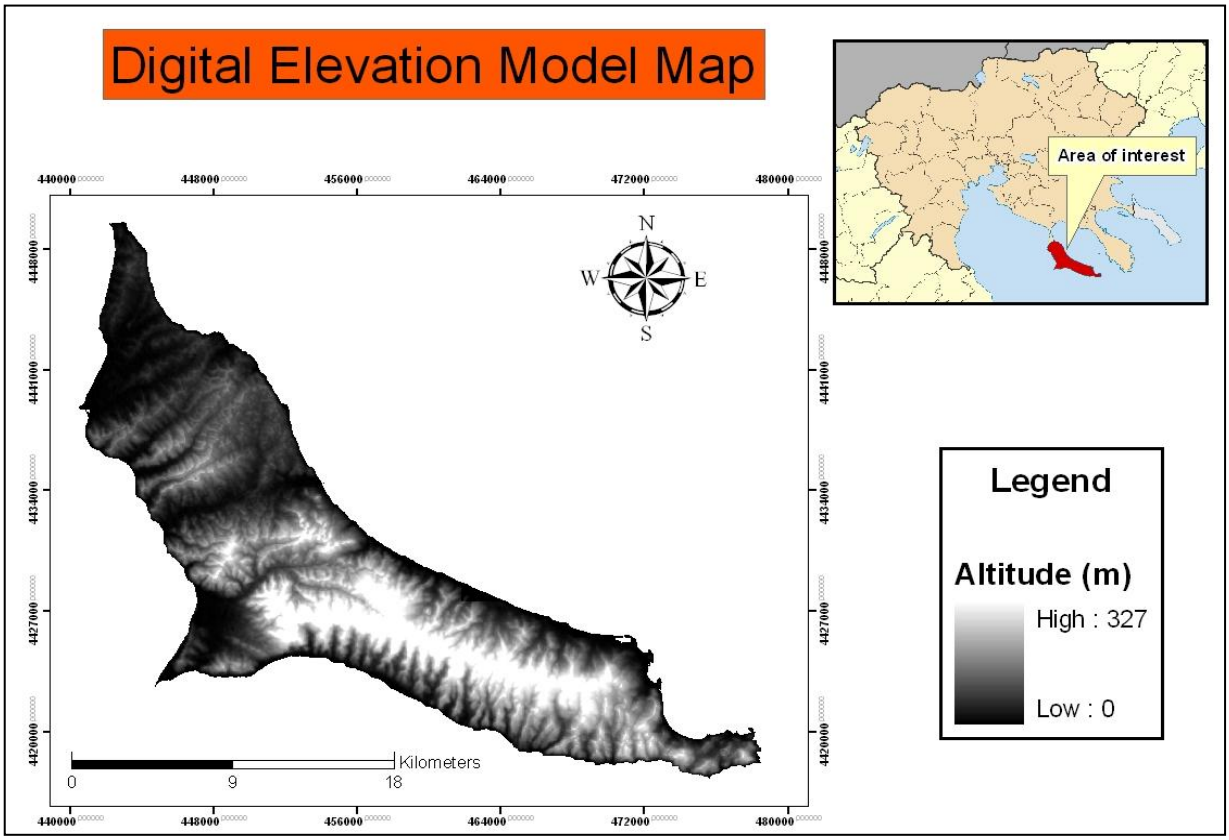

Figure 8 Digital elevation model of the study area

2.5.3 SLOPE MAP

A parameter that can be derived from further analysis of digital elevation models for further analysis, is the slope of the terrain, which is the most widely distributed known topographic size element and very important for each every geomorphological research study..

By taking into account the classification of slopes of the terrain suggested by Demek (1972), which was then adopted by the Commission Geomorphological Survey and Mapping (Commission on Geomorphological Survey and Mapping) of the International Geographical Union (IGU - International Geographical Union), the slopes of the area were classified into 6 main categories:

- Slope 0 ° - 2 ° (0% - 3.5%): Level to slightly inclined relief (floods fields, planation surfaces, terraces). Beginning of cap type erosion. Absence of problems in human activities (transport, construction, agriculture, forestry).
- Slope 2 ° - 5 ° (3.5% - 8.7%): Slightly inclined relief (foot valleys, dune slopes). Erosion of cap type and beginning of rill type erosion. In vegetated areas soil creep phenomena are observed. Measures must be taken to protect soils in cultivated areas. Slight difficulty in vehicle's movement, habitation and operation of industries. Cultivation upon the contours is suggested.
- Slope 5 ° - 15 ° (8.7% - 26.8%): Strongly inclined relief (slopes of valleys, tectonic terraces). Mass movements, strong cap and rill type erosion, intense erosive processes in areas of reduced vegetation cover, but they begin in areas of intense vegetation. Potential landslides and soil creep phenomena. In 15 ° (26.8%) is the critical angle for the formation of the whole soil surface. Significant difficulties in road construction and vehicle movement. Cultivation is impossible without the use of terraces. Difficulties in the use of agricultural machinery.
- Slope 15 ° - 35 ° (26.8% - 70%): Craggy (15°-25°) to extremely craggy (250-350) relief (slopes that belong to valleys of middle mountains). Intense denudation processes of any kind, soil creep, mudflows, very intense rill and linear erosion in both bare and vegetated areas (forests). Movement is

possible only by the use of vehicles that move on tracks. Cultivation is not feasible, logging is difficult. Area of forests and pastures.

- Slope 35 ° - 55 ° (70% - 135%): Steep relief (steep slopes of high mountain valleys, slopes of hogback formations, limestone canyon slopes). Very thin, discontinuous layer of soil, intense denudation of bedrock, strong exposure to factors of erosion and gravity. Impossible to access. Area of forests, logging exploitation limit.
- Slope > 55 ° (> 135%): Vertical relief (vertical slopes in areas of sandstone and limestone mountains). Lack of soil. Denudation of exposed rocks, collapse of rocks. Economic exploitation is impossible. Climbing. Danger of downstream rockfalls. (Nikolaidou, 2009).

The slope map of the study area resulted from the processing of digital elevation models (DEM) using the software ArcGIS (Spatial Analyst extension), and the classification of IGU (Demek, 1972):

Table 5. Spatial distribution of the slopes of the study area after Demek (1972)

Slope in Degrees	Area (km^2)	Percentage (%)
0 - 2	57	16,23
2 - 5	95	27,06
5 - 15	160	45,57
15 - 35	39	11,11
>35	0,1	0,03

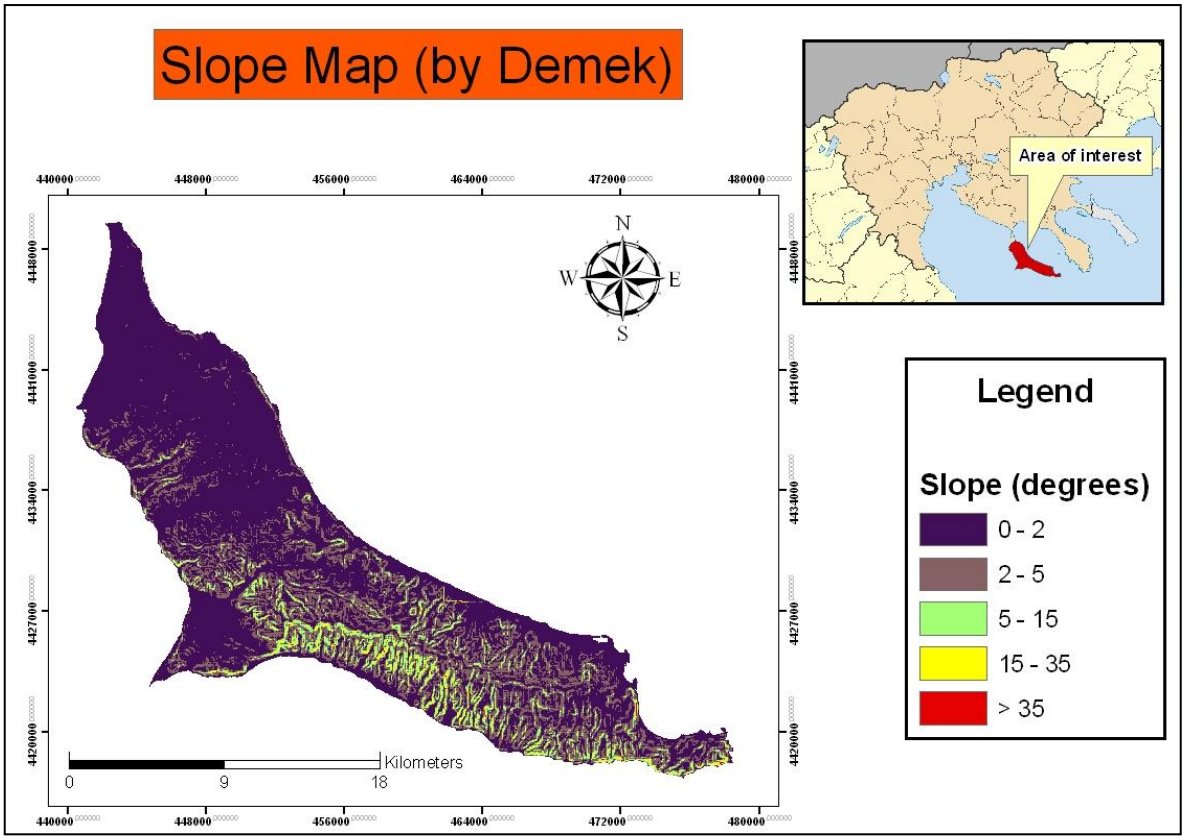

Figure 9 Slope map of Kassandra, Halkidiki (slope classification after Demek, 1972)

2.5.4 FLOW DIRECTION

The "downstream" flow (flow direction) in each pixel of DEM depends on the elevation of this point relative to its neighbors. The possible directions are eight, namely E, SE, S, SW, W, NW, N and NE. (Nikolaidou, 2009).

Flow Direction calculates the direction of flow for a given matrix. The water that is stored in each cell will flow to the neighboring cells with lower altitude. In this context, using the Hydrology Modeling tools of ArcGIS and the digital elevation model of the study area, the flow direction was calculated for each pixel.

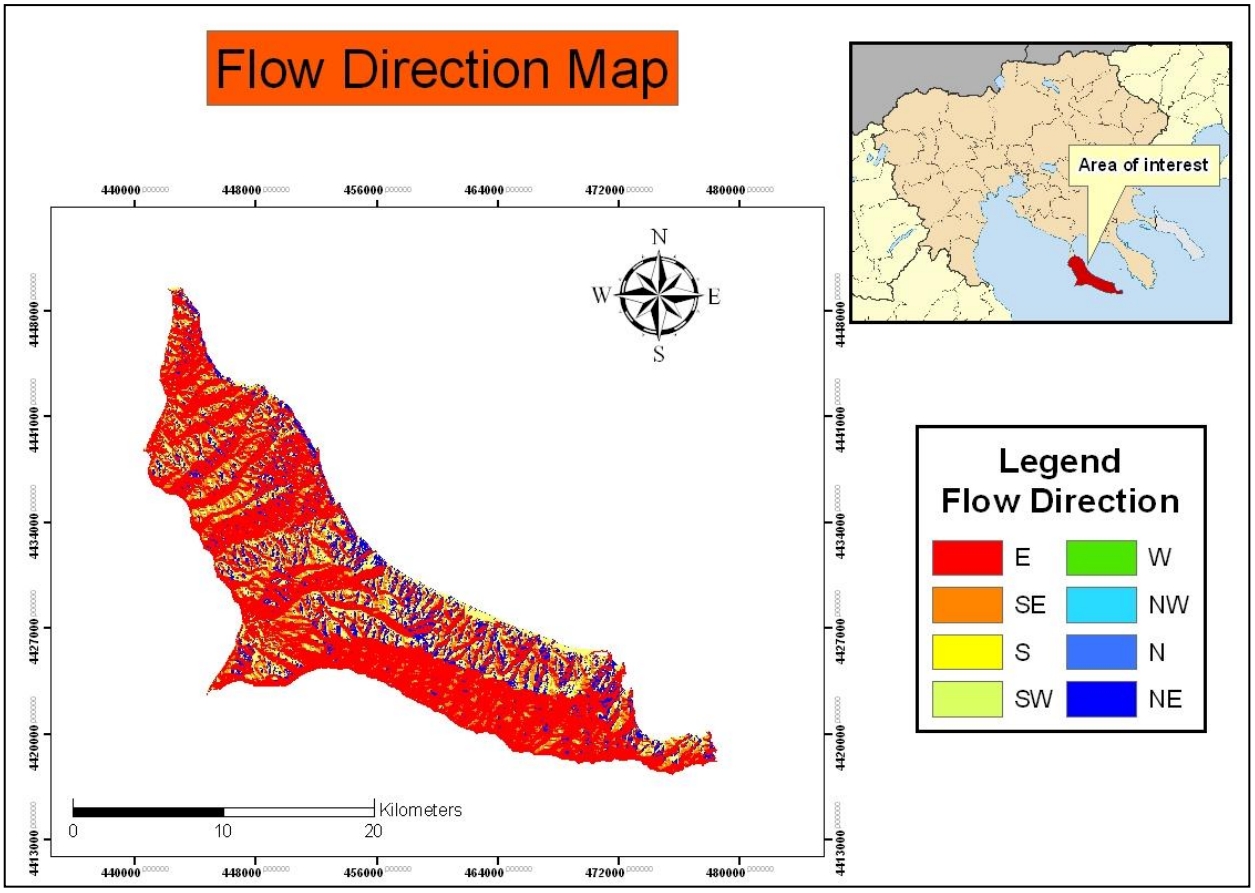

Figure 10 Flow direction map of the study area

2.5.5 FLOW ACCUMULATION

The accumulation of flow is the quantity of water, which will move to each pixel from its neighbors and will eventually be accumulated in it. The calculation of the total flux that is concentrated in each pixel is possible, based on the flow direction of the neighboring points.

The Flow Accumulation function computes the flow accumulation grid (flow accumulation grid) which includes the accumulated number of cells above the cell, for each cell of a given grid. From the Flow Accumulation Grid, opening the Properties panel and selecting the Source, one can observe how many cells there are in the grid, the size of the cell, which is the maximum flow accumulation in any cell number and what calculate the drainage area (Maidment and Robayo, 2002).

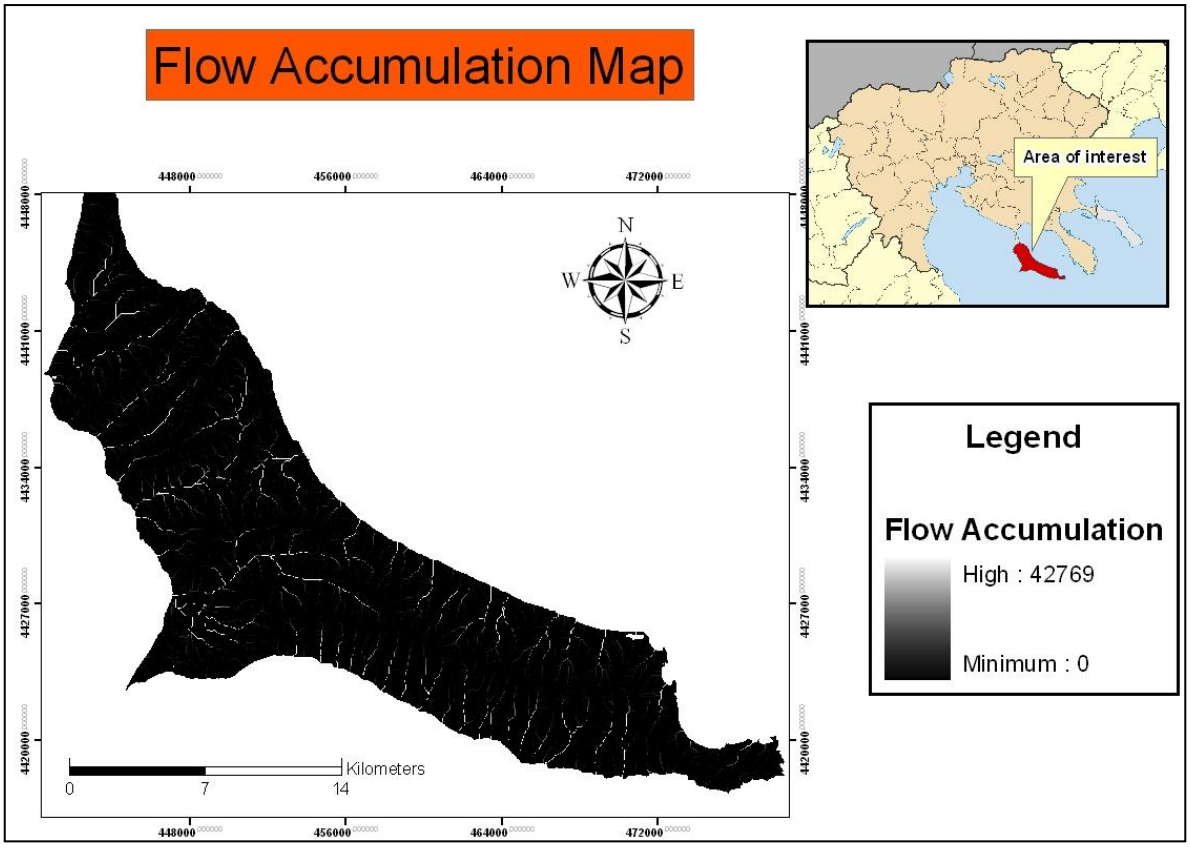

Figure 11 Flow accumulation map of the study area

2.5.6 TOPOGRAPHY - TOPOGRAPHIC MOISTURE INDEX (TOPOGRAPHIC WETNESS INDEX).

Topography is one of the most important factors controlling the spatial variation of hydrological conditions. (Burt and Butcher, 1985; Seibert et al., 1997; Rodhe and Seibert, 1999; Zinko et al., 2005) (from Sørensen, Zinko, and Seibert, 2006)

The topographic moisture index (Topographic Wetness Index / TWI) is a simple mathematical parameterization of potential soil moisture applied in many studies. The index is calculated based on slopes and therefore depends on the digital terrain data. (Haas, 2010).

TWI has been developed by Beven & Kirkby (1979) and is defined by:

$$\mathbf{TWI = \ln (a / \tan b)}$$

where **a** is the local upslope contributing area (m^2) from flow accumulation raster and **b** local slope angle. In order to convert slope angle from degrees to radians the following equation was used: Radians = (degrees x (∏/180))

The topographic moisture index (topographic wetness index) or index of moisture (wetness index) or topographic index, is the most widespread second derivative of digital elevation models (DEM) and it is used to describe the effect of topography on the distribution of soil moisture in an area.

The calculation of the location content indicator is based on the idea of water moving along slopes and its concentration on the base of the slopes. The greater the extent of the local catchment area and the smaller the slope angle, the higher the index value and the moister the soil can be expected to be (Beven and Kirkby, 1979, Quinn et al., 1991). The study of topographic index's spatial distribution in relation with various landforms, helped the classification and interpretation of its values. The ridges are characterized by low values, while the lower parts of the slopes, particularly the concave regions and bases of the valleys present high values (Rodhe and Seibert, 1999) (From Paraschou 2005).

On the map below (Figure 12), the distribution of topographic moisture index in the study area can be seen. Three categories of index values (low, medium, high) were defined, for each of which the area and the percentage of the total area were calculated.

The gradation that is given in each category corresponds to its susceptibility. Increased values of the index indicate the topographic region as more susceptible to flooding (rating 3) and low values of the index indicate an area of low susceptibility to

flooding events (rating 1). According to the TWI map 1.42% of the study area belongs to high values of the index, 17% belongs to moderate values and the remaining 81% belongs to low values.

Table 6 Percentage out of the total area for each wetness index category in the study area

Wetness Index	Area (km^2)	Percentage (%)
Low	286	81,48
Medium	60	17,09
High	5	1,42

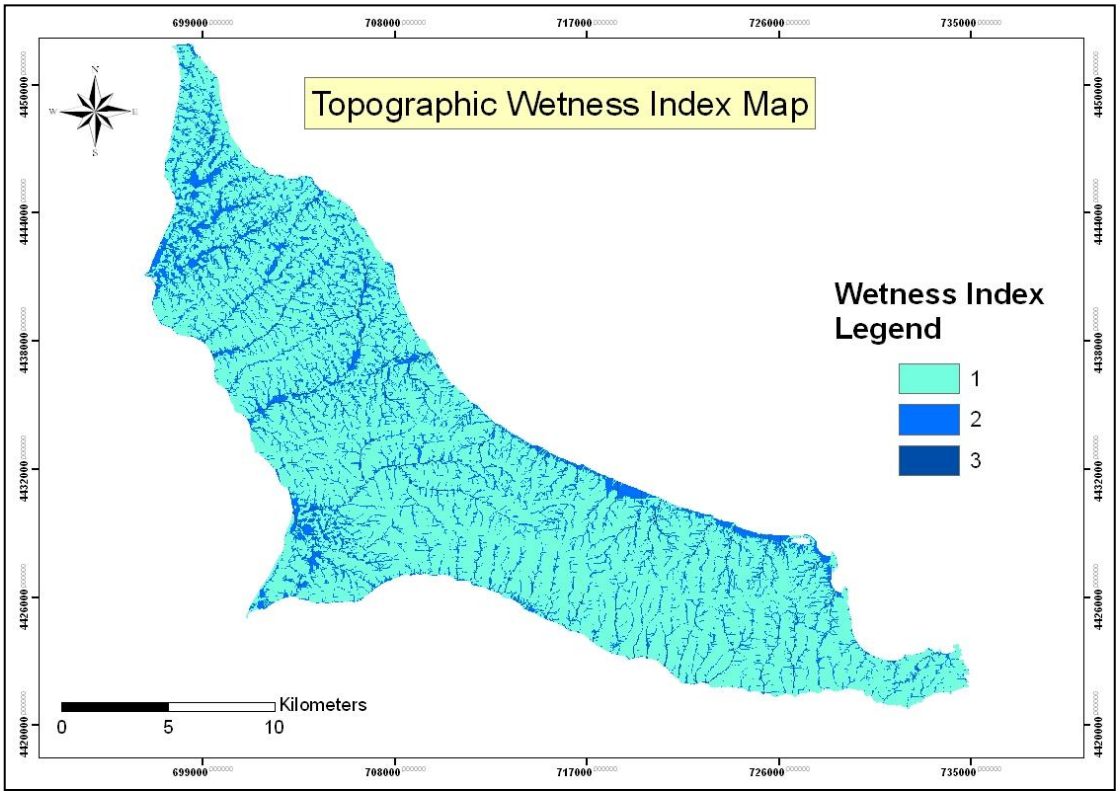

Figure 12 Topographic wetness index map of the area

2.5.7 LITHOLOGY – ROCK PERMEABILITY

Beyond the topography of a region, an important factor which affects the outflow and thus floods the runoff, is the lithology of this region. Each rock has its corresponding permeability which depends on its composition. The permeability (or hydraulic conductivity) is a property of the rock and is connected with the ease or difficulty of moving water into the mass. A measure of permeability is the permeability coefficient or the coefficient of Darcy. This factor has units m / sec, cm / sec, 1 meinzer, 1 darcy. In Europe, m / sec are commonly used (The SI Metric System of Units and SPE Metric Standard) .

The permeability coefficient depends on the pore size of the soil material and therefore it is not the material's property but varies according to the degree of concentration. For example, sand has a much higher permeability when it is dry and undisturbed rather than condensed with very dense structure. It seems therefore that the permeability coefficient depends on the type of soil material and its relative density.A rock with large permeability coefficient has relatively little resistance to the flow of water through it and may allow high speed infiltration. The exact opposite happens with a rock that has little permeability, i.e. has low permeability. The latter shows relatively large resistance to the flow of water through it and may allow really low speed flow filtration. So there are rocks more or less permeable, but it should be noted that completely impervious rocks, i.e. rocks that have zero permeability coefficient (k = 0) seem not to exist (Soulios, 1996). Yet, completely conventionally and arbitrarily, rocks are divided into three categories according to their permeability (this categorization is universally accepted and was adopted for practical reasons) (Soulios, 1996):

- Permeable rocks (high permeability) $k \geq 10^{-5}$ m / sec
- semi permeable rocks (moderate permeability) $10^{-5} > k > 10^{-7}$ m / sec
- impervious rocks (low permeability) $k \leq 10^{-7}$ m / sec

The gradation given to its category of permeability corresponds to its riskiness. So gradation 1 corresponds to permeable rocks, gradation 2 to semi permeable and gradation no 3 to impervious rocks. It is a notable fact, as derived from the

abovementioned maps and Table 8, which in the whole of the study mainly low permeability rocks prevail over the other two categories. Permeability coefficients for most common rocks are given in the following table:

Table 7 Permeability coefficients after Soulios, 1996.

FORMATIONS	**PERMEABILITY COEFFICIENT k (m/sec)**
CLAY	10^{-8} - 10^{-10}
CLAY OR MUD	10^{-6} - 10^{-9}
SANDCLAY	10^{-4} - 10^{-6}
FINE GRAINED SAND	10^{-3} - 10^{-4}
MEDIUM GRAINED SAND	10^{-2} - 10^{-3}
COARSE GRAINED SAND	10^{-1} - 10^{-2}
GRAVEL	10^{0} - 10^{-1}
SANDS-GRAVEL	10^{-2} - 10^{-3}
SANDS-GRAVEL-CLAY	10^{-3} - 10^{-4}
MARLS	10^{-6} - 10^{-9}
FLYSCH	10^{-6} - 10^{-8}
SANDSTONE	10^{-3} - 10^{-5}
CONGLOMERATES MOLASSES	10^{-4} - 10^{-5}
LIMESTONE-MARBLE	10^{-2} - 10^{-5}
SCHISTS VARIOUS	10^{-6} - 10^{-9}
OPHIOLITES	10^{-5} - 10^{-8}
GNEISSES-METAMORPHIC	10^{-6} - 10^{-9}
GRANITES	10^{-5} - 10^{-9}
VOLCANIC ROCKS	10^{-6} - 10^{-9}

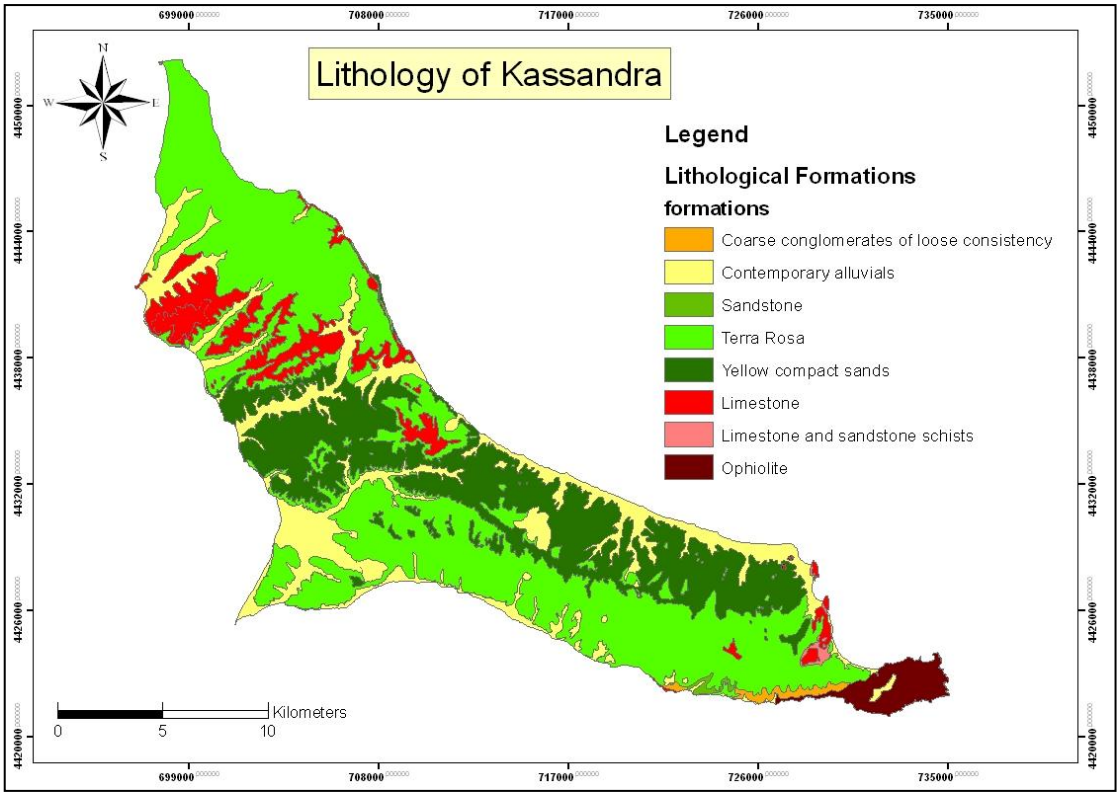

Figure 13 Lithological formations of Kassandra peninsula. (Digitization of Kassandra sheet I.G.M.E)

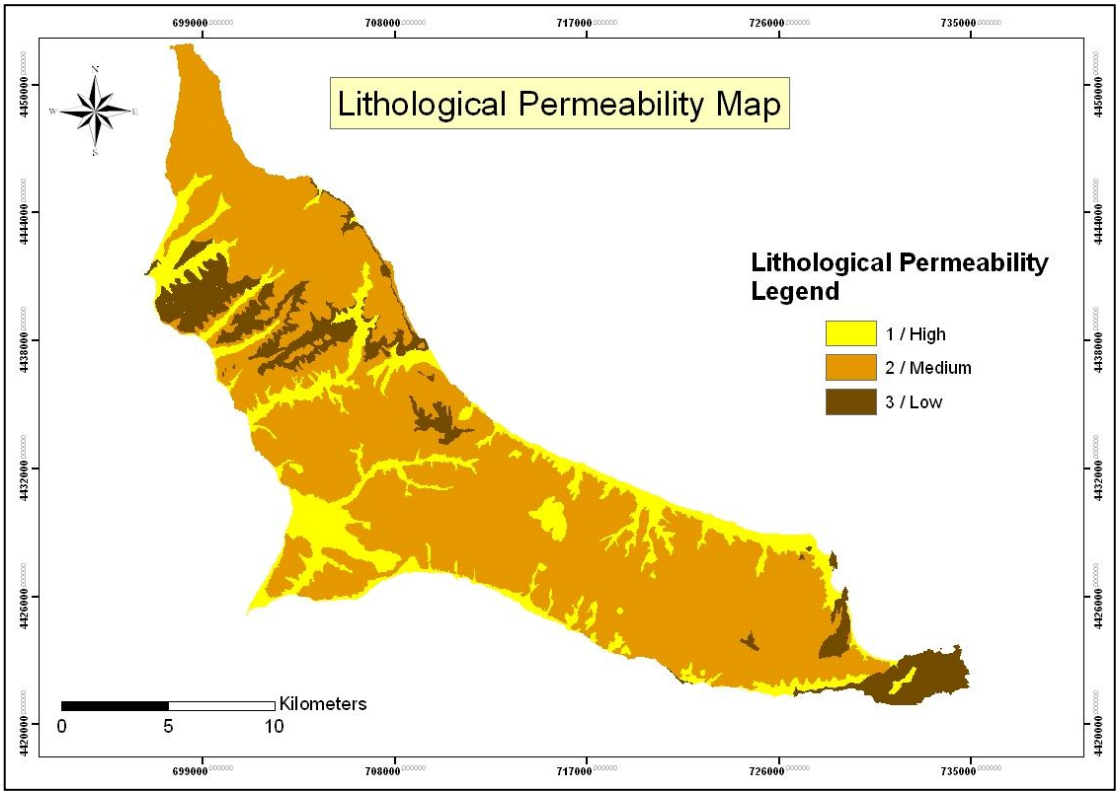

Figure 14 Lithological permeability map of the area

Table 8 Percentage distribution of rock permeability in the study area

Lithological Permeability	Area (km^2)	Percentage (%)
Low / 3	58	16,9
Medium / 2	249	72,59
High / 1	36	10,51

Thus, according to the permeability map, about 35% of the region is covered by permeable rocks, while the rest is made up of impermeable and semi permeable.

2.5.8 ROUGHNESS - LAND COVER

The land cover in the study area is given by the program CORINE LAND COVER 2000. It is based on the Strickler rate (Strickler coefficient) (e-EcoRisk, 2004), which gives a roughness value in each land cover code of the CORINE LAND COVER 2000.

Small roughness in an area (large coefficient Strickler) favors movement of water downstream which makes it more dangerous. Conversely, as the degree of roughness is increased (decreased value by Strickler), so does the resistance encountered by the water in motion with a consequent reduction in its velocity and hence it's hazardous.

In this specific study area, roughness values were defined as follows: 0.12, 4, 5, 6, 7, 8, and 10. The value 0.12 corresponds to high surface roughness and the more the numbers increase the less roughness gets.

Table 9 Roughness values in each land cover code of the study area

Land Cover Codes	112	121	142	211	223	242	243	312	313	321	323	324	421
Strickler Coefficient Codes	5	5	4	8	5	6	7	5	5	10	7	7	0,12

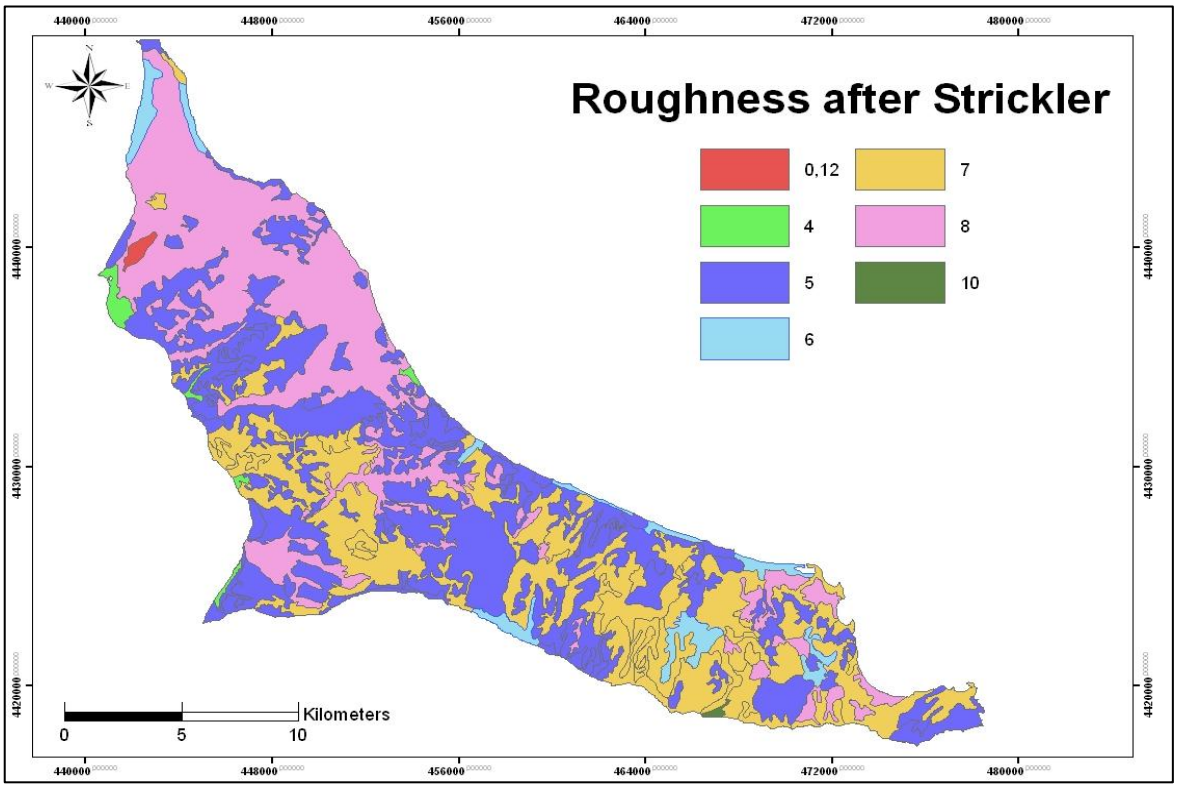

Figure 15 Land cover map based on Corine 2000

Table 10 Correlation of Srickler with Corine codes and the area they cover.

Strickler Coefficient	Corine Land Cover Codes	Corine Label Level 3	Area (km^2)	Percentage (%)
0,12	421	Salt marshes	1,02	0,03
4	142	Sport and leisure facilities	3,04	0,97
5	**112, 121, 223, 312, 313,**	**Discontinuous urban fabric, Industrial or commercial units, Olive groves, Coniferous forest, Mixed forest**	**132,65**	**38,01**
6	242	Complex cultivation patterns	12,66	3,62
7	**243, 323, 324**	**Land principally occupied by agriculture, with significant areas of natural vegetation, Sclerophyllous vegetation, Transitional woodland-shrub**	**100,49**	**28,79**
8	**211**	**Non-irrigated arable land**	**98,76**	**28,29**
10	321	Natural grasslands	0,36	0,10

2.5.9 VEGETATION INDEX (NDVI)

Bibliographically, there are several vegetation indices and many tasks related to their use, but the basic idea is, that the ratio of near infrared to red is usually high in the case of healthy vegetation. This means that in case of illness or lack of vegetation, a decrease of reflectance in the near infrared reflectance and an increase in red occurs (Syllaios, 2000).

A well-known index is the normalized difference vegetation index (Normalized Difference Vegetation Index - NDVI). This index was used in this study and was calculated by the equation:

$$NDVI = \frac{NIR - R}{NIR + R}$$

where NI.R (Near Infrared) is the spectral band of the near infrared and R (Red) the red spectral band . The satellite image which was used in the present work, is a LANDSAT 7, (acquisition date 24-08-2000). By using ENVI software the above index takes the form (Syllaios, 2000) (from Fourniadis . A., 2002):

$$\mathbf{NDVI = ((TM+4) - (TM+3)) / ((TM+4) + (TM+3))}$$

The NDVI values range theoretically from -1 to 1, as derived from the mathematical equation above. Values above zero indicate the presence of green vegetation (chlorophyll) or bare soil (values close to zero), while values below zero indicate the complete absence of vegetation and the presence of water, snow, ice and clouds. (Dalezios, 2002; Tsiro, 2006).

Table 11 Indicative values of NDVI index in different land cover types (Dalezios, 2002).

Type of Land Cover	NDVI (scale from -1 to 1)	NDVI (scale from 0 to 255)
Thick Vegetation	0.500<=NDVI<=1	210<=NDVI<=255
Medium Vegetation	0.140<=NDVI<0.500	118<=NDVI<210
Scarce Vegetation	0.090<=NDVI<0.140	105<=NDVI<118
Bare ground	0.025<=NDVI<0.090	88<=NDVI<105
Clouds	0.002<=NDVI<0.025	83<=NDVI<88
Ice and snow	-0.046<=NDVI<0.002	70<=NDVI<83
Water	-1<=NDVI<-0.046	0<=NDVI<70

Therefore, the image areas with high NDVI (light gray color) are those covered by vegetation, due to the high reflectance of vegetation in the near infrared and low in red. Instead, the image areas with low NDVI values (dark gray colors) are those where the absence of vegetation in observed, such as over residential areas, airports or bare soil (erosion areas)

For best visual results, the different shades of gray can be replaced with different colors. This method is called “false color display” (pseudocolour display). With the software ENVI, the above technique is applied to the original image NDVI (Figure 16).

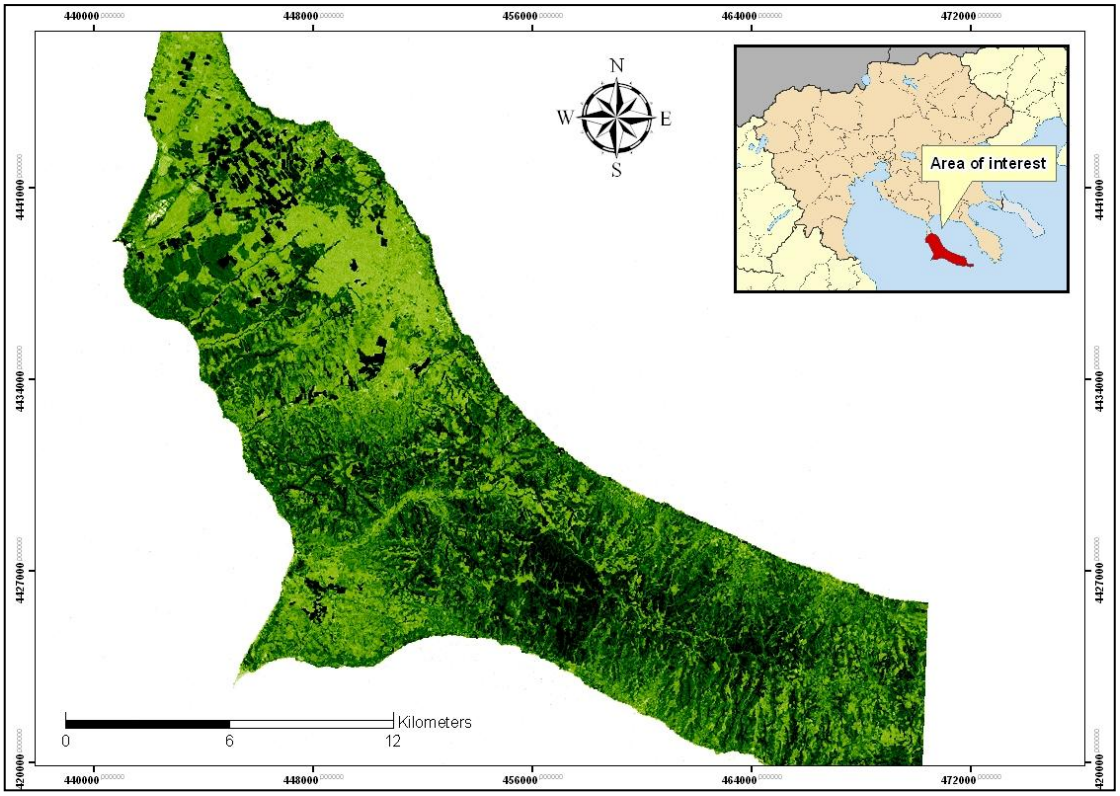

Figure 16 False color display (pseudocolour display) of the original image NDVI, with software ENVI. The classification of the NDVI value reflects the extent of vegetation. Low price NDVI (light green) involves sparse vegetation and high price NDVI (dark green) represents strong presence of vegetation.

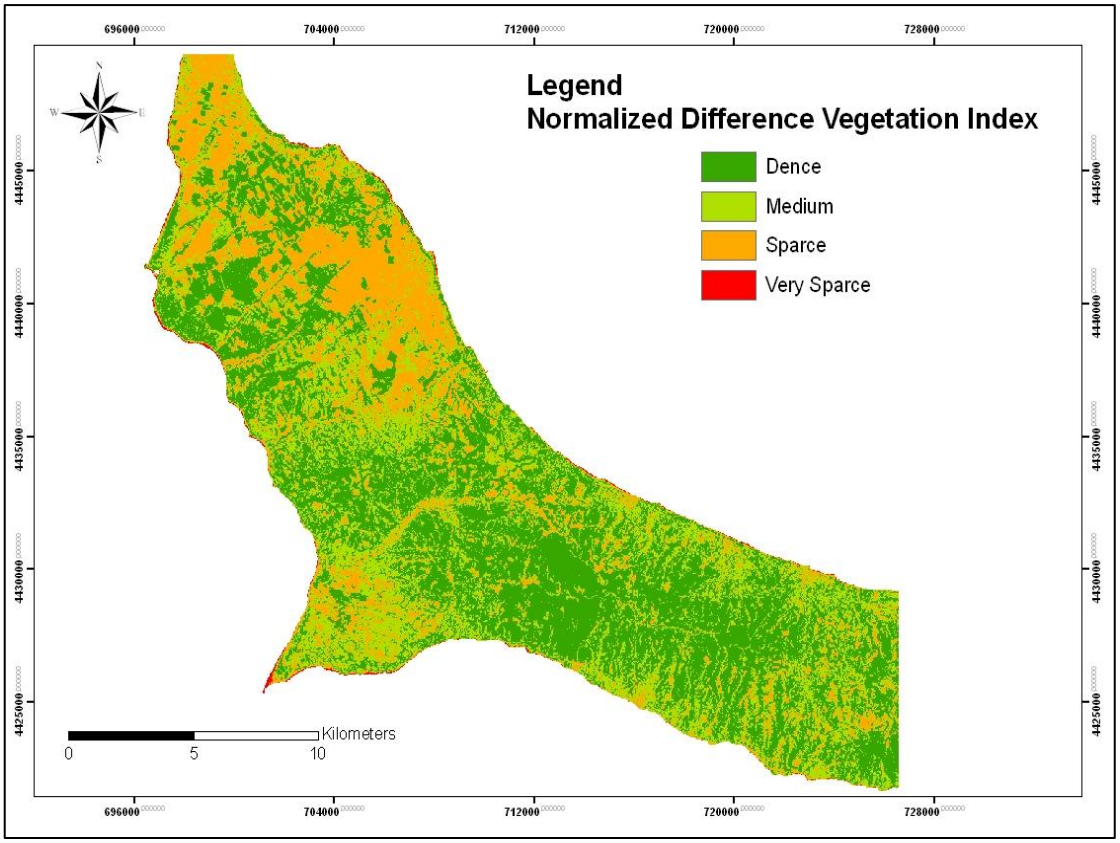

Figure 17 Normalized Difference Vegetation Index of the study area..

Having created the vegetation map of the study area, the following four categories of vegetation are discerned:

- Very Sparse (0 -100)
- Sparse vegetation (101-160)
- Medium vegetation (161-210)
- Dense vegetation (211-255).

The results are given in Table 12. Finally, the areas corresponding to the above categories were calculated, as well as their percentage with respect to the entire region. Each vegetation class was given a rating, with respect to its influence on flood occurrence.

Table 12 Percentage distribution of vegetation in the study area

Distribution of Vegetation	Area (km^2)	Percentage (%)
Very Sparse	39	12,26
Sparse	140	44,03
Medium	96	30,19
Dence	43	13,52

The lack of vegetation favors movement of the water downstream, after the water fails to be retained by the root system of plants, resulting in more rapid flow and thus becoming more dangerous. Conversely, where we have dense vegetation, water meets greater resistance to its movement as it is held in the root zone of plants, thereby reducing its speed and therefore becoming less dangerous.

2.5.10 FLOOD SUSCEPTIBILITY MAP

Each spatial component of vulnerability can be mapped under the condition that there is sufficient information on its distribution. Thus, when performing a risk assessment on natural risks for a large area, the results can be expressed in the form of hazard maps. So through mapping, the variation in the intensity of a risk is depicted from one location to another and an attempt is made for quantification based on the victims and the damage brought about. Therefore, the creation of hazard maps aims to estimate the likelihood and severity of future relative risk events in order to assess, mitigate or prevent any losses.

Despite these advantages, however, the hazard maps have some disadvantages since they are very general and represent a static view of reality, so that they must be renewed periodically, whenever relevant new data are available. Reliability, strength

and flexibility of mapping can be increased with the use of Geographic Information Systems (GIS).

To create a flood susceptibility map in the study area, initially, it is necessary to identify the factors that will be included as important and relevant to that event. The factors are not subject to a quantitative restriction. In order to select and integrate them into the model, it is necessary to have documented scientific knowledge of their adverse effect on the phenomenon and the existence of relevant data for the area to which the model is applied (Moyssiadou 2010).

In the case of flooding in the study area, the flood susceptibility map was produced after co-evaluation of the parameters of the topographic wetness index, the rock's permeability, the land cover roughness and the vegetation. The co-evaluation was determined after the percentages with which each factor affects the flood event in the region. The "weights" for each factor were calculated separately.

For the calculation of "weights" for each factor the method of "Analytic Hierarchy Process» (Analytical Hierarchy Process / AHP) is used, a methodology of multivariate modeling (multi attribute modeling) which was developed and initially implemented by Saaty (1980). In this method, all possible pairings between the factors are formed and then a numerical value from 1 to 7 is given to each factor, depending on how important the factor is considered in relation to another. The value of **1** indicates that a factor is as important as another; while the value of **7** indicates that the factor is much more important than another. Fractional values indicate that a factor is less meaningful than another. These values are chosen arbitrarily from the researcher, however, there should be subject to some restrictions which are defined by the logical relationship between the parameters, such as:

- knowledge of natural processes
- reasons for the appearance of the phenomenon
- previews experience

Also the values corresponding to each factor should not have much difference between them. The following tables record the conversion of preference factors into numerical values.

Table 13 Importance of factors and conversion in numeric value

Importance of factors	Value
Very High Importance	7
High Importance	5
Medium Importance	3
Low Importance	1

In the Table 14 are shown all possible pairings among the factors which were given a numerical value from 1 to 7, depending on how important it is believed to be in relation to another.

Table 14 Pair wise comparison of factors affecting the flood occurrence

	Topographic wetness Index	**Lithogical Permeability**	**Land Roughness**	**NDVI**
Topographic wetness Index	1	3	6	7
Lithogical Permeability	1/3	1	3	4
Land Roughness	1/6	1/3	1	2
NDVI	1/7	1/4	1/2	1
TOTAL	1,643	4,583	10,5	14

Using the table above, the method of arithmetic average (arithmetic mean method) was applied, in order to calculate the weights of the factors as follows:

- topographic wetness index → w1 = 0,584
- lithological permeability → w2 = 0,248
- land cover roughness → w3 = 0,103
- vegetation index → w4 = 0,065

In the Table 15 the results of the comparison are available.

Table 15 Calculation of weights (weights) for each factor by the arithmetic mean method

	Topographic wetness Index	**Lithogical Permeability**	**Land Roughness**	**NDVI**	**Average**
Topographic wetness Index	1/1,643=0,609	3/4,583=0,655	6/10,5=0,571	7/14=0,5	0,584
Lithogical Permeability	0,203	0,218	0,286	0,286	0,248
Land Roughness	0,101	0,073	0,095	0,143	0,103
NDVI	0,087	0,055	0,048	0,071	0,065

Then the classifications provided under each factor are multiplied by the analogous weight, and summed together to produce the final susceptibility map. Thus, the final value M for each pixel in the area of study is given by:

$$M = w1X1 + w2X2 + w3X3 + w4X4 +$$

Where X1, X2, X3, X4 are ratings for each factor (Esmali A, and Ahmadi H, 2003; Domakinis, 2005; Nikolaidou, 2009).

Based on the above methodology and using the ArcGIS 9.3 software and more particularly the Raster Calculator tool, the flood susceptibility map was created.

The susceptibility map classifies the area into 7 categories, which divide the areas in more or less susceptible to flooding as shown in the table below:

Table 16 Distribution of flood susceptibility in Kassandra

Susceptibility	**Area (km^2)**	**Percentage (%)**
Very Low	2	0,64
Low	107	34,19
Low - Medium	104	33,23
Medium	74	23,64
Medium - High	20	6,39
High	5	1,60
Very High	1	0,32

The susceptibility map was constructed using the method presented in detail above, yet contains subjective judgments, and this is because, of the factors taken into account but also because of the relevance of these which were selected empirically, because there is no specific methodology for this purpose.

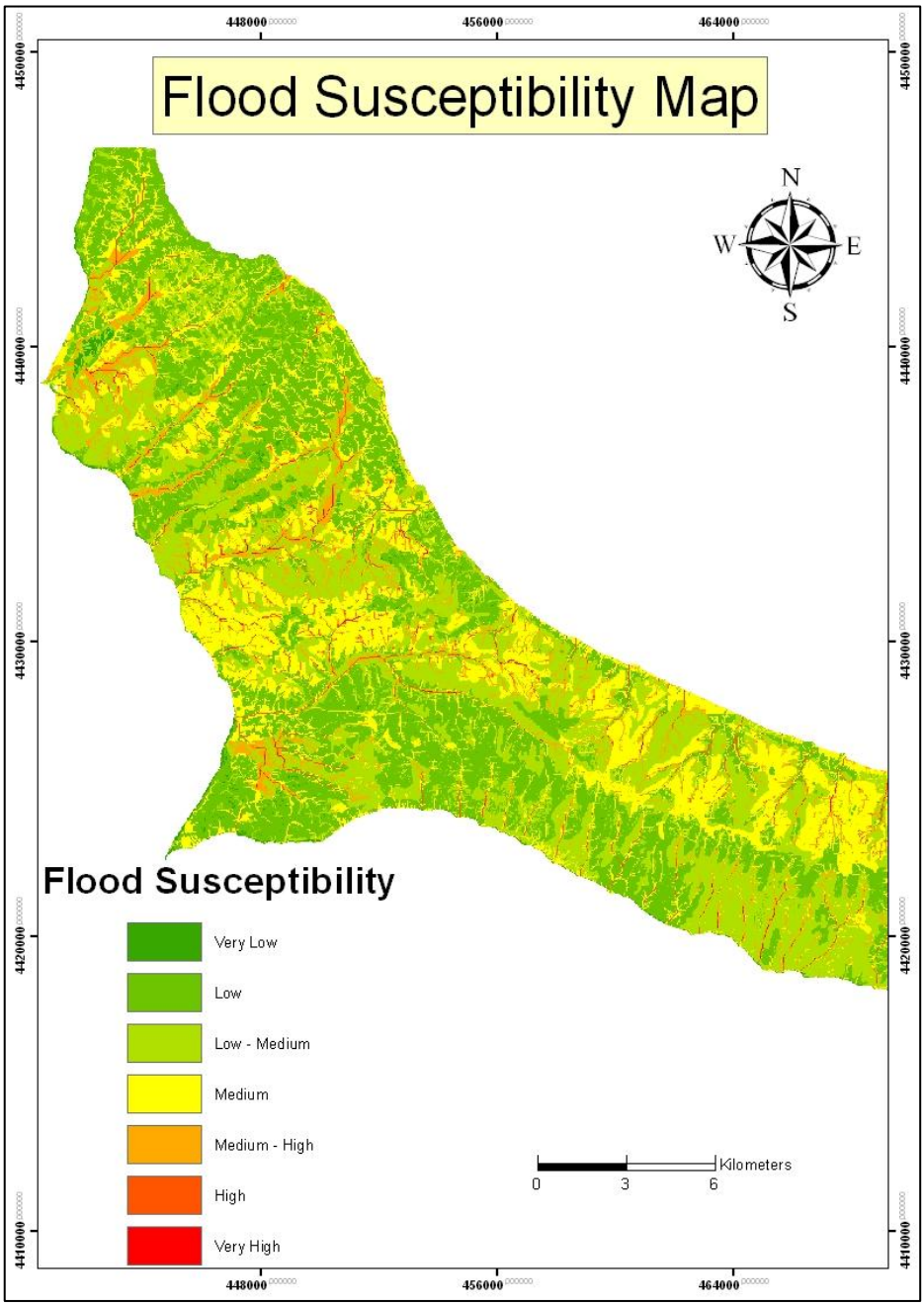

Figure 18 Flood susceptibility map of the area

The map shows that: in general, areas with high rates of susceptibility are scattered mainly in the western part of the study area.

2.6 CONCLUSIONS AND DISCUSSION

The purpose of this study was an attempt to evaluate the contribution of Remote Sensing and GIS in assessing the vulnerability of an area to flooding by constructing susceptibility maps.

This resulted in the following conclusions:

• According to the data of corine land cover 2000, the land cover map of the study area was created. From the map, it seems that about 70% of the study area consists of farmland, while 12% consists of forests.

• The map heights according to the classification after Dikau, 1989, show that the extent of the study area is divided into two types of terrain. Lowlands (84.38%), and hilly terrain (15.63%).

• Regarding the drainage network in the study area, according to the classification by Strahler, it consists of branches up to the 5th grade, but mainly the network reaches 3rd class.

• The slope map, following the classification of the IGU (Demek, 1972), showed that in the study area slopes range from 0° to43 ° degrees. Areas with slopes of 5° to 15° degrees cover 45.57% of the total of the study area. Areas with slopes between 2° and 5° degrees account for 27.06%, while the slopes from 0° to 2° degrees cover 16.23% of the total area. Finally, slopes from 15^{o} to 35^{o} cover only 11%. At this point it should be mentioned that the slopes in the settlements where there were floods range from 0° to2 ° (slightly sloping terrain).

• From the Topographic moisture indicator, which shows the distribution of moisture based on the topography of the region, it appears that 81.48% of the region has low index values, while 17.09% has moderate values and only a small percentage of order

of 1.42% gives high values. Increased wetness index shows that the region is more prone to floods and reduced-price index shows reduced susceptibility to flood events.

• From the lithological permeability map, it turns out that 35.61% of the area consists of high permeability rocks, the 32.19% of moderate permeability and also 32.19% from permeable rock.

• According to the map of land cover roughness, roughness values, which are based on the Strickler's rate, and prevail in the region, are the "5" with 38.01% percentage, the "8" with 28.29% and the "7" with 28.79%. The value of "5" corresponds to high surface roughness. The more the numbers increase the less the degree of roughness gets.

• From the digital processing and analysis of the satellite image Landsat-7 the "Normalized Difference Vegetation Index» (NDVI) was derived. The picture was given four classifications of vegetation (absence, sparse, moderate, and dense) and was incorporated into a GIS environment, where the vegetation map of the area was created. In the study it is noted that the highest percentage corresponds to sparse vegetation with 44,03%, moderate vegetation has a percentage 30.19%, dense vegetation has a percentage of 13.52% and spars vegetation is found in 12,26% of the study area. This connects to the fact that the lack of vegetation favors movement of the water downstream, after the water is not retained by the root system of the plants, leading to flow at a higher speed and thus increases the risk for flooding.

• From the co-evaluation of the parameters of the topographic wetness index, the permeability of the rock, the roughness of land cover and the vegetation cover the final flood susceptibility map was constructed, classifying the area into 7 categories. These categories show which areas are more or less vulnerable to flood. According to the final map the largest portion of the study area corresponds to:

- Low susceptibility areas which occupy 107km^2 or 34.19% of the total area and appear extensively on the S and NE part of the peninsula.
- Medium-Low susceptibility zones covering 104km^2 or 33.23% of the total, and appearing on the SE and NW.
- Areas with high susceptibility reach only 1.6%, and are located along the main branches of the drainage system throughout the peninsula. In these areas there

is a large residential development combined with low slopes and sparse vegetation, where major floods have occurred in the past (W and SW). This outlines the necessity for further quantification of the urban fabric in these areas, in order to develop a flood protection plan for affected areas.

PART B’

3. CONTEMPORARY COASTLINE CHANGES

3.1 INTODUCTION

The coastline is one of the most important linear features on the earth’s surface, which display a dynamic nature. The coastal zone and its environmental management require information about coastlines and their changes. This chapter examines the coastline change detection with a method that combines the use of satellite images and GIS. More specifically it uses Landsat images of the last 43 years and the DSAS toolbar through ArcMap. The purpose of this is to locate which coastal parts suffer from erosion and in what magnitude, and in which deposition is identified.

3.2 DEFINITIONS OF GEOMORPHOLOGICAL TERMS OF THE COASTAL ZONE

Beach: The area of accumulated sand, stone or gravel deposited along a shore by the action of waves and tides. Beaches usually slope gently towards the body of water they border and have a concave shape. They extend landward from the low water line to the point where there is a distinct change in material (as in a line of vegetation) or in land features (as in a cliff) (The American Heritage, 2002.)

Cliffs: Steep slope of earth materials, that is nearly vertical and may be over hanging. Erosional cliffs form along shorelines where the most extensive erosion takes place at the base of the slope. (Encyclopedia Britannica, 2008.)

Cliffs are common coastal features. They are formed by a combination of erosion and weathering, weathering working on the upper parts of the cliff and erosion wearing away the base of the cliff.

3.3. COASTAL CLIFF EROSION MODEL

The current cliff coast can be divided into three types (Figure 19):

• Type 1: Where sufficient coastal zone has been formed of 15-20m and erosion from the waves has stopped. In this type, the front of the cliff is not vertical, and is covered by vegetation.

• Type 2: Where small coastal zone has been formed (3-7m wide) and the normal waves do not affect the shoulder. Erosion of the cliff occurs only in cases of strong storm.

• Type 3: Where the sea undermines the cliff without forming beaches.

The relatively small energy situation of coasts causes slow-rhythm coastal transport. The erosion of the cliffs does not follow constant rates and the coast passes periodically from categories 1 and 2. When it is in category 1, the under digging of the cliff causes collapses and accumulation of material in the form of boulders at the base of the cliff. The waves are eroding these materials, evacuate the aluminous material and sand is added to the coast creating beach. The coast switches to category 2. Then the cliff has the smallest degree of erosion, because it is protected from the waves. Progressively the sand is removed by the waves and the system moves to category 1 again. The transition from one category to another is a process that takes time, more than a decade. The quantity of the remaining sand from the erosion has great diversity because the eroded formations have local variations and side transitions (Sirides, 1990). So it is possible for a capable deposition of sand to shape in some place and create a category 3 coast. The coast is relatively stable but gradually loses its balance with the rise of sea level and switches in the previous categories.

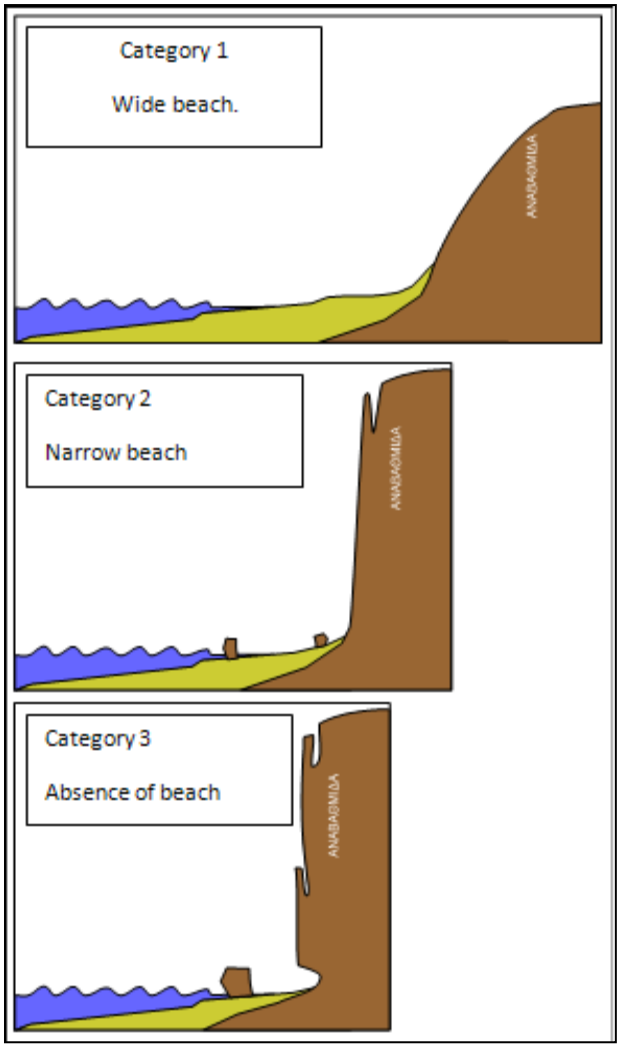

Figure 19 Cliff coast model with the 3 categories. (Albanakis, 2004)

This process within the Holocene, since the infiltration of the sea 8000 years ago (Chronis, 1986; Albanakis, 2004), is likely to erode the coastal cliffs and press the coast to recede several hundred meters. The annual rates of erosion today are of 0.1m/y.

3.4 DATA AND METHODOLOGY

3.4.1 AVAILABLE DATA

Landsat images are an important tool in remote sensing. Their resolutions of some meters, as well as their easy and costless access, render them suitable for the follow-up and the study of changes in an area. (Sabyasachi & Amit, 2011; Tucker, et. al 2004; Ding, et al, 2007).

The acquisition of the images for the study area was made with the earth explorer www.earthexplorer.usgs.gov and their further process includes the software Arc Map from ESRI, ENVI from ITT and the DSAS toolbar which is an ArcMap extension. For the definition of coastline changes, of the study area of Kassandra peninsula, Landsat multispectral images of the following dates were used: Landsat MSS of 16th of July 1977, Landsat 5TM of 19th of May 1985, 19th of July 2007 and 2nd of October 2011.

The first step is to extract images of the study area. Further through the process of the Landsat images, the NDWI (Normalized Difference Water Index) and NDVI (Normalized Difference Vegetation Index) are calculated. The final step is the calculation and the estimation of the coastal changes of the study area through the use of the DSAS (Digital Shoreline Analysis System) toolbar, which is an ArcMap extension.

3.4.2 NDWI

The Landsat images were obtained through USGS's site, www.earthexlorer.usgs.gov. After you have created a personal account, you locate the area of interest which is obtained either through coordinates or through map searching, defining at the same time the specific dates of interest. After that you choose the satellite and finally, out of the results that come up for the study area we defined, the corresponding dates of interest and the chosen satellite we make the final choice of the images that interest us.

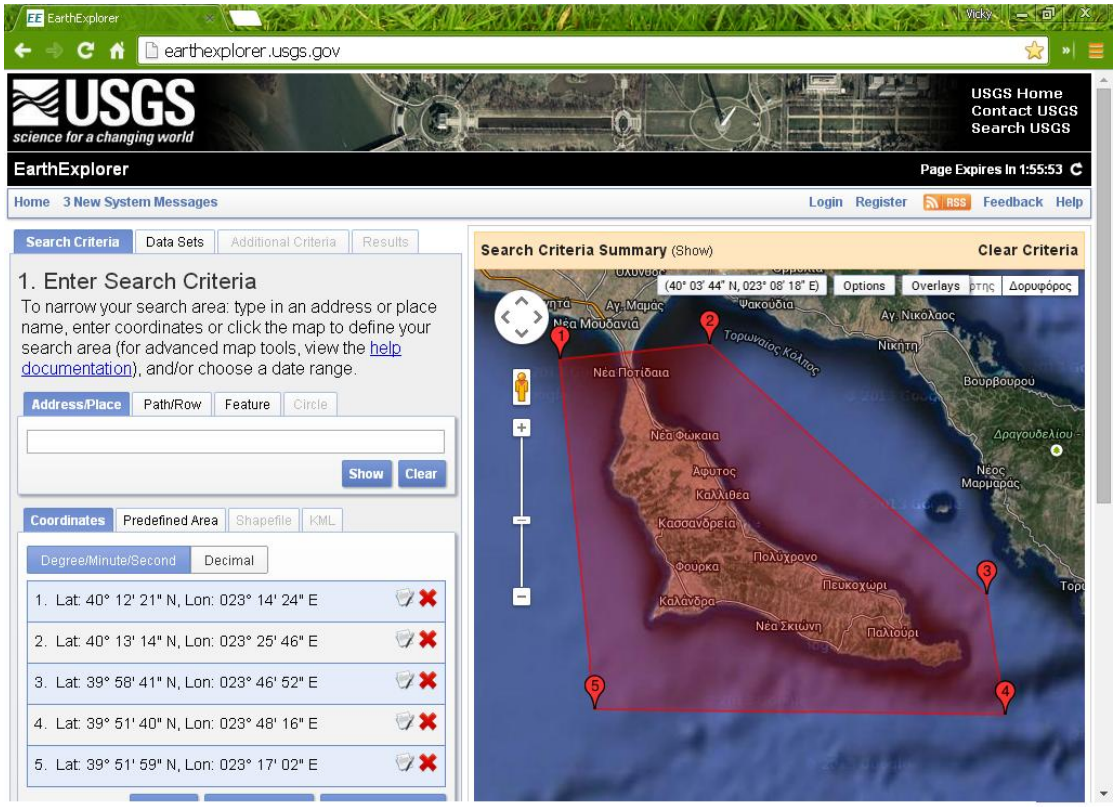

Figure 20 Earth Explorer site www.earthexplorer.usgs.gov .

The NDWI is calculated for the images that have been chosen according to (McFeeters 1996):

NDWI= (Green-NIR) / (Green+NIR)

Every Landsat image consists of certain spectral zones.

- The Landsat 2 MSS consists of 4 spectral zones where the green corresponds to the 2nd spectral zone and the near infrared to the 4th zone (NIR).
- The Landsat 5 TM consists of 7 spectral zones where the Green corresponds to the 2nd zone and the NIR (Near Infrared) to the 4th zone.

This index is designed to (1) maximize reflectance of water by using green wavelengths; (2) minimize the low reflectance of NIR by water features; and (3) take

advantage of the high reflectance of NIR by vegetation and soil features. As a result, water features have positive values and thus are enhanced, while vegetation and soil usually have zero or negative values and therefore are suppressed (McFeeters 1996, Hanqiu, 2006). The calculation of the NDWI is achieved with the LOC-Water wizard though the ENVI software.

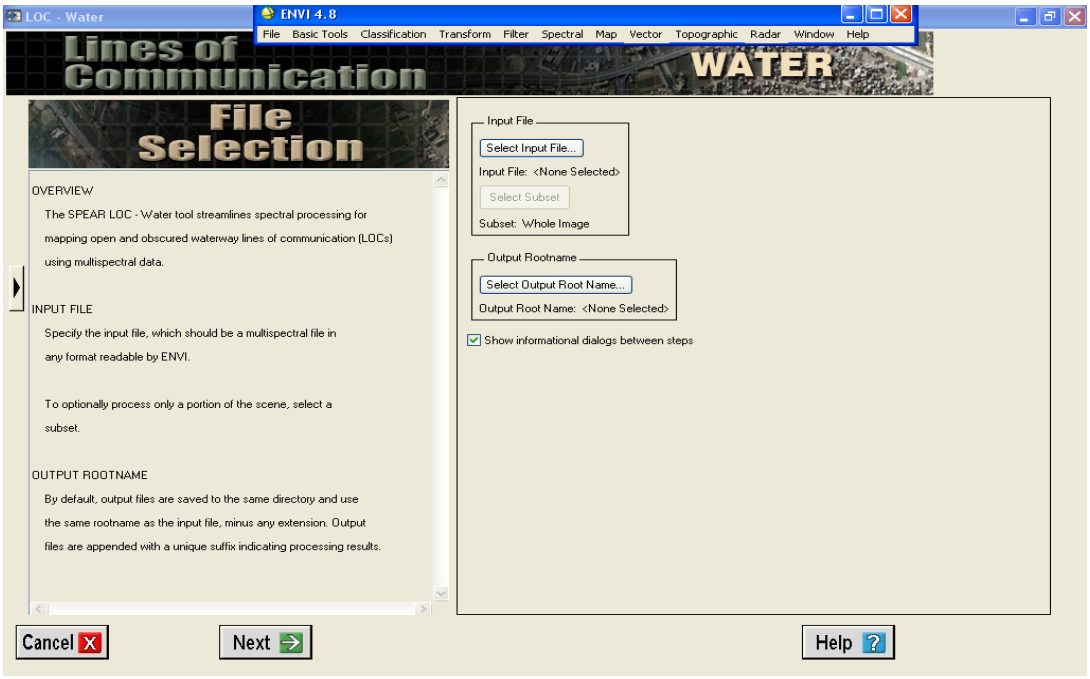

Figure 21 Loc – Water wizard through ENVI software in order to create an NDWI image of the area of interest.

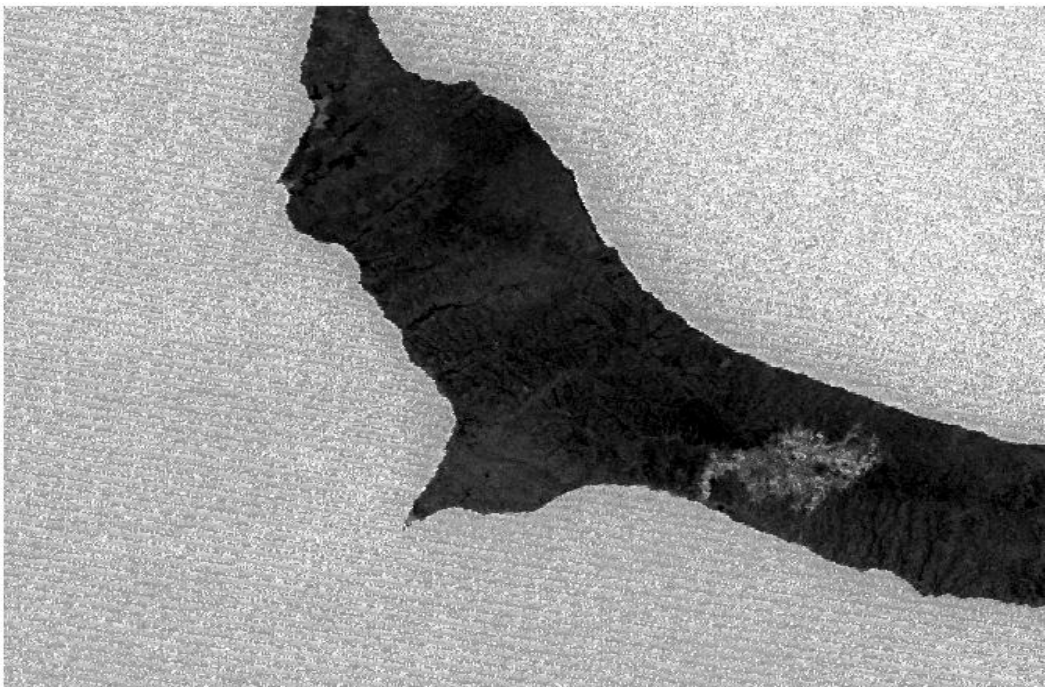

Figure 22 NDWI image of Kassandra peninsula for the year 1977.

In the central part of the peninsula is an area affected by fire (Figure 22), very close to the date of the image, therefore the reflectance in all bands including the infrared part of the spectral, is very low. (The reflectance of the water in the infrared is also very low, therefore this area is expected to be classified as water and has to be corrected manually.)

In the next phase of the process of the images, the Auto Threshold command through Arc Map is applied, on the NDWI processed image. This command separates the image into two parts, in land and sea.

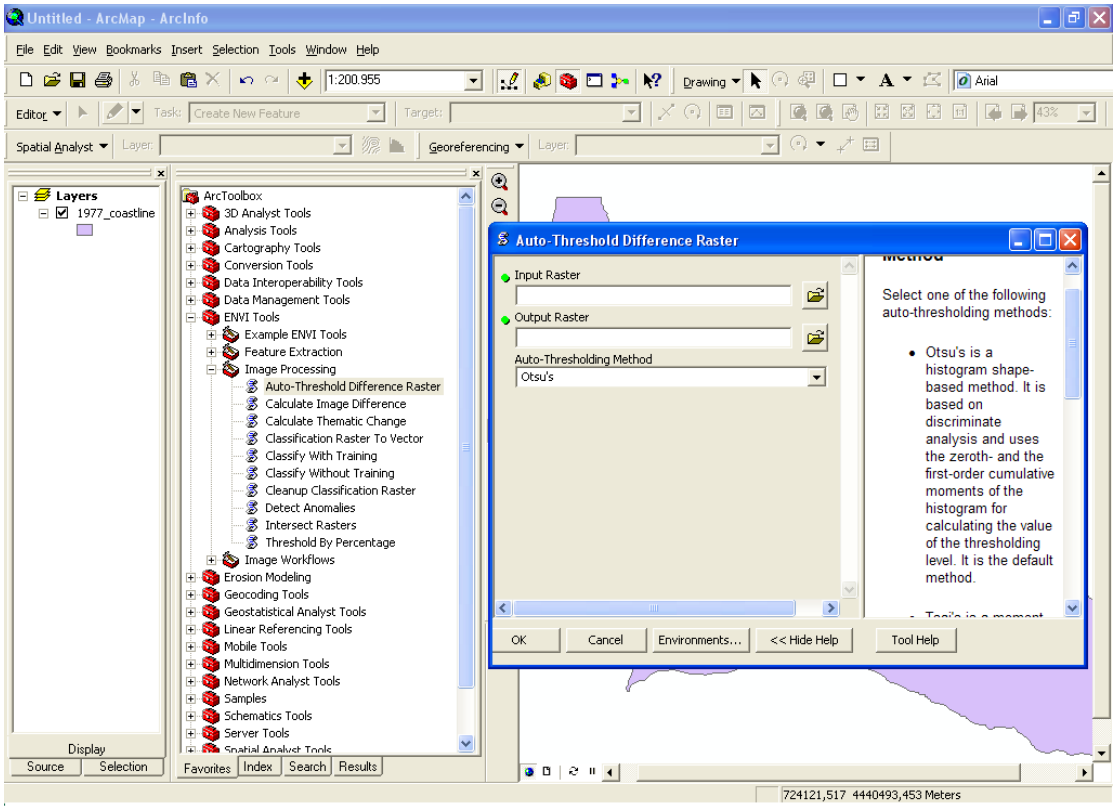

Figure 23 Path for auto threshold's tool in Arc Map 9.3 environment

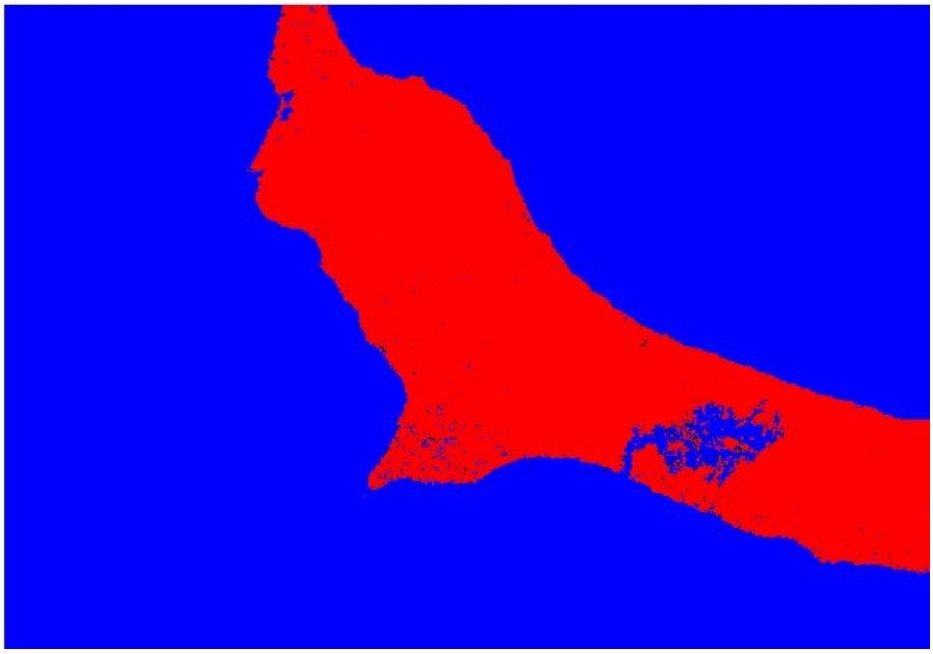

Figure 24 Image result after Kittler's threshold for the year 1977.

Recent bush and forest fires are classified by the algorithm (NDWI) as water and have to be corrected manually (Figure 24).

Further the command «raster to polygon» is applied on the achieve which comes out, so as a polyline to be created between land and water.

Figure 25 Image result after «raster to polygon» convert of the year 1977.

Finally the study area is chosen through the command “clip” of the Arc Map, so as to obtain the final coastline in which we are interested.

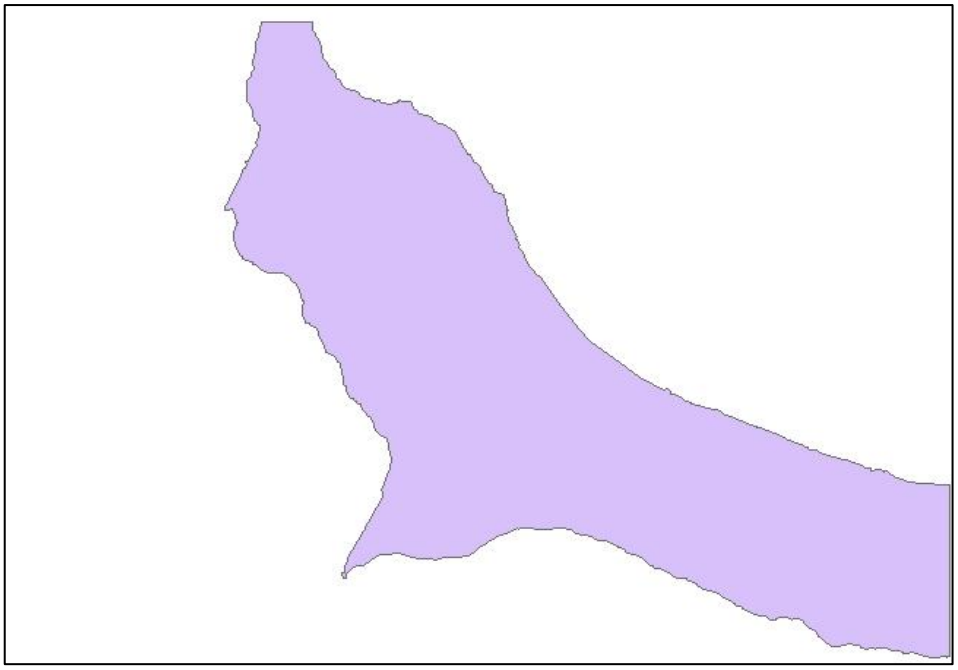

Figure 26 Final polygon of the coastline of Kassandra peninsula of the year 1977.

The same procedure is followed for the all of the dates.

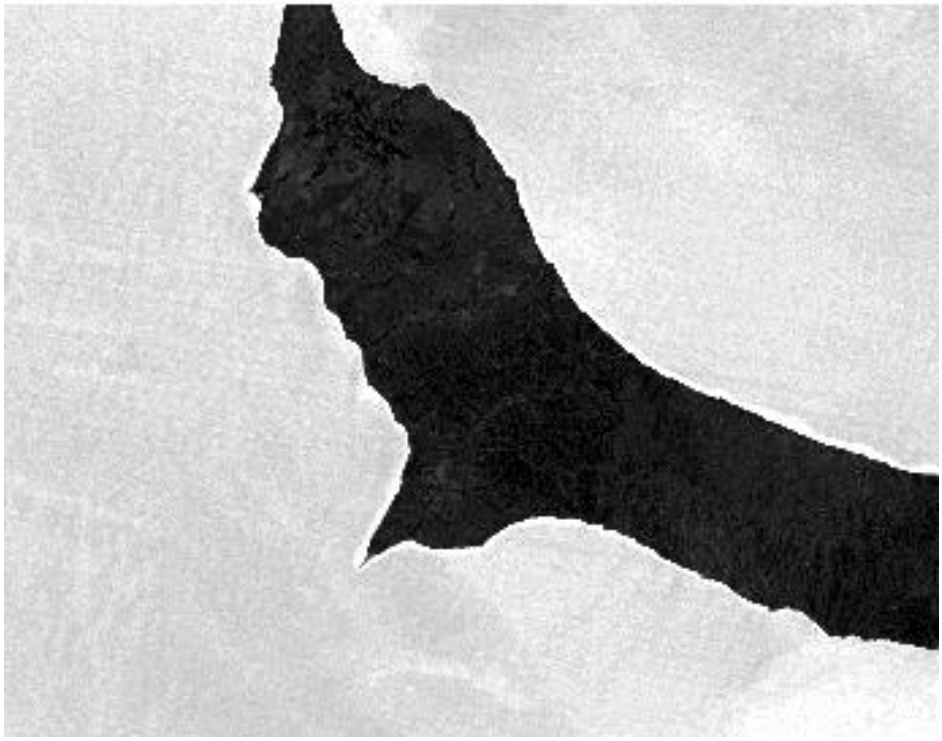

Figure 27 NDWI of Kassandra peninsula of the year 1985.

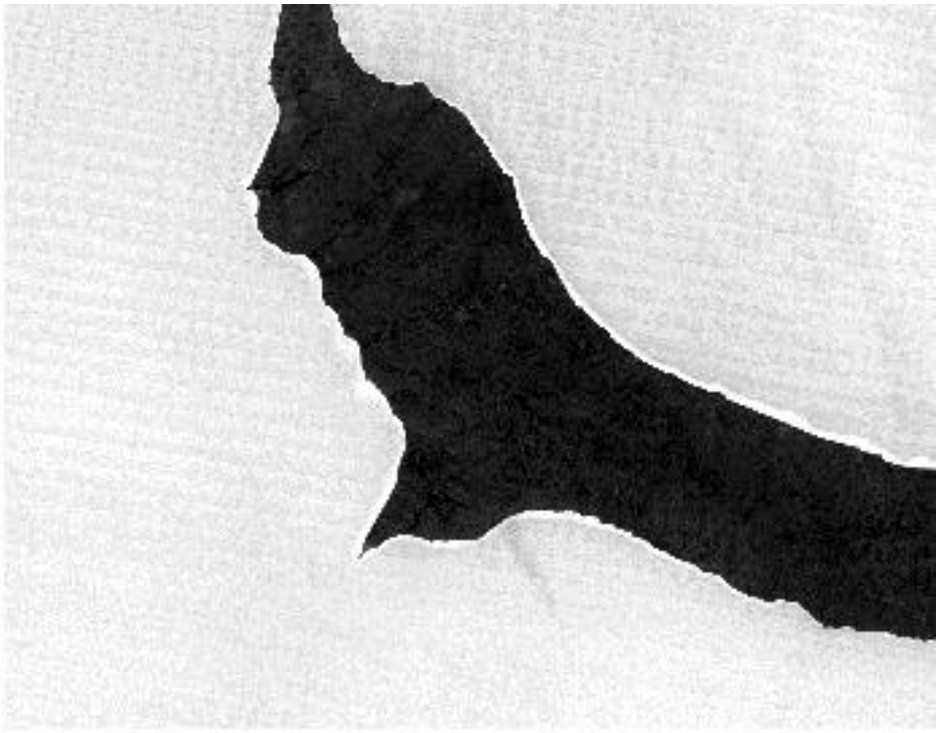

Figure 28 NDWI of Kassandra peninsula of the year 2007.

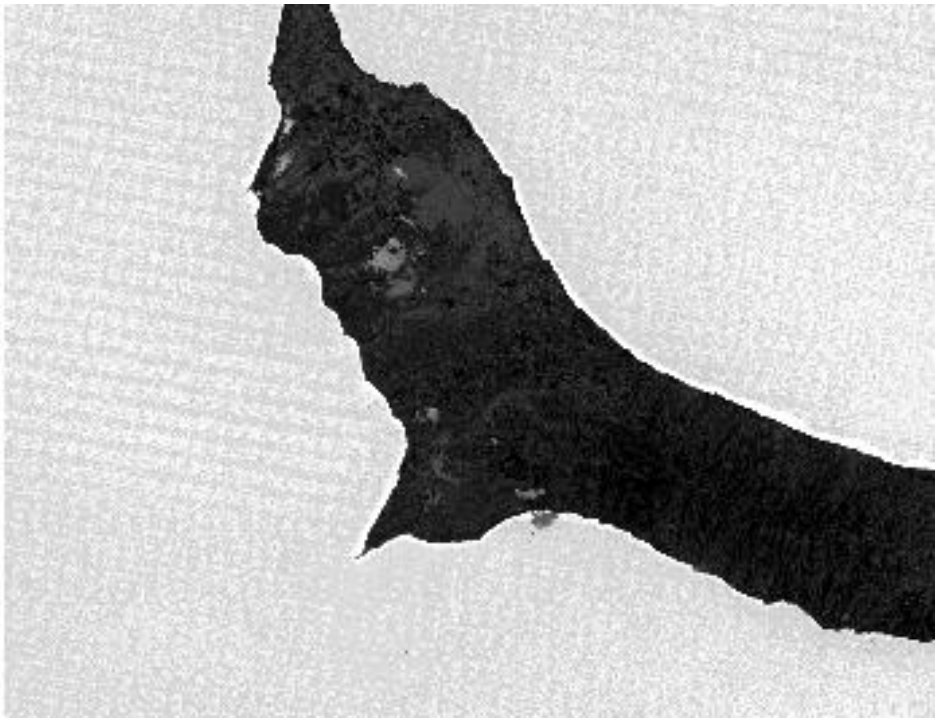

Figure 29 NDWI of Kassandra peninsula of the year 2011.

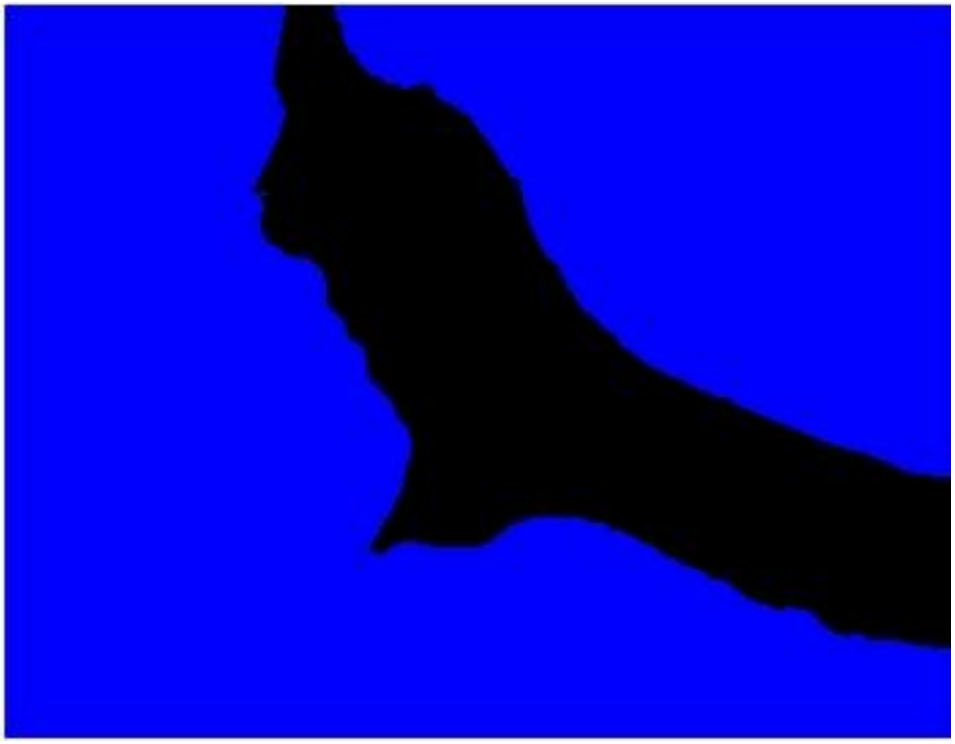

Figure 30 Image result after Otsu's threshold of the year 1985.

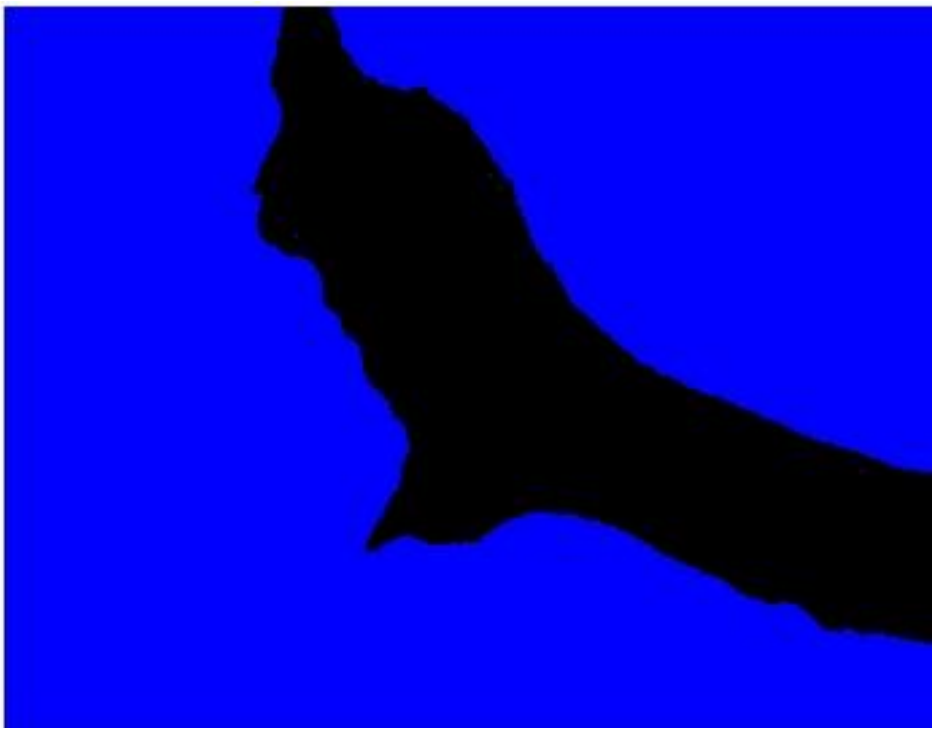

Figure 31 Image result after Otsu's threshold of the year 2007.

Figure 32 Image result after Otsu's threshold of the year 2011.

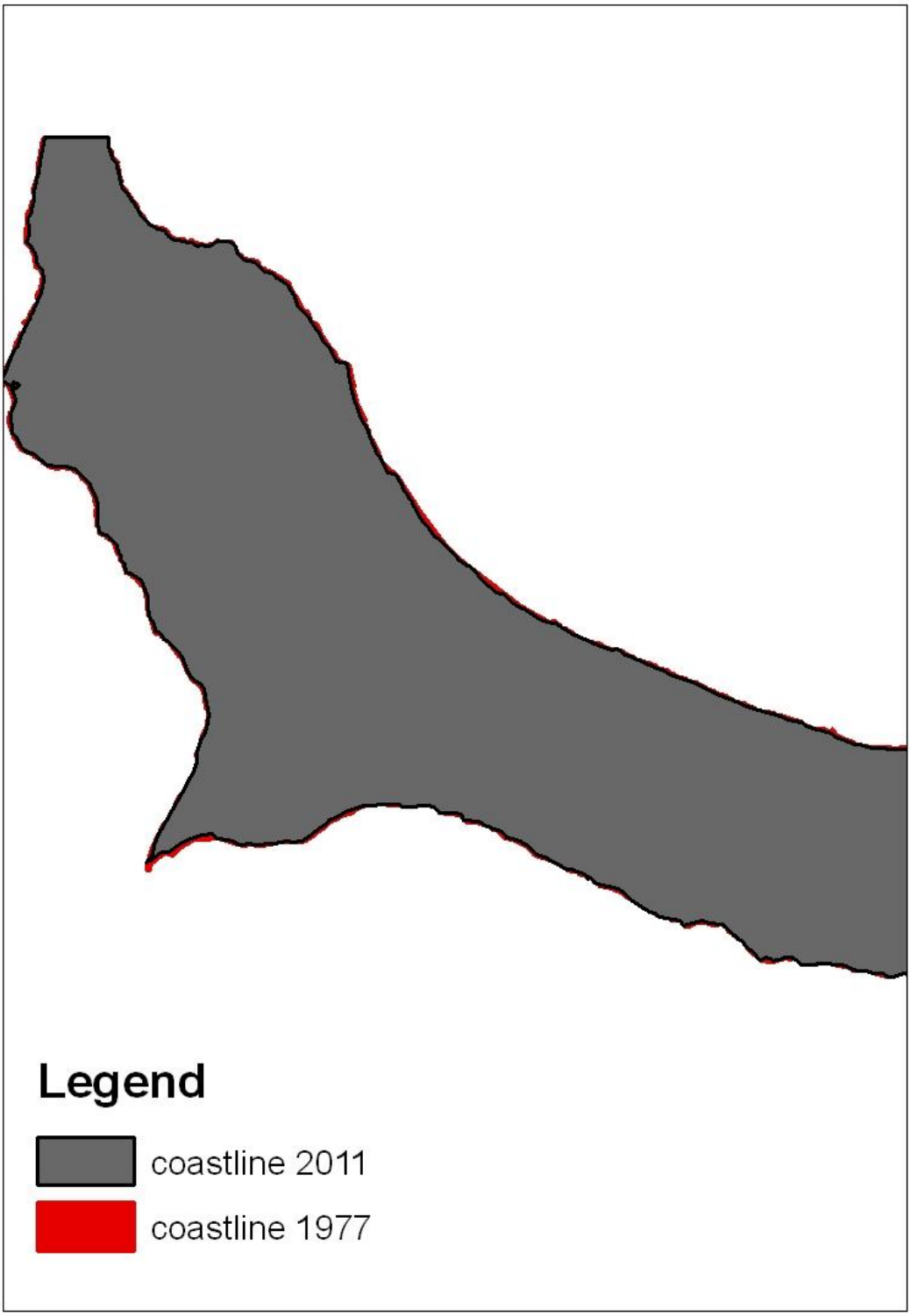

Figure 33 Coastlines of 1977 and 2011 of the study area.

3.4.3 NDVI

The physical NDVI values are between -0.1 and 0.92, where higher values indicate denser and healthier (higher green density) vegetation. NDVI values of 0.1 and below, for instance, typically correspond to areas with little to no vegetation (rocks, ice, and desert). Moderate values (around 0.2 and 0.3) correspond to shrub and grasslands and high values (0.5 and above) typically correspond to dense vegetation like rainforests. In the legend of the image viewer, the NDVI is not given as physical value, but as a qualitative indicator.

Table 17 NDVI density and physical values

Vegetation health & density	Physical NDVI value
Very Dense	0.72 till 0.92
Dense	0.42 till 0.72
Normal	0.22 till 0.42
Sparse	0.12 till 0.22
Very Sparse	-0.10 till 0.12

In order to calculate the normalized difference vegetation index (NDVI) we worked on ENVI software for each Landsat image for the years 1977, 1985, 2007, 2011.

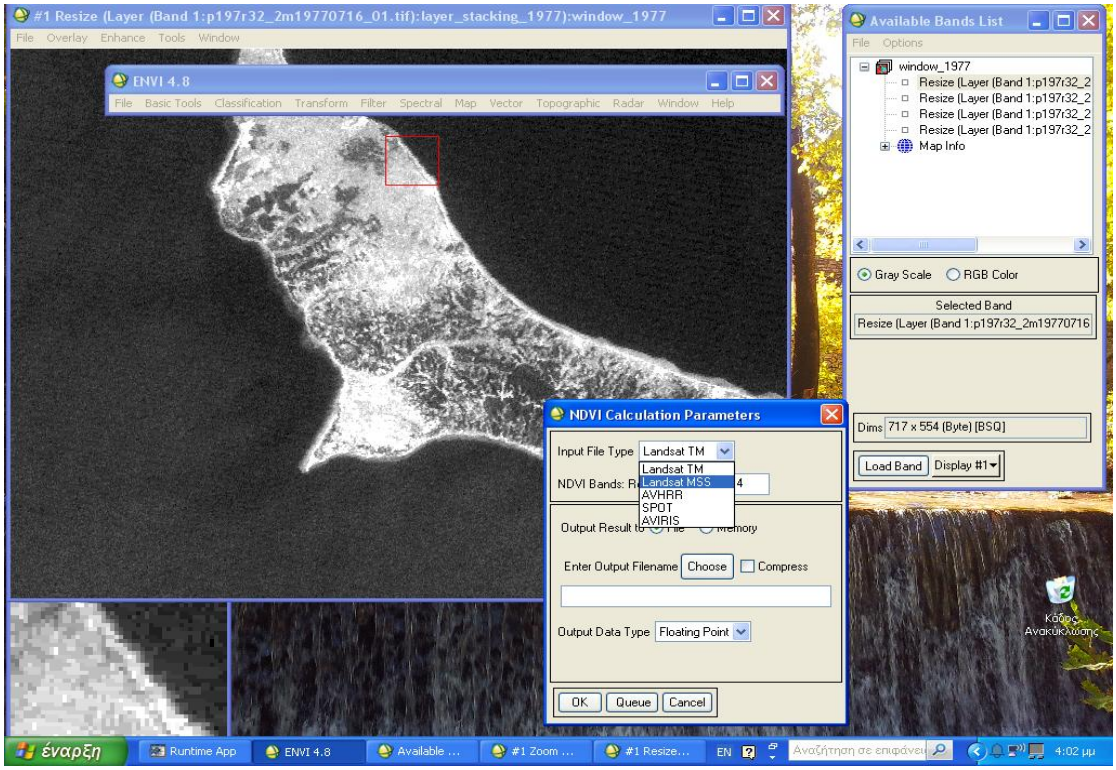

Figure 34 Working on Envi software with MSS Landsat image of 1977

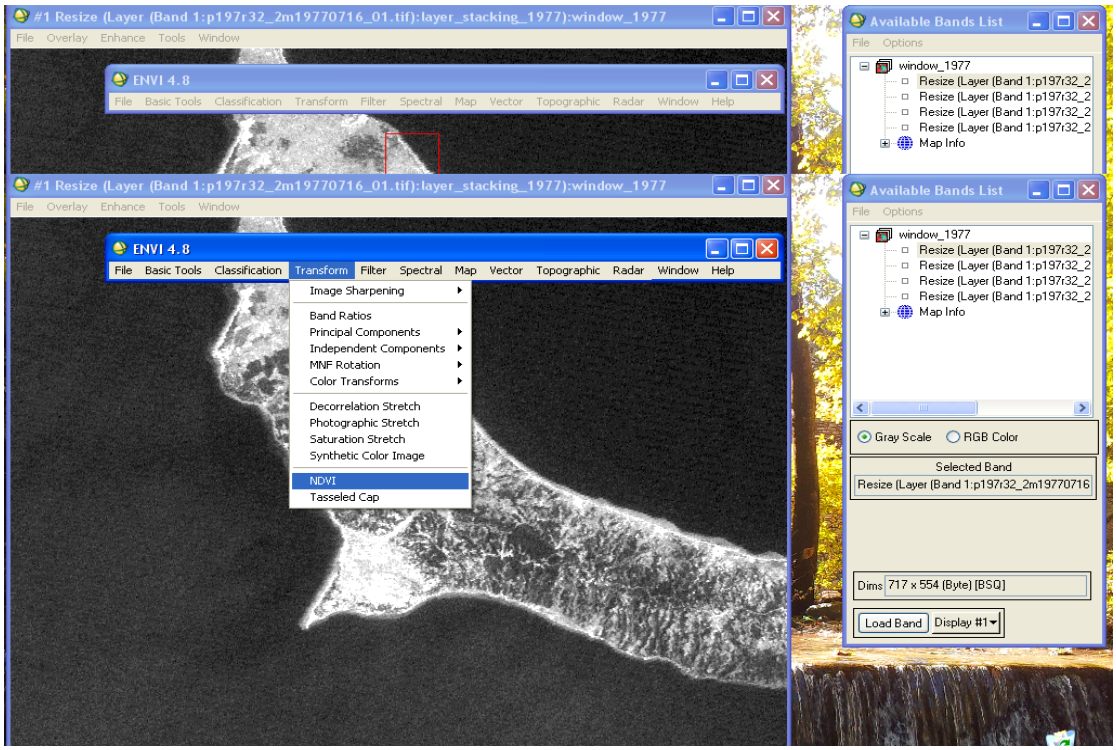

Figure 35 Calculating NDVI with ENVI software

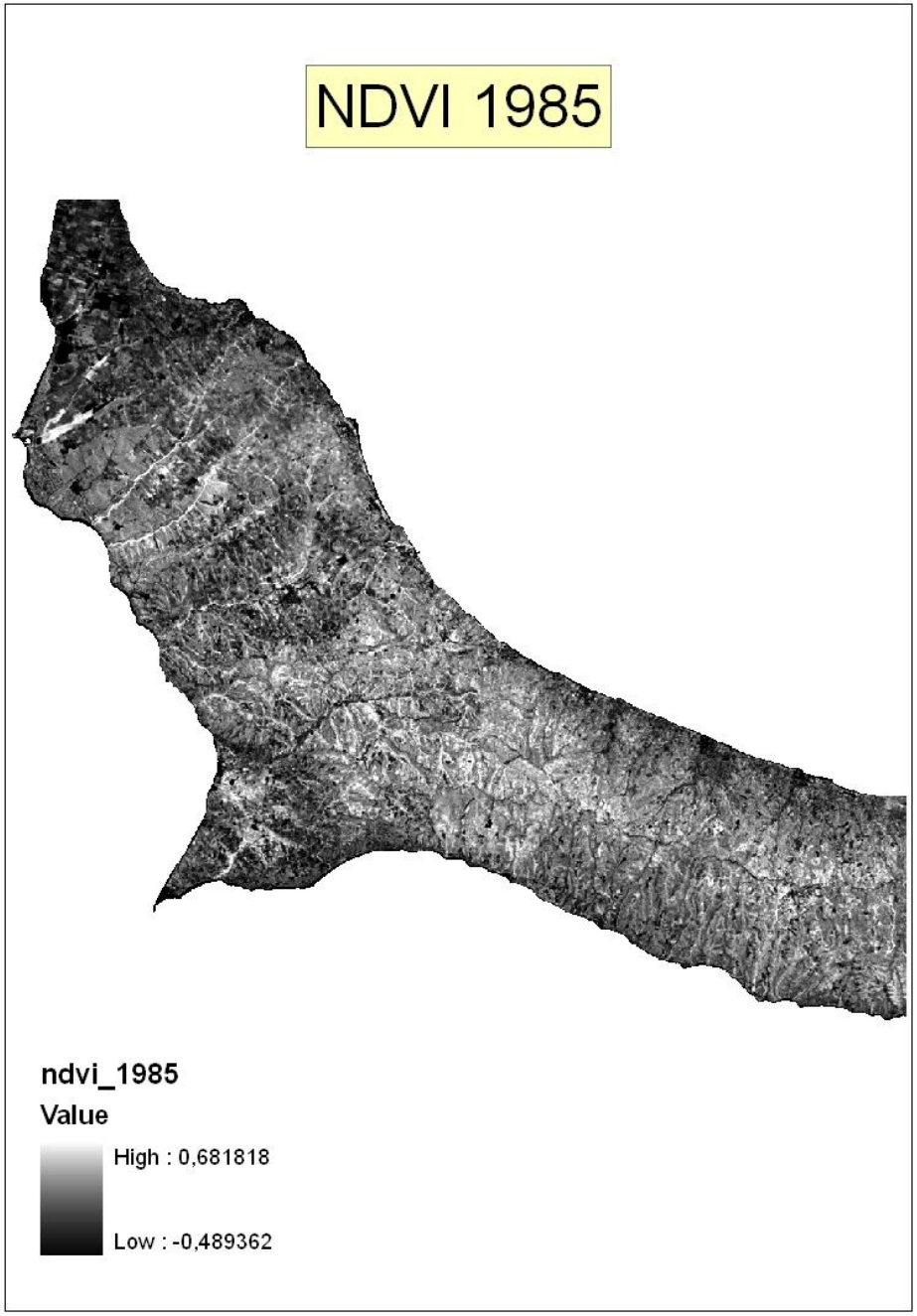

Figure 36 NDVI value with scale from -1 to 1 exported from ENVI for the years 1977 and 1985

Figure 37 NDVI value with scale from -1 to 1 exported from ENVI for the years 2007 and 2011.

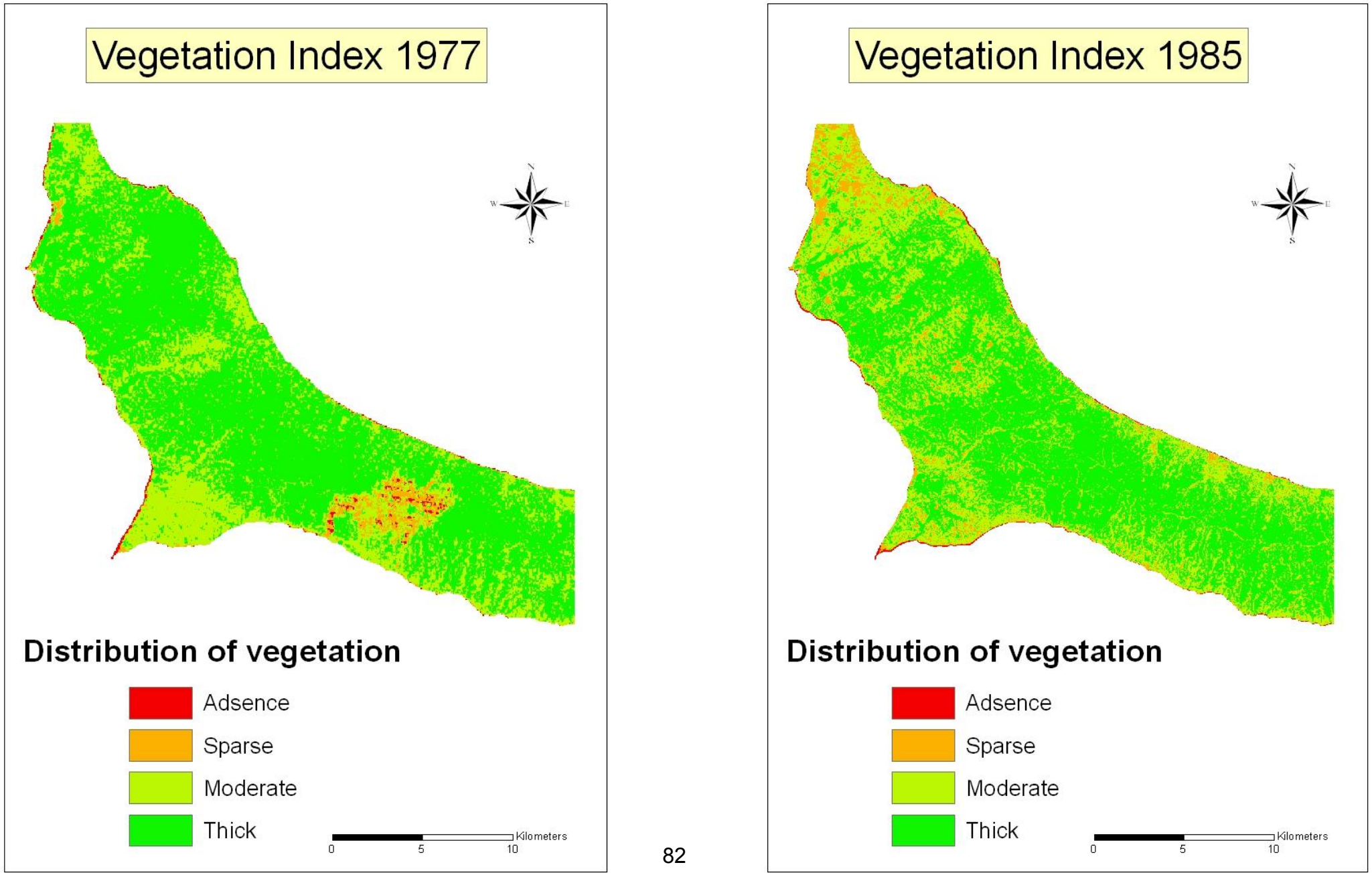

Figure 38 NDVI index of the years 1977 and 1985.

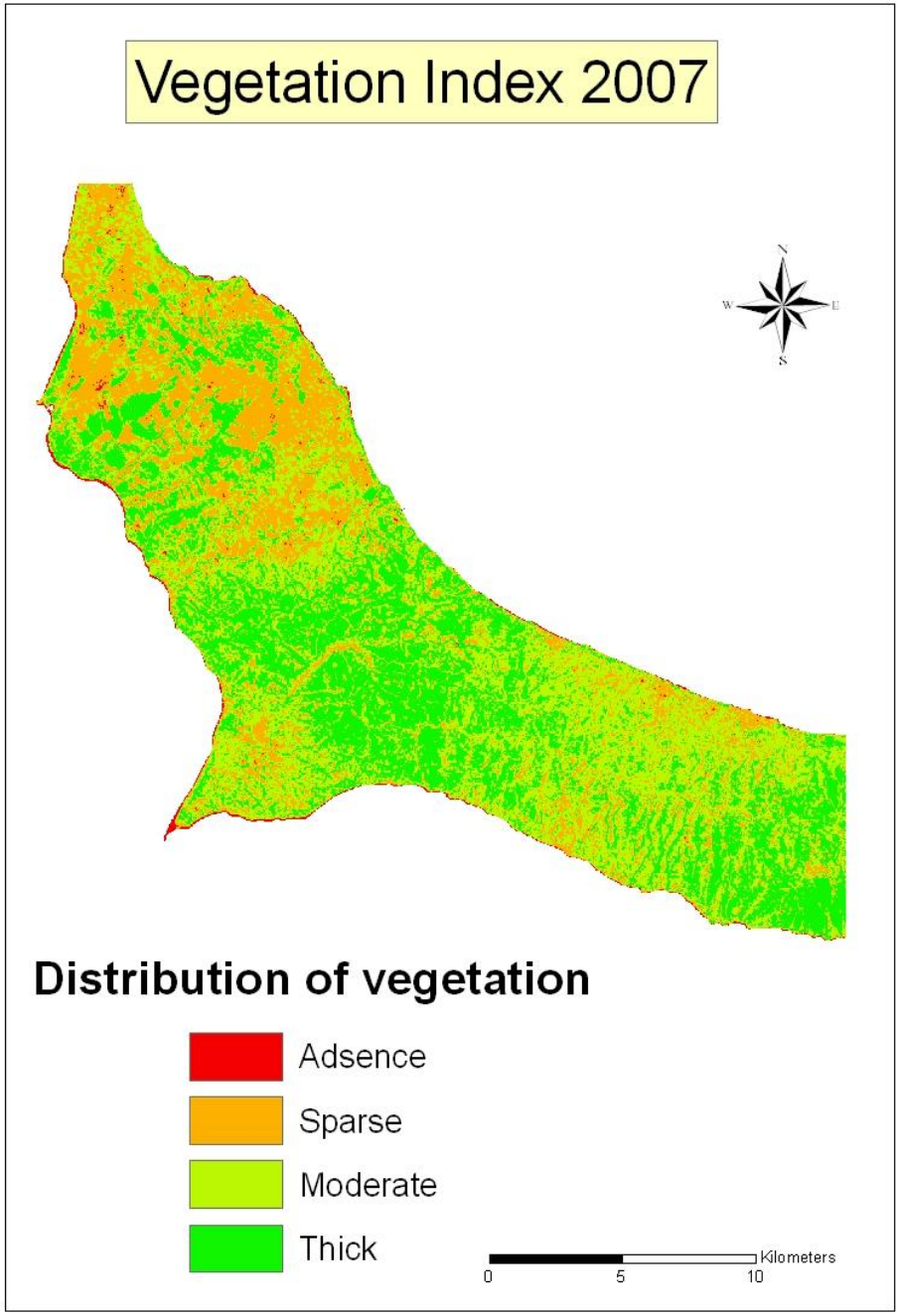

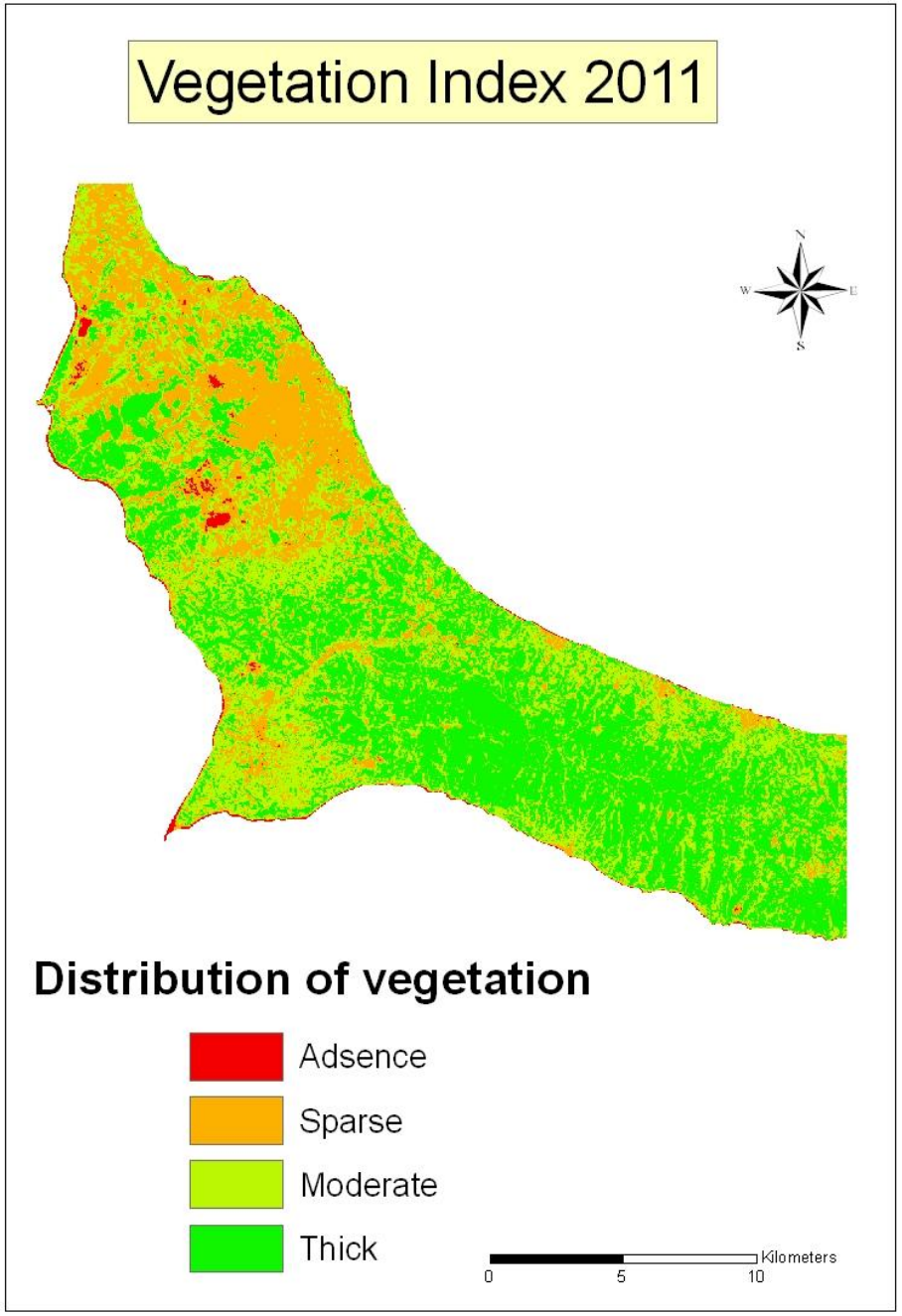

Figure 39 NDVI index of the years 2007 and 2011.

Table 18 Overview table of the area in km^2 occupied by each NDVI range for the years 1977, 1985, 2007, 2011.

GRIDCODE	NDVI	Range	Area km^2 1977	Area km^2 1985	Area km^2 2007	Area km^2 2011
1	Very Sparse	-0,10 till 0,12	0,092132	6,661311	41,359086	54,668846
2	Sparse	0,12 till 0,22	12,68349	24,715557	85,61066	54,081847
3	Normal	0,22 till 0,42	191,509789	222,424884	159,321001	157,263958
4	Dense	0,42 till 0,72	115,85913	65,564342	33,369995	53,633313

3.4.4 DSAS (Digital Shoreline Analysis System)

The Digital Shoreline Analysis System (DSAS) is a freely available software application that works within the Environmental Systems Research Institute (ESRI) Geographic Information System (ArcGIS) software. DSAS computes rate-of-change statistics for a time series of shoreline vector data. Version 4.3 was released in April 2012 and is only compatible with ArcGIS v.10.

On this thesis, we will make a brief reference on the software and the necessary inputs. For more details, you can download the DSAS manual from the official site http://woodshole.er.usgs.gov/project-pages/DSAS/.

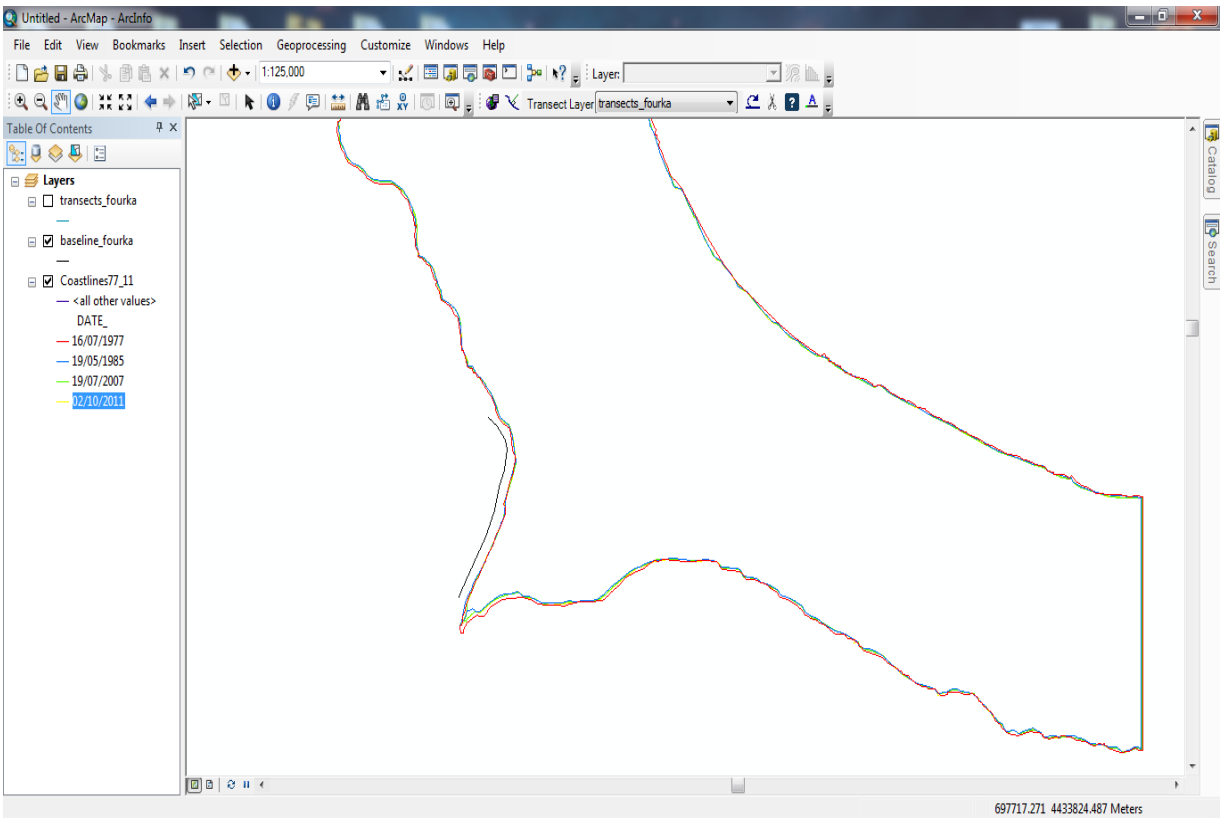

Figure 40 DSAS toolbar in Arc Map 10 environment.

3.4.4.1 DSAS TOOLBAR

This section provides a quick reference and explanation for each button on the DSAS toolbar interface.

Table 19 Explanation table for each button on the DSAS toolbar interface.(Himmelstoss, E.A. 2009)

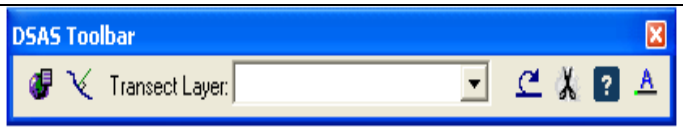	**Set/Edit default parameters** specifies file names for the baseline and shoreline inputs and other settings, such as transect spacing
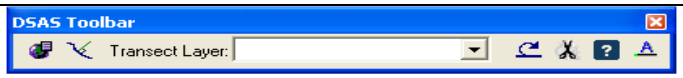	**Cast transects** generates a new (or overwrites an existing) transect feature class based on the user-specified default parameters.
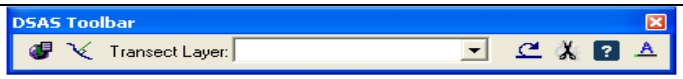	The drop-down menu lists all recognized transect files added to the active ArcMap project.
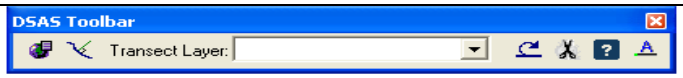	**Calculate statistics** launches a dialog box populated with a selectable list of change-rate statistics to be calculated.
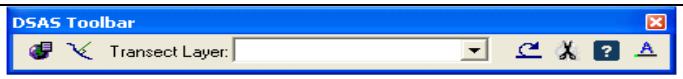	**Clip transects to SCE** launches a dialog box providing users with the option to generate a copy of the specified transect file that is clipped to the shoreline change envelope (SCE) or the maximum distance between all shorelines
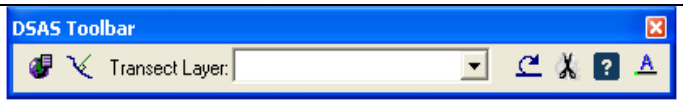	Launches the **DSAS help** feature.
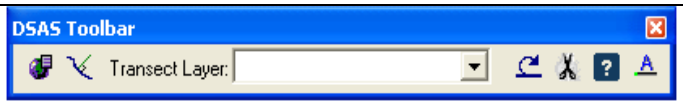	**About DSAS** provides information about the software, including the version number.

3.4.4.2 REQUIRED INPUTS

This section describes the data requirements, including file format and field attributes that are necessary for DSAS to properly recognize and compute rate-of-change statistics. It includes instruction on how to produce the required files and field elements.

Geodatabase

All DSAS input data must be managed within a personal geodatabase, which also serves as the storage location for the program-generated transect feature class and related statistical output tables.

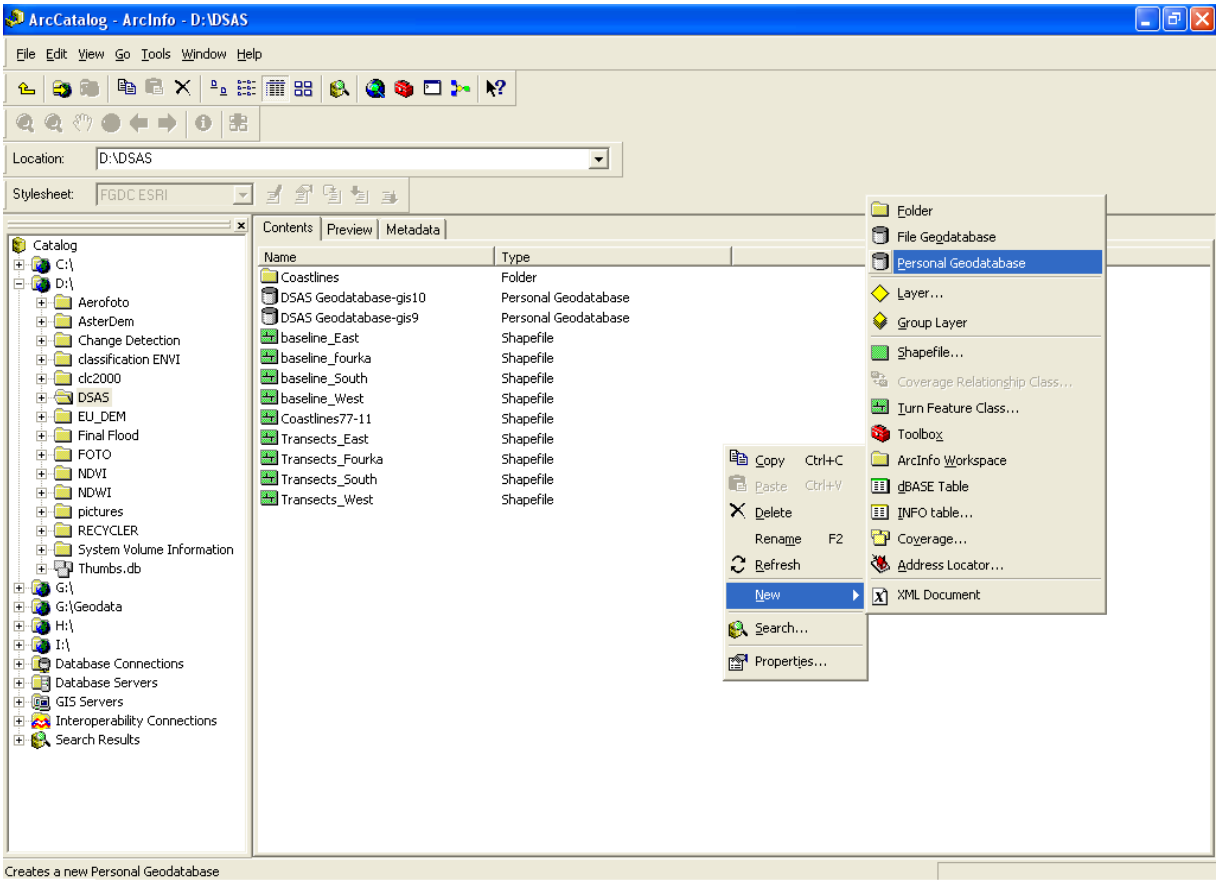

Figure 41 Creating a new personal geodatabase in Arc Catalog. (Himmelstoss, E.A. 2009)

Shorelines

All shoreline data must reside in a single feature class within a personal geodatabase. If the shorelines are collected as shapefiles, they must be appended to a single file and then imported into a geodatabase within ArcCatalog. DSAS also requires that the feature class be in meter units in a projected coordinate system and meet the attribute field requirements.

Field name	Data type		
OBJECTID	Object ID	Auto-generated	
SHAPE	Geometry	Auto-generated	
SHAPE_Length	Double	Auto-generated	
DATE_	Text	User-created	Length = 10 or Length = 22
UNCERTAINTY	Any numeric field	User- created	

DATE_	This field is required but not name-specific (meaning you can use something other than "Date_" as the field name). A length of 10 is used for shoreline change spanning days, months or years, and dates are set up as mm/dd/yyyy. In the sample data provided, the default when month and day are unknown is July 1st (07/01). A length of 22 is used for shoreline data spanning different hours within the same day and will have dates set up as mm/dd/yyyy hh:mm:ss (using either 24-hour time or AM/PM).
UNCERTAINTY	This field is required but not name-specific (meaning you can use something other than "Uncertainty" as the field name). The calculated rates of change provided by DSAS are only as reliable as the measurement and sampling errors that the user must account for when compiling each shoreline position (Anders and Byrnes, 1991; Crowell and others, 1991; Thieler and Danforth, 1994; and Moore, 2000). Different measurement uncertainties can be provided for each shoreline segment. The uncertainty value should ideally account both for positional uncertainties associated with natural influences over the shoreline position (wind, waves, tides) and measurement uncertainties (for example, digitization or global-positioning-system errors). For any shoreline vectors assigned a value of zero or null, DSAS will use the value specified by the user in the Set Default parameters window (des

Figure 42 Shoreline attribute field requirements. (**Himmelstoss, E.A. 2009**)

Baseline

DSAS uses a measurement baseline method (Leatherman and Clow, 1983) to calculate rate-of-change statistics for a time series of shorelines. The baseline is constructed by the user and serves as the starting point for all transects cast by the DSAS application. The transects intersect each shoreline at the measurement points used to calculate shoreline-change rates.

Field name	Data type		
OBJECTID	Object ID	Auto-generated	Required
SHAPE (alias: Shape)	Geometry	Auto-generated	Required
SHAPE_Length (alias: Shape_Leng)	Double	Auto-generated	Required
ID	Long Integer	User-created	Required
Group	Long Integer	User-created	Optional
OFFshore	Short Integer	User-created	Optional
CastDir	Short Integer	User-created	Optional

ID	This field is required by DSAS and the name is specific. DSAS uses this value to determine the ordering sequence of transects when the baseline feature class contains multiple segments. If you create this attribute field prior to drawing baseline segments, the ID value defaults to zero. You must edit the attribute table and designate a unique ID value for each segment of the baseline. DSAS will not cast transects along baseline segments where the ID value is zero.
Group	This optional field can be used for data-management purposes to aggregate transects on the basis of physical variations alongshore (for example, tidal inlets, change in coastal type, or hard stabilization features). Providing a group value will not affect any of the change statistics provided within DSAS, but if used, a group field will be added to the transect feature class to facilitate later sorting and analysis of the data.
OFFshore	This field is required if a combination of onshore and offshore baselines is used. The name of this field is specific, meaning that the field must be called OFFshore and is case-sensitive. A value of "0" indicates that the baseline segment is onshore or landward of the input shorelines. A value of "1" indicates that the baseline is offshore or seaward of the input shorelines.
CastDir	This field is required in conjunction with OFFshore. The name of this field is specific, meaning the field must be called CastDir, and case sensitive. A value of "0" will result in transects being cast to the left of the baselineon the basis of the segment flow (flow from the start vertex of the line segment to the last vertex that the ends line segment). Similarly, a value of 1 will result in transects being cast towards the right of the baseline on the basis of the flow direction (**fig. 14**).

Figure 43 Baseline attribute field requirements (Himmelstoss, E.A. 2009)

3.4.4.3 DSAS Workflow

Once the required geodatabase and input-feature classes have been created or imported from shapefiles and all necessary feature classes have been added and properly attributed, the DSAS Application can be used within ArcMap to establish transect locations and calculate change statistics.

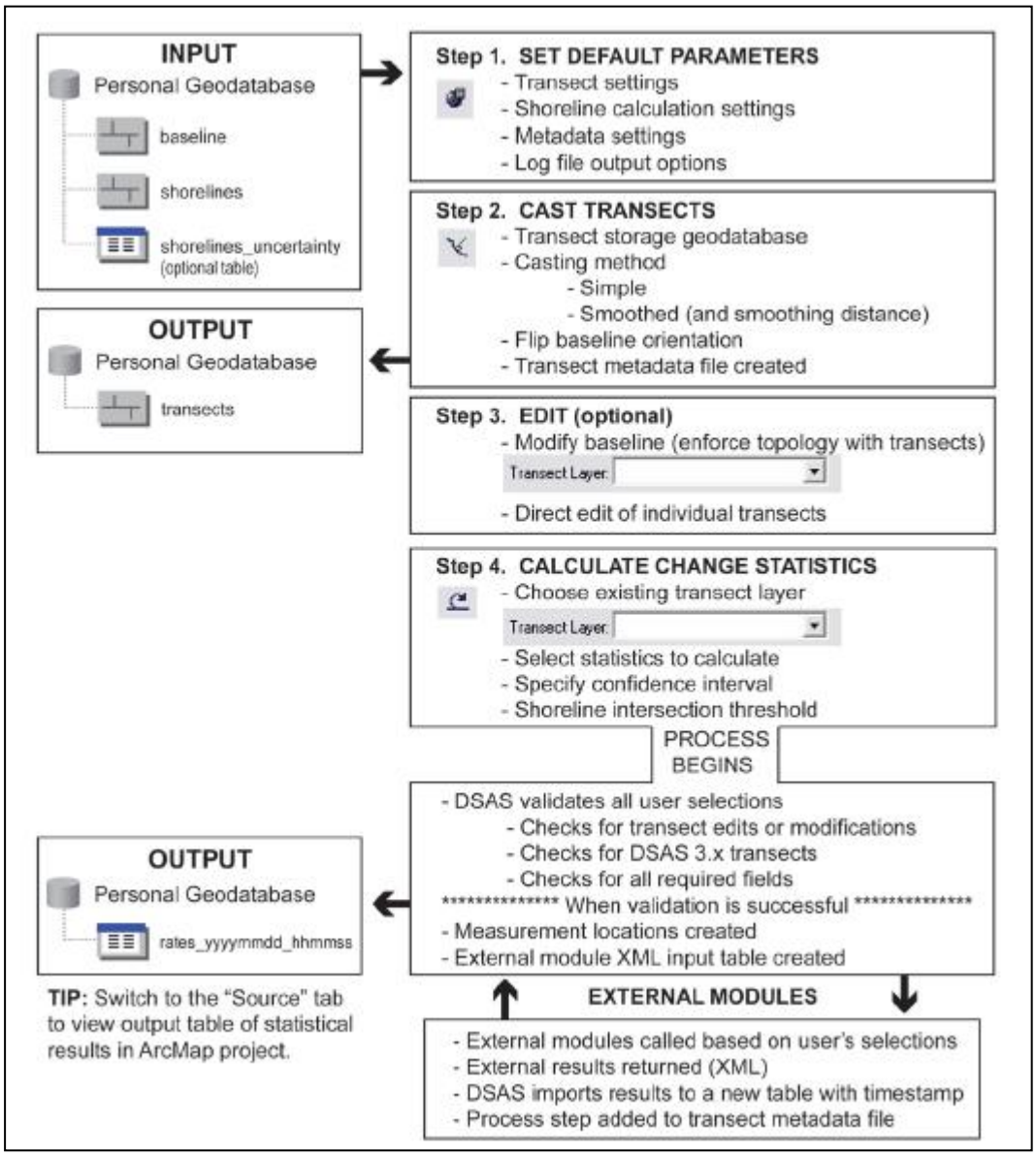

Figure 44 Diagram illustrating the steps necessary to establish transect locations and compute change-rate statistics by using the DSAS application. (Himmelstoss, E.A. 2009)

Set Default Parameters window

Begin the transect-generation process by selecting your preferred default settings in the Set Default Parameters window. This window can be accessed from the DSAS toolbar and contains three tabs: (1) Cast Transect Settings, (2) Shoreline Calculation Settings, and (3) Metadata Settings.

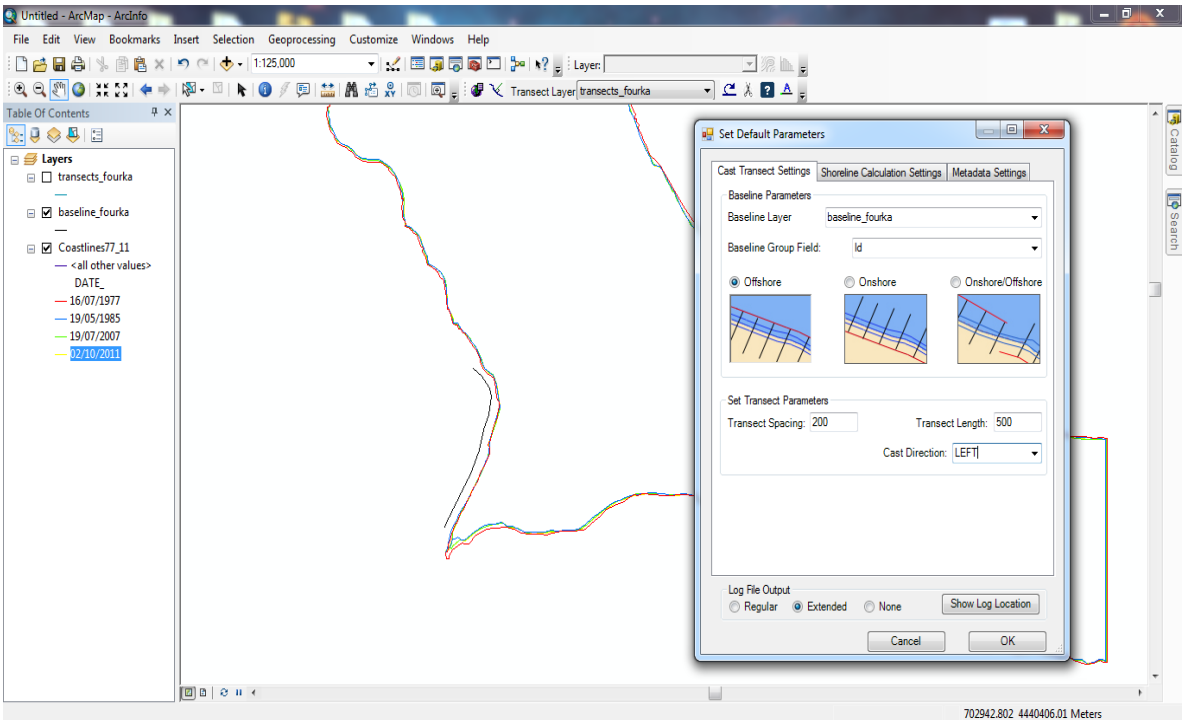

Figure 45 Screenshot showing the DSAS Set Default Parameters window and the Cast Transect Settings tab.

The Shoreline Calculation Settings tab is one of the three components of the default parameters. These settings specify the attribute fields containing the date and shoreline uncertainty values. The available options are described below.

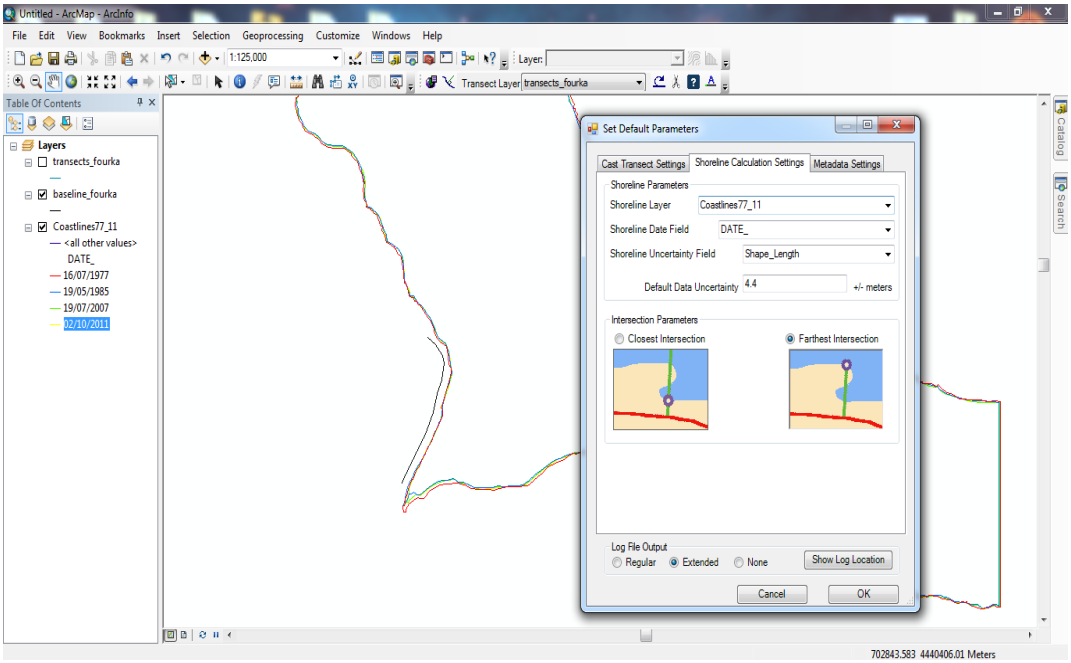

Figure 46 Screenshot showing the DSAS Set Default Parameters window and the Shoreline Calculation Settings tab.

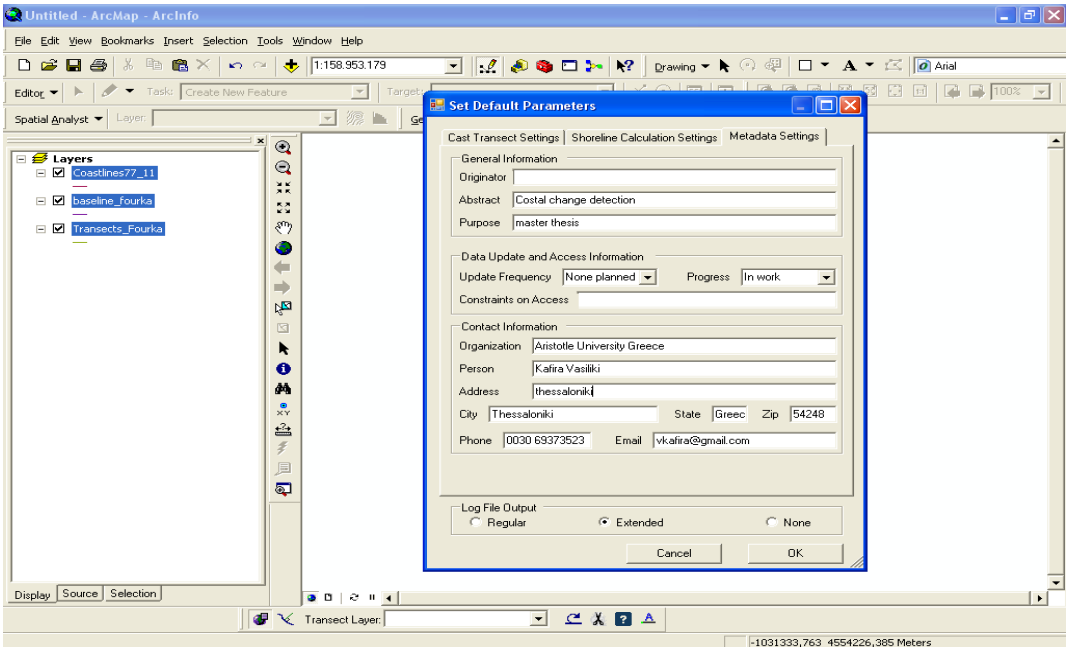

Figure 47 Screenshot showing the DSAS Set Default Parameters dialog box and the Metadata Settings tab.

Cast Transcects

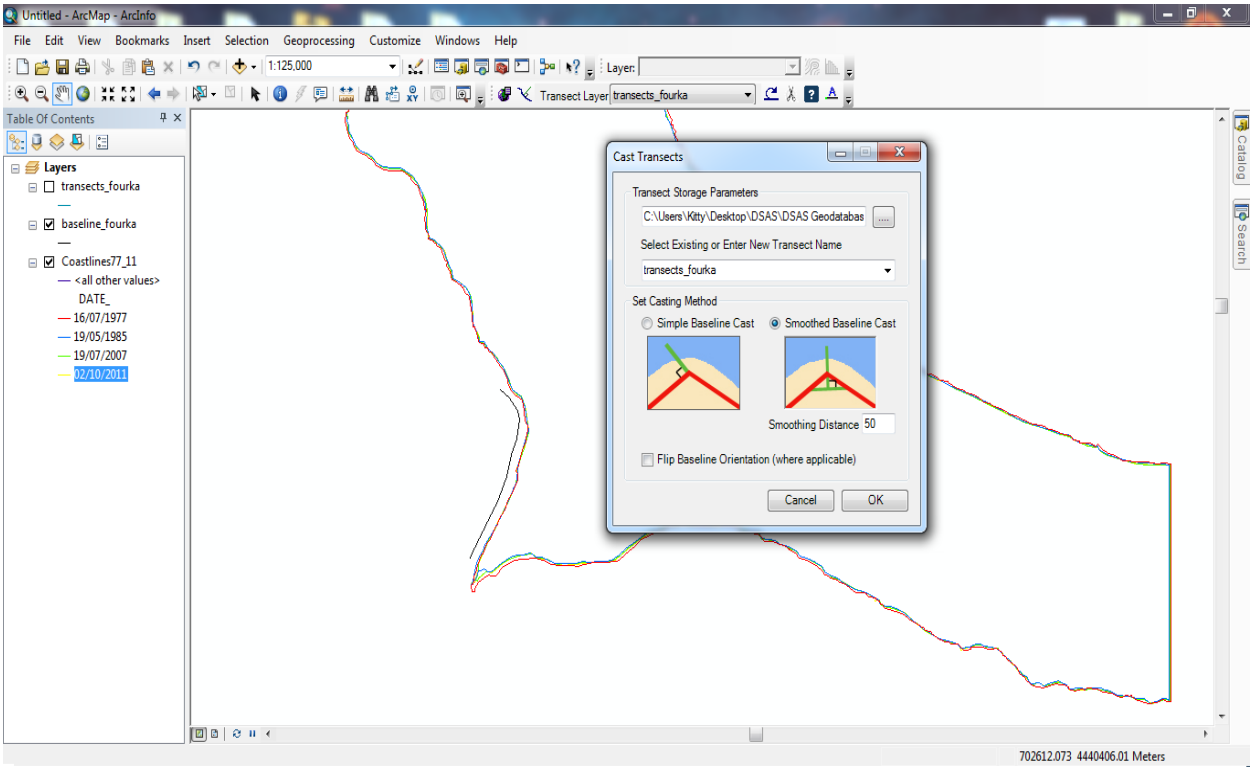

Figure 48 Screenshot showing the DSAS Cast Transects window.

Field name	Data type	Field purpose
OBJECTID (aliases: object identifier, OID, or FID)	Object ID	The object identification field is automatically created and maintained by ArcGIS. It establishes a unique ID for each row in the attribute table. This number is used by DSAS to relate all shoreline-change result tables with the transects. Depending on the way in which your file was created, the field name may be called OID or FID.
SHAPE (alias: Shape)	Geometry	The geometry field is automatically created and maintained by ArcGIS. It provides a definition of the feature type (point, line, polygon).
BaselineID	Long Integer	Values in this field are assigned by DSAS to identify the baseline segment used to generate the measurement transect. Baseline segments assigned an ID = 0 are ignored by DSAS and no transects will be cast along those line segments. See **section 5.3.2** for more information.
Group	Long Integer	Values in this field assigned by DSAS are based on input by user for grouping transects. Groups are assigned by DSAS by using the following logic: if a user selects a baseline-group field as input, then DSAS will use the group ID provided by the user for assigning to output transects; if user does not select a baseline-group field as input, then DSAS will assign all transects a group value of zero. This field is used to aggregate shoreline data and the resulting measurement locations established by the transects into groups. Please refer to the baseline field requirements in **section 5.3.2** for more information.
TransOrder	Long Integer	Assigned by DSAS on the basis of transect order along the baseline or baselines. This field provides the user with a method to sort transect data from the start of the baseline segment with an ID=1 and increment sequentially to the end of the final baseline segment (**fig. 23**).
Proctime	Text	DSAS automatically records the date and time each transect was processed.
Autogen	Text	Indicates whether or not a transect was automatically created by DSAS (1= transect was auto-generated by DSAS; 0=transect was added by user).
StartX	Double	Used by DSAS to record the X coordinate of the beginning of the transect.
StartY	Double	Used by DSAS to record the Y coordinate of the beginning of the transect.
EndX	Double	Used by DSAS to record the X coordinate of the end of the transect.
EndY	Double	Used by DSAS to record the Y coordinate of the end of the transect.
Azimuth	Double	Used to record the azimuth of the transect measured in degrees clockwise from north.

Figure 49 The attribute fields generated for the transect feature class by DSAS (Himmelstoss, E.A. 2009)

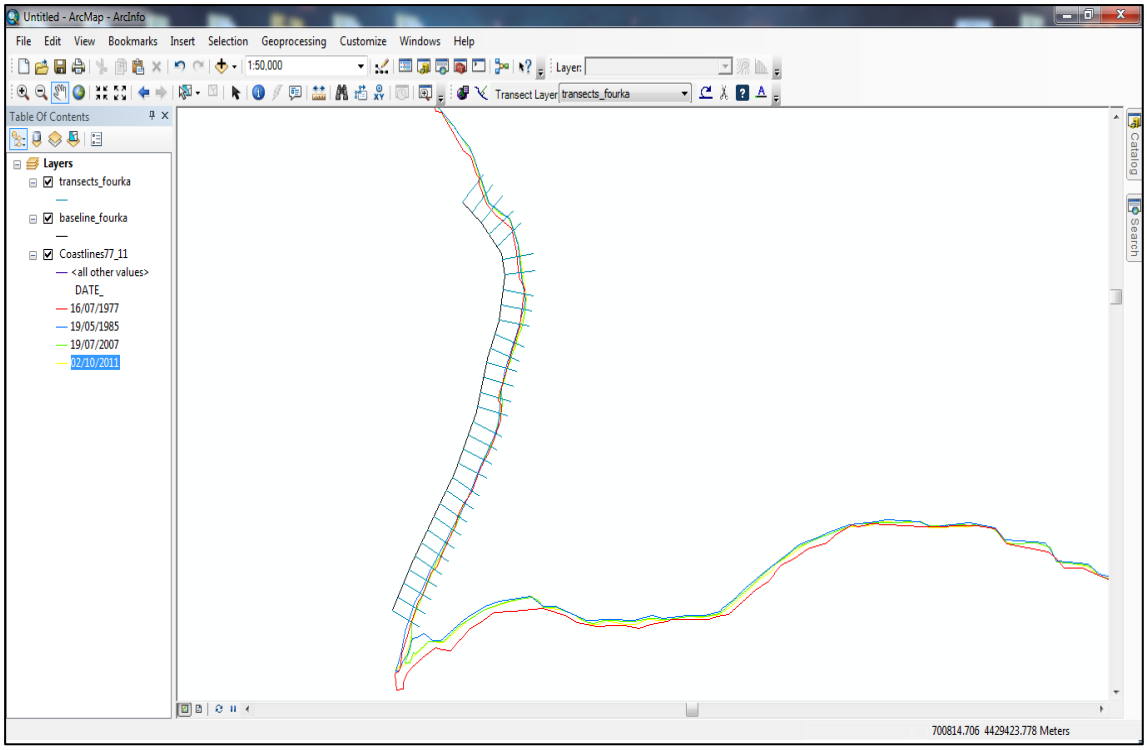

Figure 50 Transects at the area of Fourka in Kassandra peninsula, created with DSAS in ArcMap 10 environment.

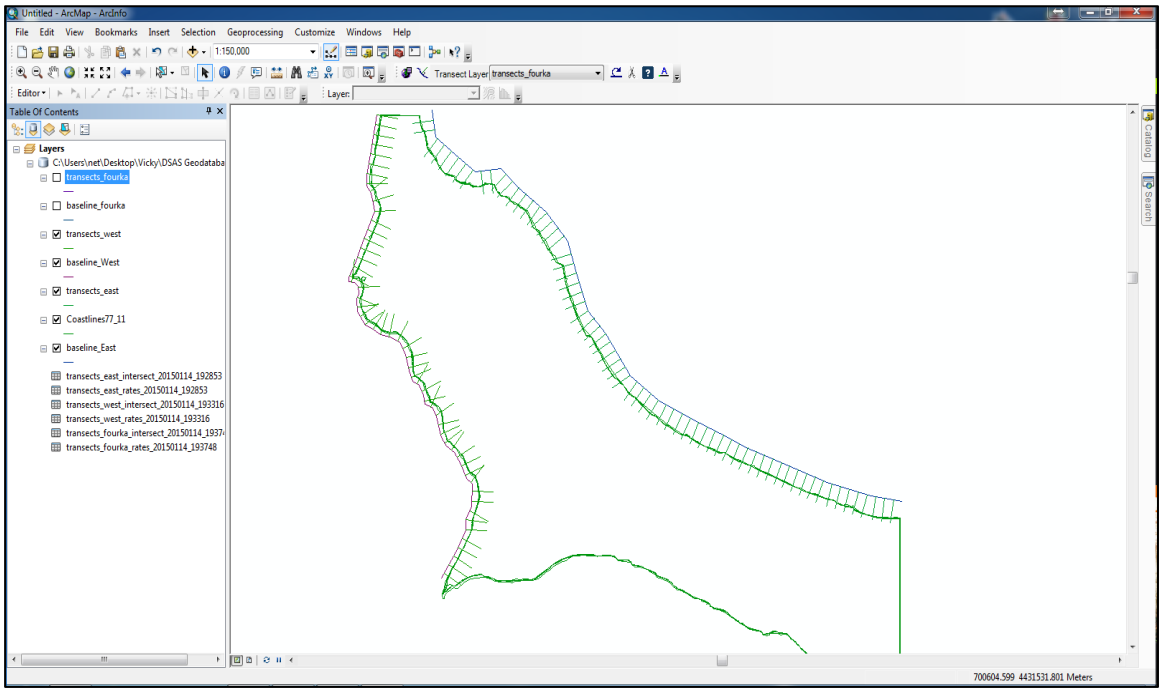

Figure 51 Transects of the west and east part of Kassandra peninsula.

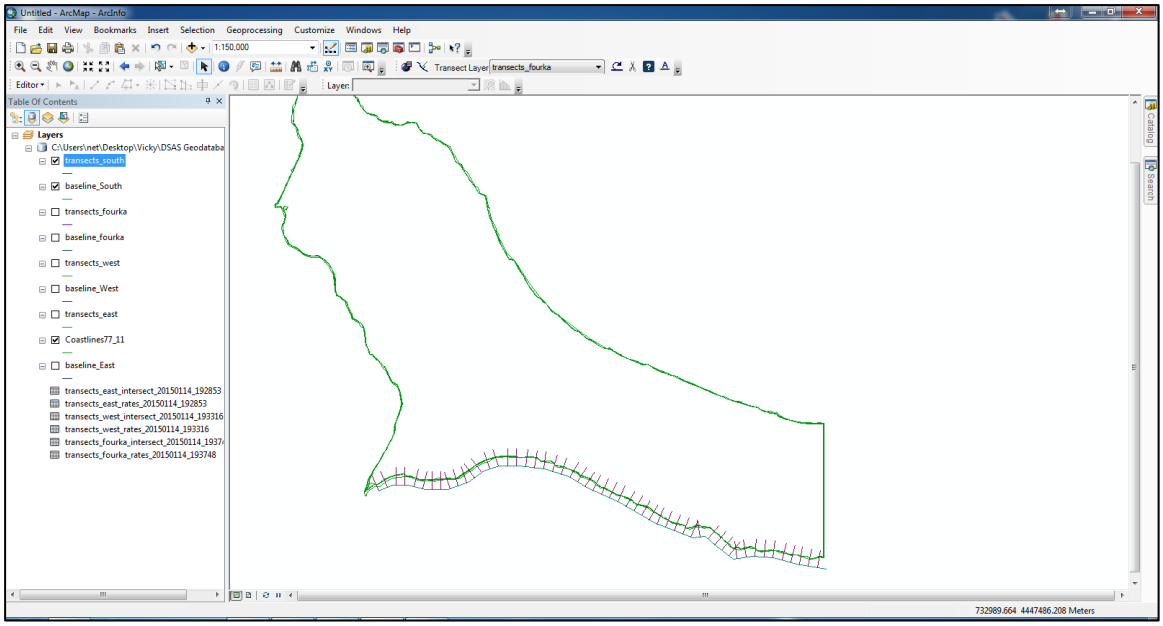

Figure 52 Transects created with DSAS for the south part of Kassandra peninsula.

3.4.4.3 Calculating Change Statistics

Once the transect feature class has been created and all updates or modifications have been made, the data can be used to compute change statistics.

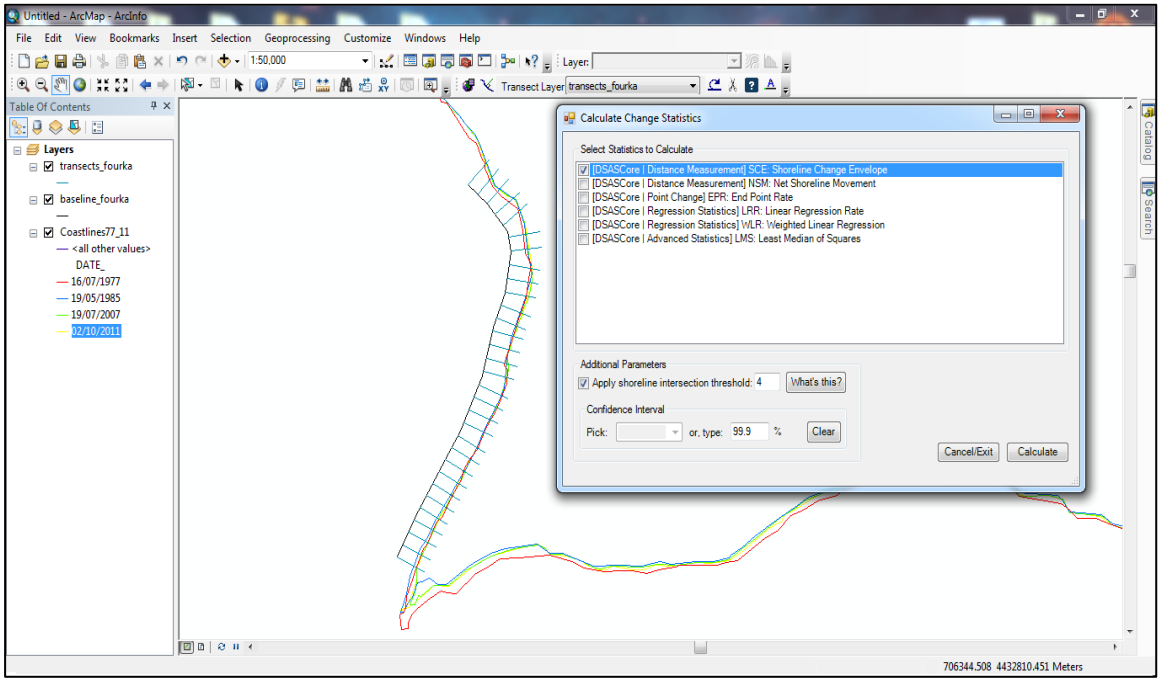

Figure 53 Screenshot of the Calculate Change Statistics window.

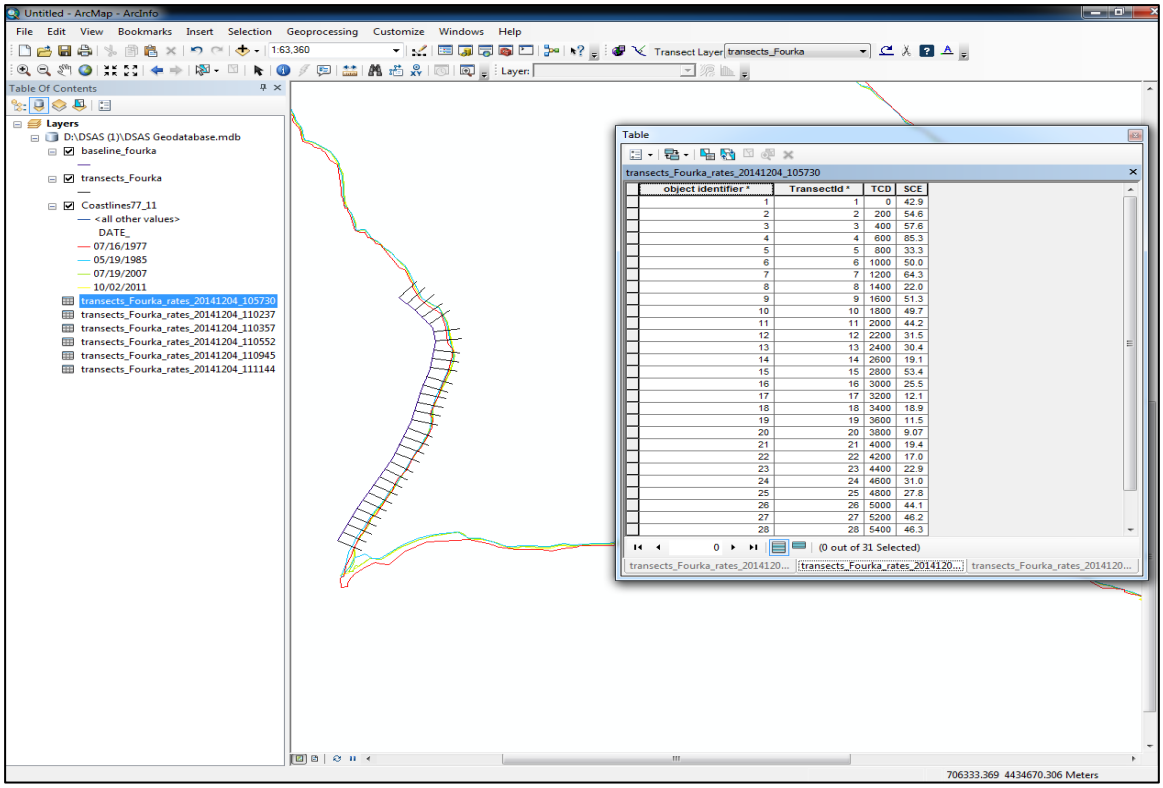

Figure 54Table with the SCE results after the calculation, for the area of Fourka in Kassandra peninsula.

Clipping transects to the Shoreline Change Envelope (SCE)

This is a stand-alone option on the DSAS toolbar which can be performed any time after change statistics have been run. The clipping process will create a copy of the specified transect file, cropped to the greatest extent between shorelines.

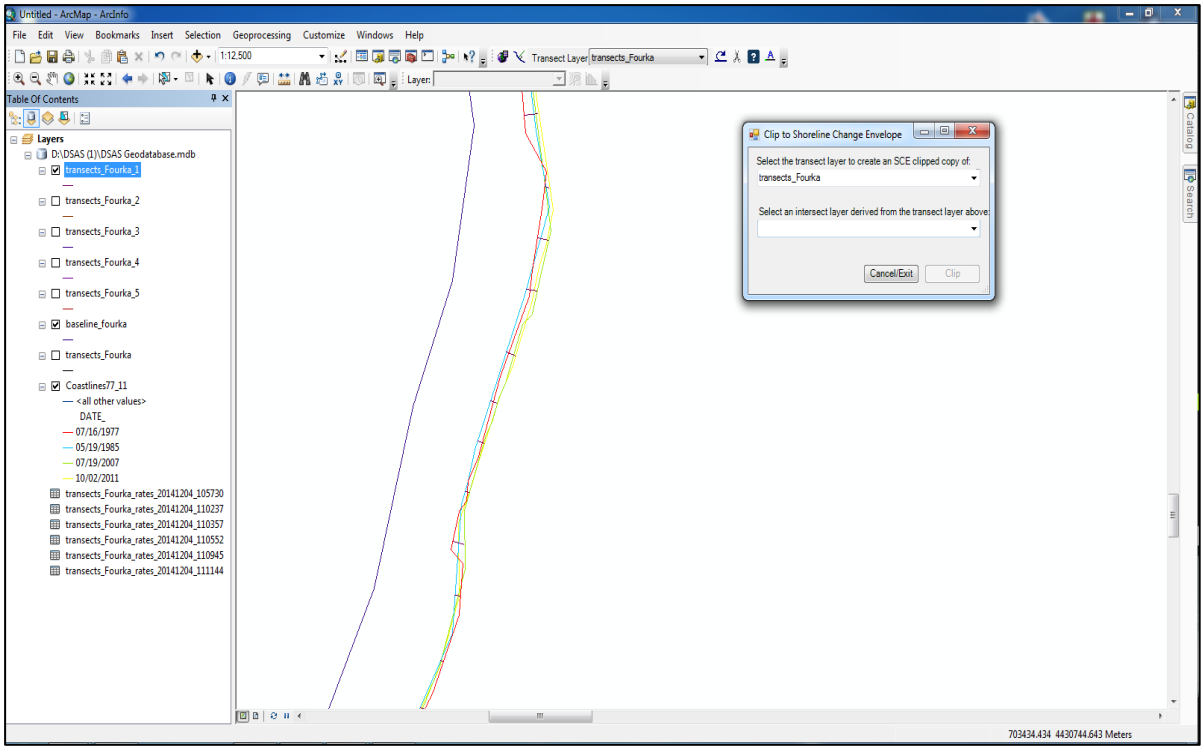

Figure 55 Screenshot of the Clip to Shoreline Change Envelope window with example of required parameters, at the area of Fourka in Kassandra.

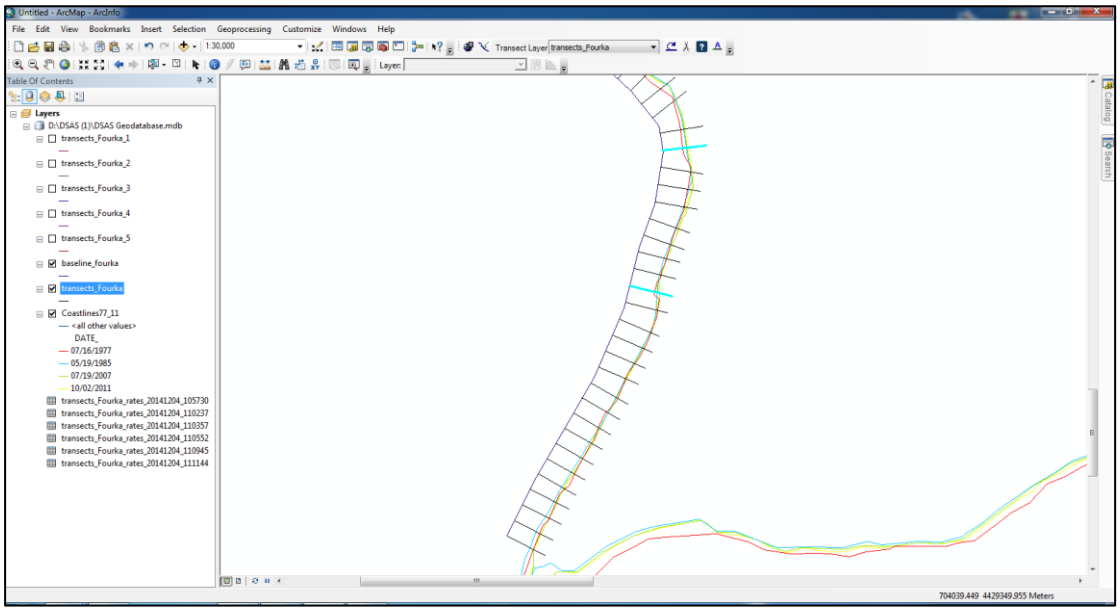

Figure 56 Example of the biggest rate of shoreline change envelope (sce) in Fourka are.

3.4.4.4 Statistics

Each method used to calculate shoreline rates of change is based on measured differences between shoreline positions through time. The reported rates are expressed as meters of change along transects per year. When the user-selected rate-change calculations have finished processing, DSAS merges the individual module calculations, and the output is made available as a table in ArcMap.

Table 20 Table of the standardized field headings provided by the DSAS for change calculations

SCE	Shoreline Change Envelope
NSM	Net Shoreline Movement
EPR	End Point Rate
LRR	Linear Regression Rate

Shoreline Change Envelope (SCE)

The shoreline change envelope reports a distance, not a rate. The SCE is the distance between the shoreline farthest from and closest to the baseline at each transects. This represents the total change in shoreline movement for all available shoreline positions and is not related to their dates.

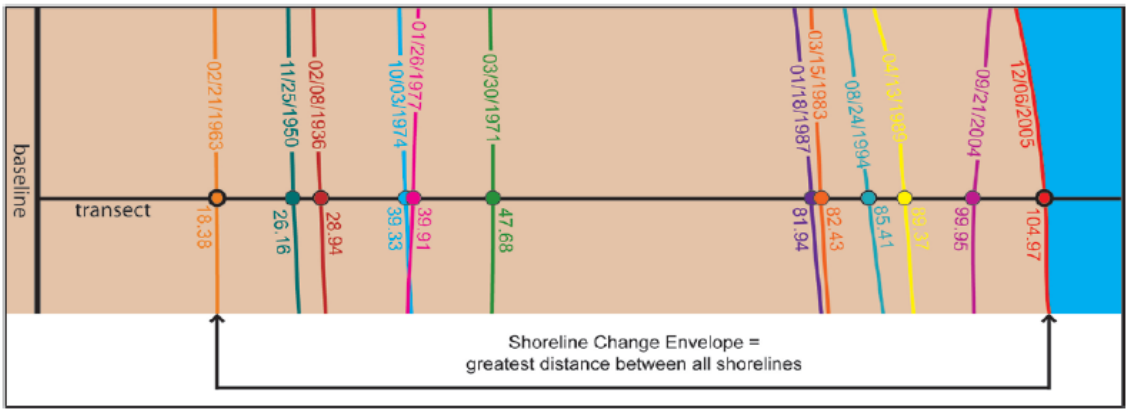

Figure 57 In the example above, the shoreline change envelope is the distance between the 2005 and 1963 shorelines of 86.59 meters; this distance is not associated with the age of the shorelines. (DSAS 4.0 Installation Instructions and User Guide) (Himmelstoss, E.A. 2009)

Net Shoreline Movement (NSM)

The net shoreline movement reports a distance, not a rate. The NSM is associated with the dates of only two shorelines. It reports the distance between the oldest and youngest shorelines for each transect. This represents the total distance between the oldest and youngest shorelines.

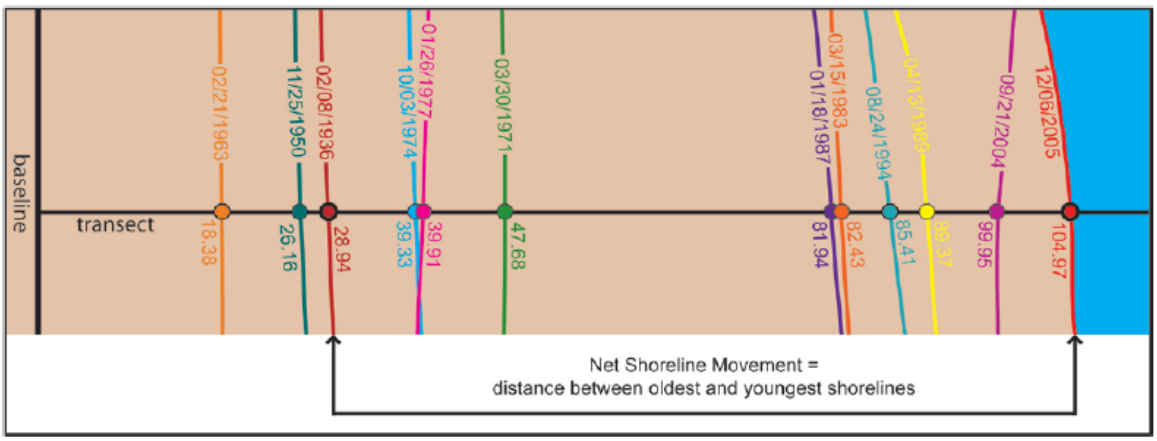

Figure 58 In the example above, the net shoreline movement is the distance of 76.03 meters between the most recent shoreline from 2005 and the oldest shoreline from 1936. (DSAS 4.0 Installation Instructions and User Guide) (Himmelstoss, E.A. 2009)

End Point Rate (EPR)

The end point rate is calculated by dividing the distance of shoreline movement by the time elapsed between the oldest and the most recent shoreline. The major advantages of the EPR are the ease of computation and minimal requirement of only two shoreline dates. The major disadvantage is that in cases where more data are available, the additional information is ignored. Changes in sign (for example, accretion to erosion), magnitude, or cyclical trends may be missed (Crowell and others, 1997; Dolan and others, 1991).

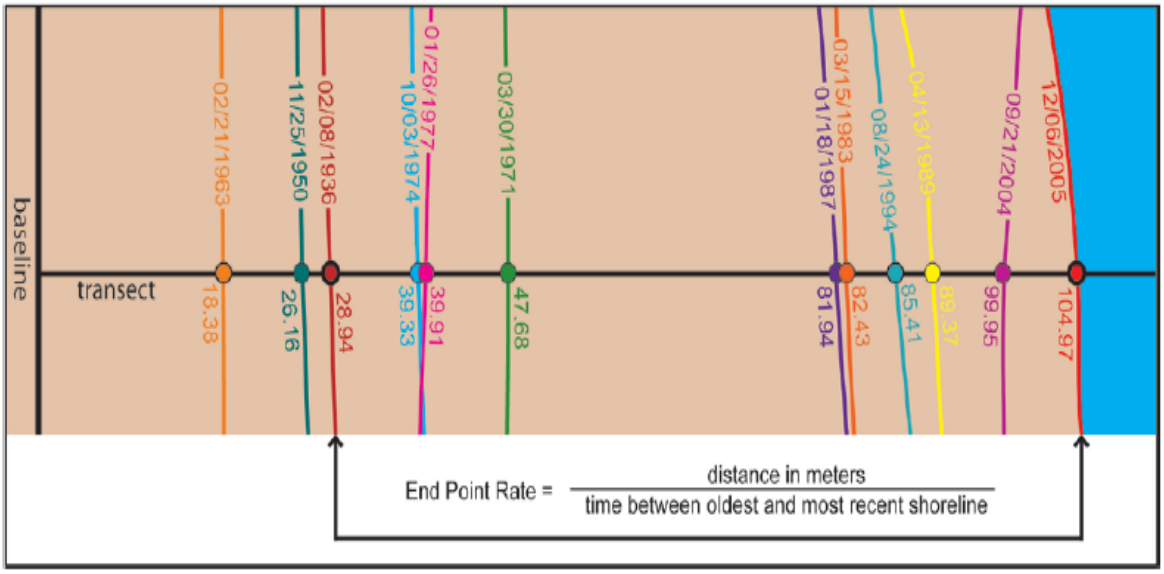

Figure 59 In the example above, the end point rate of 1.09 meters per year is the distance between the 2005 and 1936 shorelines (76.03 meters) divided by the span of time elapsed between the two shoreline positions (69.82 years). All other shoreline data are ignored in this computation. (Himmelstoss, E.A. 2009)

Linear Regression (LRR)

A linear regression rate-of-change statistic can be determined by fitting a least-squares regression line to all shoreline points for a particular transect. The regression line is placed so that the sum of the squared residuals (determined by squaring the offset distance of each data point from the regression line and adding the squared

residuals together) is minimized. The linear regression rate is the slope of the line. The method of linear regression includes these features: (1) All the data are used, regardless of changes in trend or accuracy, (2) The method is purely computational, (3) The calculation is based on accepted statistical concepts, and (4) The method is easy to employ (Dolan and others, 1991). However, the linear regression method is susceptible to outlier effects and also tends to underestimate the rate of change relative to other statistics, such as EPR (Dolan, and others, 1991; Genz and others, 2007). In conjunction with the linear regression rate, the standard error of the estimate (LSE), the standard error of the slope with user-selected confidence interval (LCI), and the R-squared value (LR2) are reported.

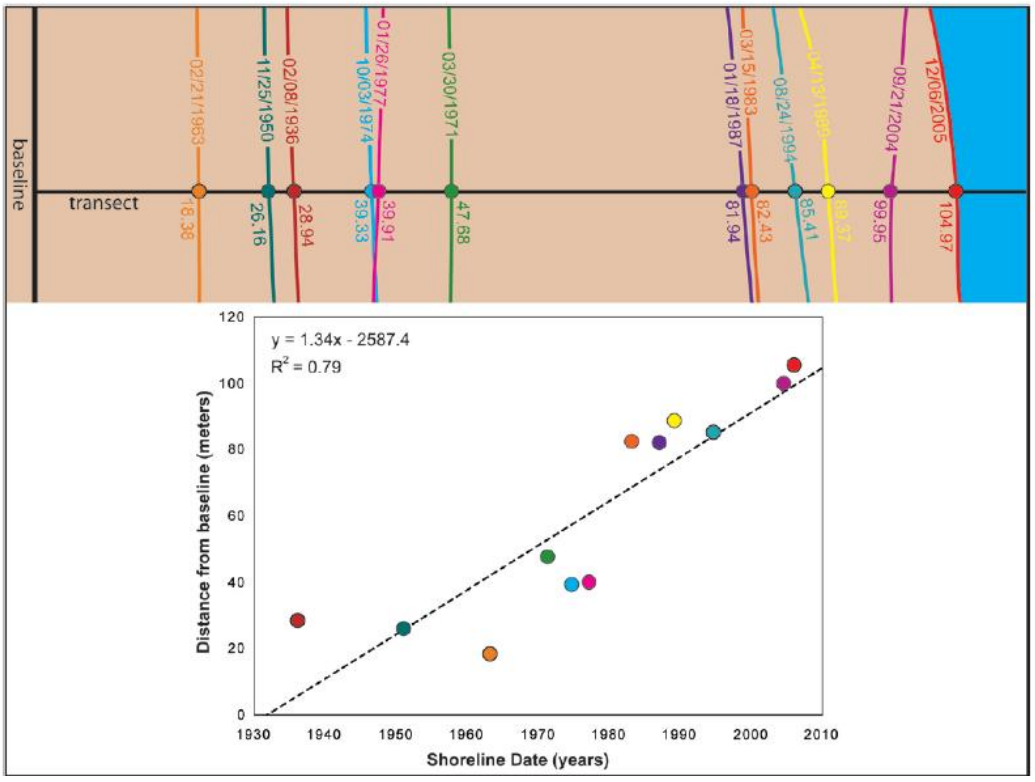

Figure 60 In the example above, the linear regression rate was determined by plotting the shoreline positions with respect to time and calculating the linear regression equation of y = 1.34x – 2587.4. The slope of the equation describing the line is the rate (1.34m/yr). (Himmelstoss, E.A. 2009)

3.5. RESULTS

Table 21 Table of results of the DSAS change calculations for the area of Fourka in Kassandra peninsula.

Transect Id	SCE Greater distance between all shorelines	NSM Distance between older and youngest shorelines	EPR NSM/time between older and youngest shorelines	LRR Linear regression rate	LR2 Squared linear regression
1	42,98	20,27	0,59	0,47	0,15
2	81,82	51,48	1,5	0,97	0,21
3	50,06	50,06	1,46	1,19	0,79
4	47,44	47,44	1,39	1,05	0,78
5	44,25	32,56	0,95	1,1	0,82
6	24,07	10	0,29	0,51	0,58
7	25,53	-5,64	-0,16	0,04	0
8	16,69	-14,15	-0,41	-0,21	0,23
9	19,42	-19,42	-0,57	-0,37	0,45
10	25,4	-2,83	-0,08	0,28	0,2
11	44,17	-19,21	-0,56	-0,01	0
12	43,33	1,15	0,03	0,57	0,26
13	54,09	11,64	0,34	0,79	0,29

Table 22 Table of results of the DSAS change calculations for the east part of Kassandra peninsula.

Transect Id	SCE Greater distance between all shorelines	NSM Distance between older and youngest shorelines	EPR NSM/time between older and youngest shorelines	LRR Linear regression rate	LR2 Squared linear regression
1	15,79	-15,79	-0,46	-0,39	0,86
2	88,39	83,85	2,45	1,83	0,49
3	85,65	63,75	1,86	1,11	0,25
4	74,33	54,71	1,6	0,93	0,24
5	89,93	77,69	2,27	1,7	0,43
6	34,38	21,37	0,62	0,41	0,21
7	51,06	51,06	1,49	1,06	0,56
8	96,35	96,35	2,82	2,46	0,84
9	21,27	6,61	0,19	0,4	0,5
10	14,91	-14,91	-0,44	-0,31	0,55
12	25,13	-20,39	-0,6	-0,54	0,68
13	19,61	19,61	0,57	0,43	0,55
14	41,75	32,36	0,95	0,83	0,57
15	56,26	40,58	1,19	1,21	0,73
16	62,22	62,22	1,82	1,07	0,38
17	69,49	63,12	1,84	1,42	0,5
18	112,38	104,24	3,05	2,37	0,55
19	77,09	70,68	2,07	1,22	0,34
20	115,57	100,86	2,95	1,96	0,38
21	85,43	85,43	2,5	1,74	0,57
23	99,34	99,34	2,9	2,06	0,51
24	90,49	69,15	2,02	1,72	0,51
25	76,93	76,93	2,25	1,76	0,64
26	69,51	60,73	1,78	1,48	0,61
27	89,16	89,16	2,61	1,93	0,53
28	80,1	61,12	1,79	1,16	0,3
29	80,22	63,71	1,86	1,12	0,28
30	46,41	32,34	0,95	0,58	0,23
31	101,2	101,2	2,96	2,36	0,85

32	46,8	46,8	1,37	1,16	0,9
33	65,3	50,97	1,49	1,37	0,65
34	92,1	80,34	2,35	2,13	0,75
35	123,85	123,85	3,62	2,72	0,57
36	148,07	130,2	3,81	2,91	0,47
37	46,63	46,63	1,36	0,99	0,72
38	54,96	38,15	1,12	0,62	0,2
39	18,79	-4,75	-0,14	0,16	0,09
40	82,71	82,71	2,42	1,89	0,65
41	114,57	114,57	3,35	2,52	0,55
42	69,44	67,56	1,97	1,53	0,58
43	68,19	68,19	1,99	1,6	0,75
44	66,75	66,75	1,95	1,57	0,71
45	17,39	15,71	0,46	0,55	0,92
46	22,03	15,09	0,44	0,6	0,82
47	21,03	3,33	0,1	0,33	0,3
48	14,66	6,76	0,2	0,32	0,6
49	47,05	47,05	1,38	1,33	0,95
50	19,25	17,67	0,52	0,62	0,93
51	39,3	38,82	1,13	1,11	0,95
52	32,44	32,44	0,95	0,82	0,93
53	26,63	26,44	0,77	0,81	0,99
54	36,32	36,32	1,06	0,95	0,91
55	30,77	27,53	0,8	0,79	0,89
56	45,58	45,58	1,33	1,17	0,86
57	40,57	38,59	1,13	1,08	0,91
58	44,3	44,3	1,29	1,18	0,93
59	60,19	60,19	1,76	1,42	0,69
60	26,33	24,64	0,72	0,75	0,97
61	49,52	49,52	1,45	1,26	0,84
62	31,09	30,35	0,89	0,86	0,94
63	6,95	1,64	0,05	-0,02	0,02
64	78,75	63,42	1,85	1,77	0,75
65	104,06	88,14	2,58	2,04	0,5
66	58,64	53	1,55	1,42	0,81
67	26,34	26,34	0,77	0,79	1
68	65,77	61,83	1,81	1,62	0,8
69	44,28	41,59	1,22	1,2	0,93

Table 23 Table of results of the DSAS change calculations for the south part of Kassandra peninsula.

Transect Id	SCE Greater distance between all shorelines	NSM Distance between older and youngest shorelines	EPR NSM/time between older and youngest shorelines	LRR Linear regression rate	LR2 Squared linear regression
1	40,84	-5,94	-0,17	-0,45	0,17
2	29,03	4,68	0,14	0,11	0,02
3	27,64	-1,34	-0,04	-0,38	0,26
4	47,64	13,71	0,4	-0,14	0,01
5	67,45	51,54	1,51	0,92	0,27
6	21,93	-10,18	-0,3	-0,43	0,56
7	40,46	-0,56	-0,02	-0,23	0,04
8	42,51	10,26	0,3	0,13	0,01
9	53,78	5,39	0,16	-0,46	0,09
10	112,78	88	2,57	1,59	0,29
11	133,99	92,02	2,69	1,46	0,19
12	30,47	22,63	0,66	0,4	0,25
13	12,79	-7,74	-0,23	-0,11	0,11
14	39,02	38,62	1,13	0,92	0,68
15	110,03	93,47	2,73	1,43	0,24
16	107,84	59,84	1,75	0,85	0,1
17	34,26	-10,15	-0,3	-0,08	0,01
18	48,86	17,62	0,52	0,09	0,01
19	13,18	-13,03	-0,38	-0,36	0,88
20	30,68	-30,68	-0,9	-0,65	0,61
21	35,04	31,85	0,93	0,67	0,44
22	79,25	68,11	1,99	1,34	0,38
23	68,61	53,54	1,56	1,09	0,34
24	21,67	-21,42	-0,63	-0,7	0,98
25	33,76	24,29	0,71	0,41	0,22
26	44,2	36,34	1,06	0,89	0,55
27	43,85	32,74	0,96	0,65	0,3
28	68,44	62,26	1,82	1,24	0,42
29	88,81	61,71	1,8	0,97	0,19
30	70	58,59	1,71	1,27	0,4

31	48,42	35,07	1,03	0,69	0,29
32	64,46	41,13	1,2	0,76	0,2
33	13,12	-9,96	-0,29	-0,19	0,25
34	71,17	42,76	1,25	0,57	0,1
35	16,93	1,23	0,04	-0,18	0,14
36	30,94	-1,18	-0,03	-0,17	0,04
37	62,32	62,32	1,82	1,18	0,51
38	70,13	33,59	0,98	0,27	0,02
39	34,2	-12,59	-0,37	-0,47	0,31
40	113,49	92,39	2,7	1,87	0,36
41	79,13	55,54	1,62	1,11	0,27
42	126,04	88,01	2,57	1,67	0,25
43	127,87	76,34	2,23	1,37	0,17
44	61,32	31,52	0,92	0,41	0,07
45	40,92	18,44	0,54	0,19	0,03
46	64,76	28,22	0,82	0,5	0,08
47	84,52	28,95	0,85	0,52	0,05
48	79,8	69,19	2,02	1,33	0,37
49	73,45	72,91	2,13	1,6	0,54
50	129,67	123,14	3,6	2,79	0,56
51	143,98	118,99	3,48	2,33	0,35
52	158,67	110,29	3,22	2,02	0,24
53	605,5	-2,98	-0,09	7,25	0,16

Table 24 Table of results of the DSAS change calculations for the western part of Kassandra peninsula.

Transect Id	SCE Greater distance between all shorelines	NSM Distance between older and youngest shorelines	EPR NSM/time between older and youngest shorelines	LRR Linear regression rate	LR2 Squared linear regression
1	2,21	128,91	75,71	0,99	0,1
2	1,04	37,23	35,65	0,9	0,76
3	2,32	79,43	79,43	2,1	0,89
4	1,29	46,55	44,11	1,27	0,94
5	0,13	15,68	4,6	0,29	0,45
6	2,17	76,72	74,35	1,75	0,64
7	2,84	97,18	97,18	1,87	0,52
8	2,3	91,15	78,66	1,84	0,52
9	1,36	59,82	46,45	1,12	0,48
10	3,51	120,2	120,2	2,56	0,6
11	1,79	71,24	61,24	1,91	0,94
12	-0,22	42,97	-7,55	0,38	0,1
13	1,44	49,52	49,14	1,21	0,75
14	0,25	11,63	8,51	0,28	0,86
15	0,91	39,69	30,97	0,81	0,61
16	0,57	24,06	19,49	0,63	0,92
17	2	68,52	68,52	1,93	0,99
18	4,12	148,44	141,04	3,59	0,76
20	2,02	83,07	69,09	2,01	0,84
21	1,52	52,6	51,94	1,54	0,98
22	1,21	55,66	41,48	0,71	0,25
23	1,87	86,99	63,82	1,1	0,24
24	1,72	81,52	58,87	1	0,23
25	1,64	84,25	55,99	0,97	0,2
26	1,31	79,17	44,82	0,64	0,11
27	1,93	83,8	66,18	1,22	0,3
28	1,16	55,08	39,72	0,64	0,21
29	1,74	62,71	59,66	1,22	0,46
30	2,29	78,37	78,37	1,98	0,84
31	1,57	53,59	53,59	1,43	0,89
32	0,76	28,88	25,9	0,63	0,62

33	1,45	49,48	49,48	0,8	0,34
34	1,9	70,4	64,86	1,41	0,47
35	0,91	44,78	31	0,18	0,02
36	0,96	52,05	32,99	0,62	0,21
37	1,2	59,82	41,18	0,82	0,27
38	1,29	44,2	44,2	1,14	0,84
39	0,36	24,45	12,28	0,47	0,6
40	0,55	19,57	18,81	0,48	0,79
41	0,56	39,61	19,13	0,16	0,03
42	2,04	73,67	69,81	1,46	0,47
43	0,93	51,68	31,94	0,75	0,27
44	1,37	61	46,76	0,85	0,28
45	1,6	67,08	54,7	1,26	0,45
46	1,65	56,31	56,31	1,27	0,79
47	0,8	45,72	27,37	1,18	0,8
48	0,39	32,08	13,28	0,68	0,57
49	0,28	27,29	9,66	0,45	0,43
50	-0,47	17,95	-16,12	-0,51	0,96
51	0,23	11,83	7,97	0,32	0,85
52	0,45	16,89	15,29	0,33	0,45
53	-0,09	31,04	-3,06	0,33	0,16
54	-0,05	37,27	-1,82	0,29	0,08
55	-4	182,55	-136,93	-2,65	0,3

3.5.1 SUMMARY OF RESULTS

The results given in the above tables were divided into three categories in order for conclusions to be drawn.

- **1st Category**: Correlation Coefficient $R^2 > 0.5$ and Net Shoreline Movement (NSM) > +20m
- **2nd Category**: Correlation Coefficient $R^2 > 0.5$ and Net Shoreline Movement (NSM) < -20m
- **3rd Category**: Correlation Coefficient $R^2 < 0.5$ and Net Shoreline Movement (NSM) > 20m

Values that **do not** fall under one of the aforementioned categories are not taken into account.

3.5.1.1 AREAS OF HIGH CORRELATION (R2>0.5)

These areas present high correlation and the movements are either positive (erosion) or negative (deposition) and they all are above 20 m.

EROSION

Table 25 WEST KASSANDRA

Transect Id	NSM Distance between older and youngest shorelines	LRR Linear regression rate	LR2 Squared linear regression
2	35,65	0,9	0,76
3	79,43	2,1	0,89
4	44,11	1,27	0,94
6	74,35	1,75	0,64
7	97,18	1,87	0,52
8	78,66	1,84	0,52
10	120,2	2,56	0,6
11	61,24	1,91	0,94
13	49,14	1,21	0,75
15	30,97	0,81	0,61
16	19,49	0,63	0,92
17	68,52	1,93	0,99
18	141,04	3,59	0,76
20	69,09	2,01	0,84
21	51,94	1,54	0,98
30	78,37	1,98	0,84
31	53,59	1,43	0,89
32	25,9	0,63	0,62
38	44,2	1,14	0,84
46	56,31	1,27	0,79
47	27,37	1,18	0,8

Table 26 FOURKA AREA

Transect Id *	NSM Distance between older and youngest shorelines	LRR Linear regression rate	LR2 Squared linear regression
3	50,06	1,19	0,79
4	47,44	1,05	0,78
5	32,56	1,1	0,82
6	10	0,51	0,58

Table 27 SOUTH KASSANDRA

Transect Id *	NSM Distance between older and youngest shorelines	LRR Linear regression rate	LR2 Squared linear regression
14	38,62	0,92	0,68
26	36,34	0,89	0,55
37	62,32	1,18	0,51
49	72,91	1,6	0,54
50	123,14	2,79	0,56

Table 28 EAST KASSANDRA

Transect Id *	NSM Distance between older and youngest shorelines	LRR Linear regression rate	LR2 Squared linear regression
7	51,06	1,06	0,56
8	96,35	2,46	0,84
13	19,61	0,43	0,55
14	32,36	0,83	0,57
15	40,58	1,21	0,73
17	63,12	1,42	0,5
18	104,24	2,37	0,55
21	85,43	1,74	0,57
23	99,34	2,06	0,51
24	69,15	1,72	0,51
25	76,93	1,76	0,64
26	60,73	1,48	0,61
27	89,16	1,93	0,53
31	101,2	2,36	0,85
32	46,8	1,16	0,9
33	50,97	1,37	0,65
34	80,34	2,13	0,75
35	123,85	2,72	0,57
37	46,63	0,99	0,72
40	82,71	1,89	0,65
41	114,57	2,52	0,55
42	67,56	1,53	0,58
43	68,19	1,6	0,75
44	66,75	1,57	0,71
49	47,05	1,33	0,95
51	38,82	1,11	0,95
52	32,44	0,82	0,93
53	26,44	0,81	0,99
54	36,32	0,95	0,91
55	27,53	0,79	0,89
56	45,58	1,17	0,86
57	38,59	1,08	0,91
58	44,3	1,18	0,93
59	60,19	1,42	0,69

60	24,64	0,75	0,97
61	49,52	1,26	0,84
62	30,35	0,86	0,94
64	63,42	1,77	0,75
65	88,14	2,04	0,5
66	53	1,42	0,81
67	26,34	0,79	1
68	61,83	1,62	0,8
69	41,59	1,2	0,93

Figure 61 Areas with erosion in Kassandra peninsula.

Table 29 SOUTH KASSANDRA

Transect Id *	NSM Distance between older and youngest shorelines	LRR Linear regression rate	LR2 Squared linear regression
20	-30,68	-0,65	0,61
24	-21,42	-0,7	0,98

Table 30 EAST KASSANDRA

TransectId *	NSM Distance between older and youngest shorelines	LRR Linear regression rate	LR2 Squared linear regression
12	-20,39	-0,54	0,68

Figure 62 Coasts with deposition on Kassandra peninsula.

3.4.1.2 AREAS OF LOW CORRELATION AND HIGH DISPLACEMENT (R2<0.5, NSM>20m)

These areas present displacements above 20m. but very low correlation. In this case we are not dealing with a steady process of deposition or erosion but with alternating processes.

Having observed these areas we reach the conclusion that we are dealing with Clift coasts, where due to seasonal variation a coast cannot be formed.

Table 31 WEST KASSANDRA

Transect Id *	NSM Distance between older and youngest shorelines	LRR Linear regression rate	LR2 Squared linear regression
1	75,71	0,99	0,1
9	46,45	1,12	0,48
22	41,48	0,71	0,25
23	63,82	1,1	0,24
24	58,87	1	0,23
25	55,99	0,97	0,2
26	44,82	0,64	0,11
27	66,18	1,22	0,3
28	39,72	0,64	0,21
29	59,66	1,22	0,46
33	49,48	0,8	0,34
34	64,86	1,41	0,47
35	31	0,18	0,02
36	32,99	0,62	0,21
37	41,18	0,82	0,27
41	19,13	0,16	0,03
42	69,81	1,46	0,47
43	31,94	0,75	0,27
44	46,76	0,85	0,28
45	54,7	1,26	0,45
55	-136,93	-2,65	0,3

Table 32 FOURKA AREA

Transect Id *	NSM Distance between older and youngest shorelines	LRR Linear regression rate	LR2 Squared linear regression
1	20,27	0,47	0,15

2	51,48	0,97	0,21
9	-19,42	-0,37	0,45
11	-19,21	-0,01	0

Table 33 SOUTH KASSANDRA

Transect Id *	NSM Distance between older and youngest shorelines	LRR Linear regression rate	LR2 Squared linear regression
5	51,54	0,92	0,27
10	88	1,59	0,29
11	92,02	1,46	0,19
12	22,63	0,4	0,25
15	93,47	1,43	0,24
16	59,84	0,85	0,1
21	31,85	0,67	0,44
22	68,11	1,34	0,38
23	53,54	1,09	0,34
25	24,29	0,41	0,22
27	32,74	0,65	0,3
28	62,26	1,24	0,42
29	61,71	0,97	0,19
30	58,59	1,27	0,4
31	35,07	0,69	0,29
32	41,13	0,76	0,2
34	42,76	0,57	0,1
38	33,59	0,27	0,02
40	92,39	1,87	0,36
41	55,54	1,11	0,27
42	88,01	1,67	0,25
43	76,34	1,37	0,17
44	31,52	0,41	0,07
46	28,22	0,5	0,08
47	28,95	0,52	0,05
48	69,19	1,33	0,37
51	118,99	2,33	0,35
52	110,29	2,02	0,24

Table 34 EAST KASSANDRA

Transect Id *	NSM Distance between older and youngest shorelines	LRR Linear regression rate	LR2 Squared linear regression
2	83,85	1,83	0,49
3	63,75	1,11	0,25
4	54,71	0,93	0,24
5	77,69	1,7	0,43
6	21,37	0,41	0,21
16	62,22	1,07	0,38
19	70,68	1,22	0,34
20	100,86	1,96	0,38
28	61,12	1,16	0,3
29	63,71	1,12	0,28
30	32,34	0,58	0,23
36	130,2	2,91	0,47
38	38,15	0,62	0,2

Figure 63 Cliff coasts on Kassandra peninsula.

3.6. CONCLUSIONS AND DISCUSSION

Based on the research of the current study that involved satellite image analysis, from 1977 to 2011 according to Digital Shoreline Analysis System, in the area of Kassandra Halkidiki were located areas where:

1. There is continuous deposition during the study's time frame.
2. Continuous erosion.
3. Also areas where there is no apparent correlation but there is high alternation in the rates of deposition and erosion.

To go into further detail for the three types of coasts that were found:

1. 3 areas of continuous **deposition** where found, in 3 piscatorial refuges (N. Fokea, N. Skioni, Loutra), with deposition located by the groyne. In these areas (100% of the cases), the deposition occurs due to coastal works for protection and redevelopment of the coastal area. (see Appendix 2).
2. Continuous **erosion** was found in **25 regions of the West coast** which corresponds to 1region/km, **43 regions in the East coast** which correspond to 1.2 regions/km and **5 regions in the South coast** which correspond in 0.2 regions/km (1 area/5 km).
    a. In the **West Coast** there is an increase of the residential zone in the downstreams of the drainage basins, as well as near riverbeds of the drainage network, a fact that decreases the input of material from the upstreams. In the region of Fourka in particular one observes the greatest displacement. Along with the erosion at the coastal area there occurs a reduction of the NDVI along the road hubs as a result of residential development as well as an increase of the NDVI (at the south east part of the basin) with an increase of vegetation, as a result of forestation. The result is less material transported to the coastline by the torrents (see Appendix III)
    b. In the **East Coast**, the great coastal residential development combined with the small extent of the drainage basins, leads to phenomena of coastal erosion.

c. The **South Part** is where the areas with least erosion is observed, the human intervention is the least and, as a result, there is the least possible effect in the conditions of solid matter transportation. It was observed that 100% of the cases of great variation in the coastal system (alternating deposition-erosion) are cliff coasts (high coasts with terraces). (Figure 19)

It would be interesting to correlate human activity, mainly in the form of expanded residential activity related to resorts, with the phenomenon of erosion in the study area. This was not feasible in the present study as the available satellite images were of too low spatial resolution to allow the extraction of reliable results on the matter. To underline the importance of further study let us comment that the Municipality of Kassandra has 18.000 residents while during the summer months 400.000 seasonal residents relocate there.

APPENDIX I

Figure 64 Flooding in Fourka, Kassandra, in 2011 (URL1)

Figure 65 Flooding in Siviri, Kassandra, in 2007(URL2)

Figure 66Flooding in Sani, Kassandra, in 2010 (URL3)

Figure 67 Flooding in Siviri, Kassandra, in 2007 (URL4) (URL5)

Figure 68 Flooding in Skioni, Kassandra, 2007 (URL6)

Figure 69 Flooding in Skioni, Kassandra, 2007 (URL7)

APPENDIX II

WEST PART OF KASSANDRA

CLIFF COASTS

Cliff coasts of the western part of Kassandra peninsula, starting from the North to the South.

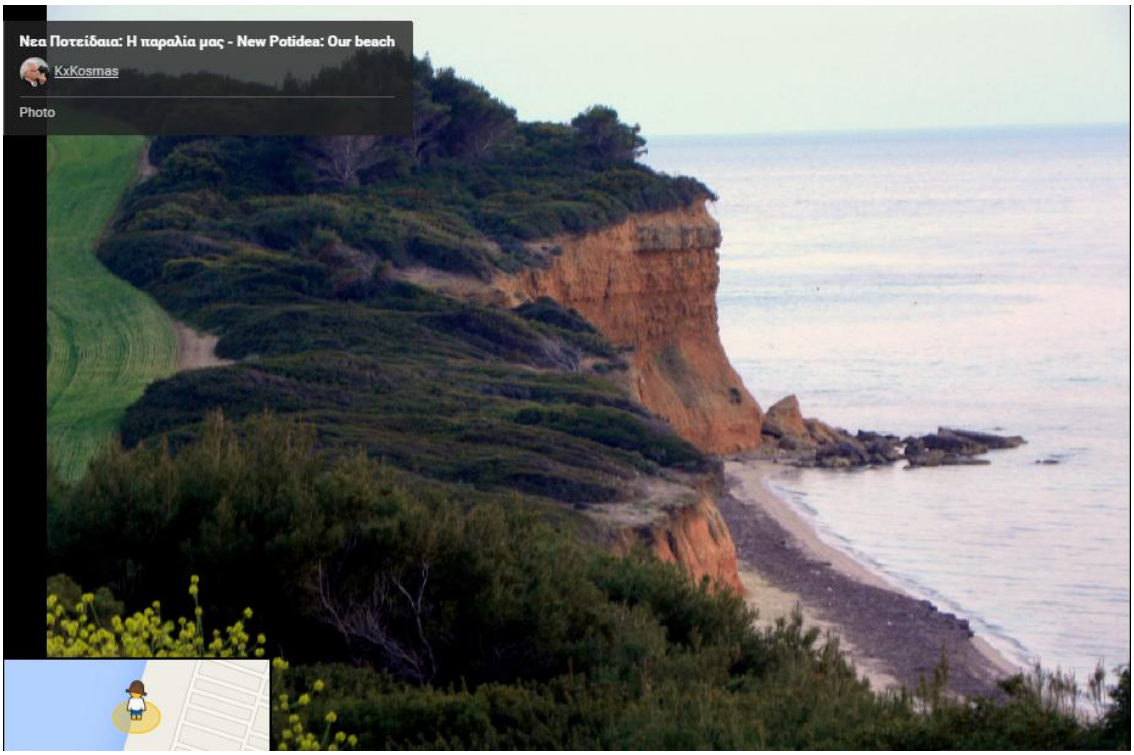

Figure 70
(https://www.google.gr/maps/@40.15887,23.321357,3a,75y,90t/data=!3m5!1e2!3m3!1s34328743!2e1!3e10)

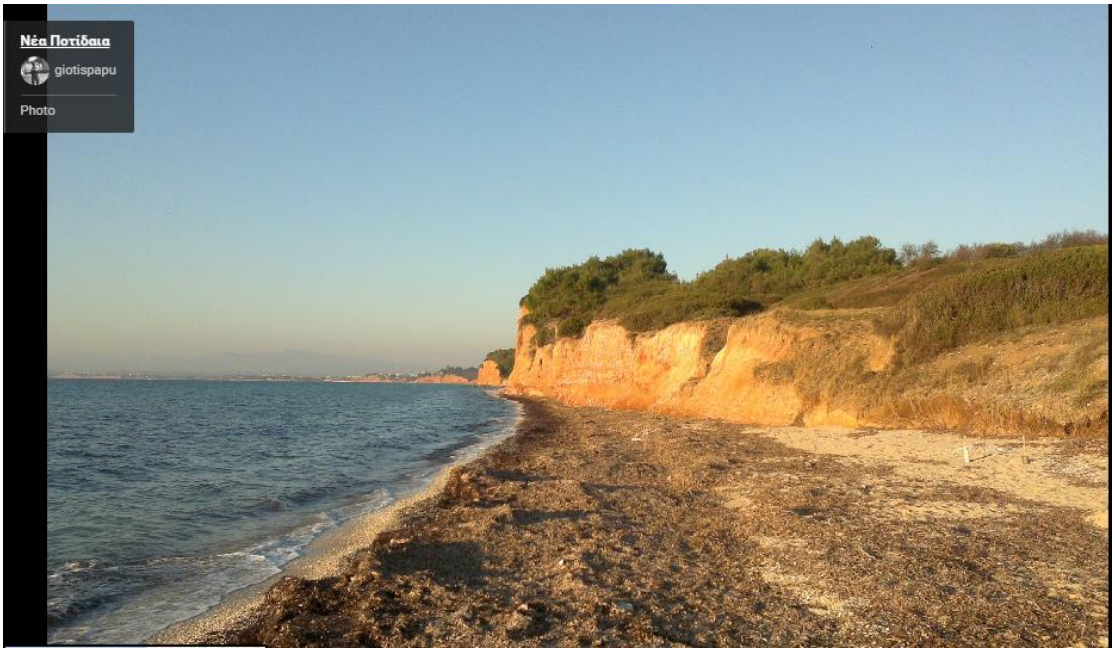

Figure 71
(https://www.google.gr/maps/@40.157541,23.320831,3a,75y,90t/data=!3m5!1e2!3m3!1s47999240!2e1!3e10)

Figure 72
(https://www.google.gr/maps/@40.167706,23.323814,3a,75y,90t/data=!3m5!1e2!3m3!1s107987980!2e1!3e10)

Figure 73
(https://www.google.gr/maps/@40.157451,23.320766,3a,75y,90t/data=!3m5!1e2!3m3!1s48005119!2e1!3e10)

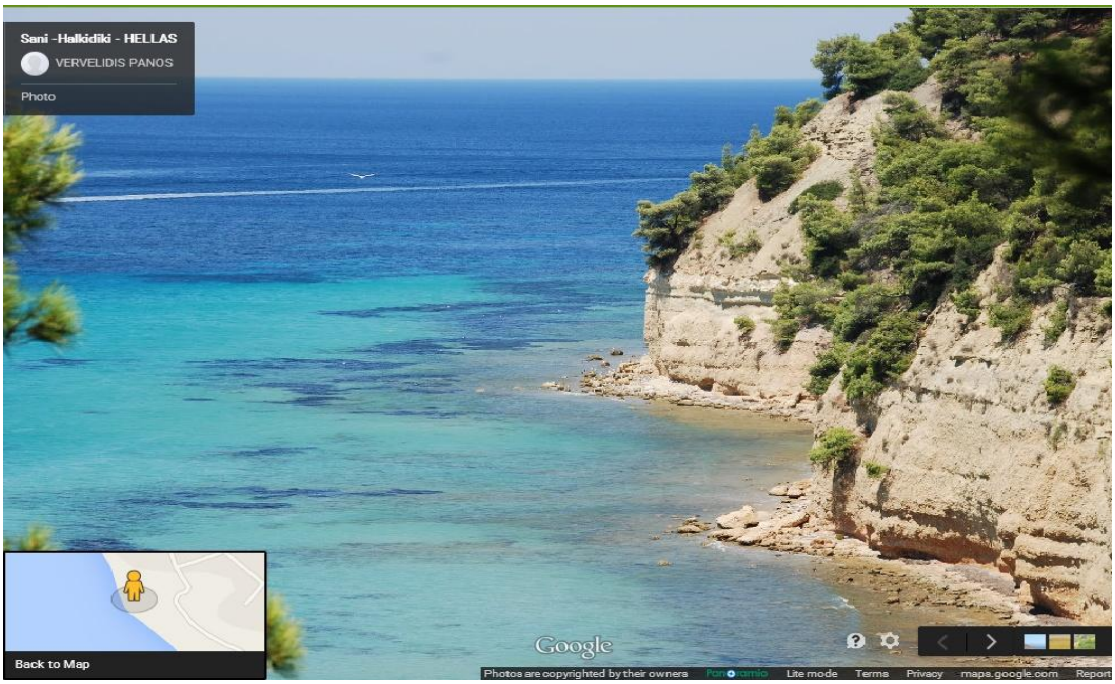

Figure 74

(https://www.google.gr/maps/@40.080895,23.31213,3a,75y,90t/data=!3m5!1e2!3m3!1s13212385!2e1!3e10)

Figure 75

(https://www.google.gr/maps/@40.077677,23.317966,3a,75y,90t/data=!3m5!1e2!3m3!1s13201710!2e1!3e10)

Figure 76

(https://www.google.gr/maps/@40.0787778,23.316575,3a,75y,90t/data=!3m5!1e2!3m3!1s-EnT73I9pv0w%2FU5x_D3FZIVI%2FAAAAAAAAHLg%2FINYPaGTZG4k!2e4!3e12)

Figure 77

(https://www.google.gr/maps/@40.07725,23.318546,3a,75y,90t/data=!3m5!1e2!3m3!1s2006777!2e1!3e10)

SOUTH PART OF KASSANDRA

CLIFF COASTS

Cliff coasts of the south part of Kassandra peninsula, starting from the West to the East.

Figure 78
(https://www.google.gr/maps/@39.9618264,23.3869851,3a,75y,90t/data=!3m5!1e2!3m3!1s-x7CPbMYf-e0%2FUCAYXpgTJ-I%2FAAAAAAAAAISE%2FWw7FYSHxa4A!2e4!3e12)

Figure 79
(https://www.google.gr/maps/@39.962043,23.38433,3a,75y,90t/data=!3m5!1e2!3m3!1s84668618!2e1!3e10)

Figure 80
(https://www.google.gr/maps/@39.961814,23.3868563,3a,75y,90t/data=!3m5!1e2!3m3!1s-zqzKYa3TJOc%2FUCAYMkgi2pI%2FAAAAAAAAAIRs%2FZQTun5J1i3Q!2e4!3e12)

Figure 81
(https://www.google.gr/maps/@39.944699,23.532907,3a,75y,90t/data=!3m5!1e2!3m3!1s62778272!2e1!3e10)

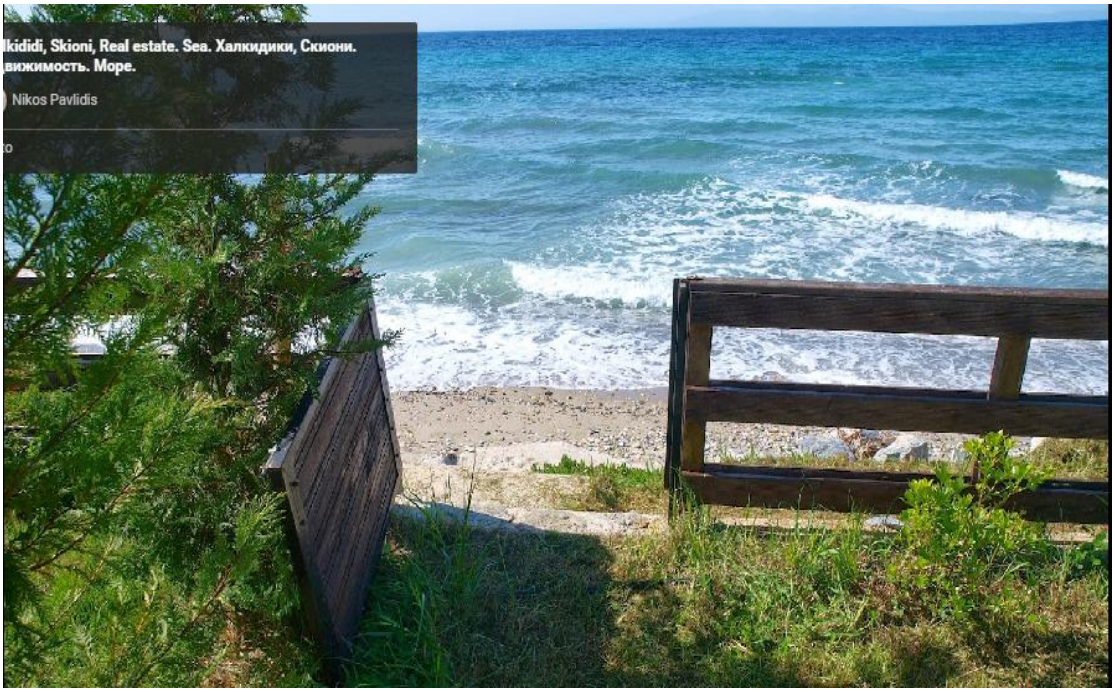

Figure 82
(https://www.google.gr/maps/@39.948752,23.524695,3a,75y,90t/data=!3m5!1e2!3m3!1s-rzTGehq2DFk%2FU0er4IEnXCI%2FAAAAAAAAAC1Q%2Fg4YzcbJv7oE!2e4!3e12)

Figure 83
(https://www.google.gr/maps/@39.933115,23.570145,3a,75y,90t/data=!3m5!1e2!3m3!1s50264655!2e1!3e10)

Figure 84
(https://www.google.gr/maps/@39.922865,23.593065,3a,75y,90t/data=!3m5!1e2!3m3!1s16887624!2e1!3e10)

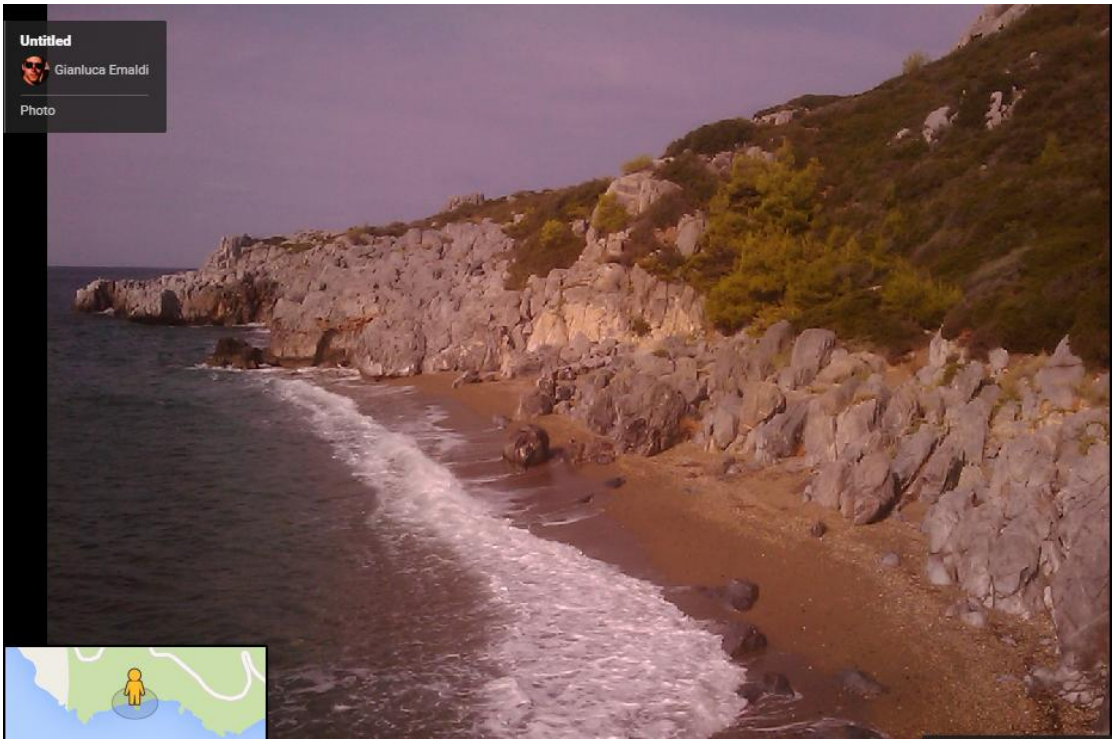

Figure 85
(https://www.google.gr/maps/@39.921575,23.5951361,3a,75y,90t/data=!3m5!1e2!3m3!1s-lCbl0fzEjYI%2FTJmvYLrRyPI%2FAAAAAAAACbE%2Fc5Y4aEvUDxE!2e4!3e12)

COASTS WITH DEPOSITION
(South part of the peninsula with direction from West to East.)

Figure 86 Small marina at Nea Skioni. (Google Earth)

Figure 87 Groyne at Loutra beach (Google Earth)

EAST PART OF KASSANDRA

CLIFF COASTS

Cliff coasts of the eastern part of Kassandra peninsula, starting from the North to the South.

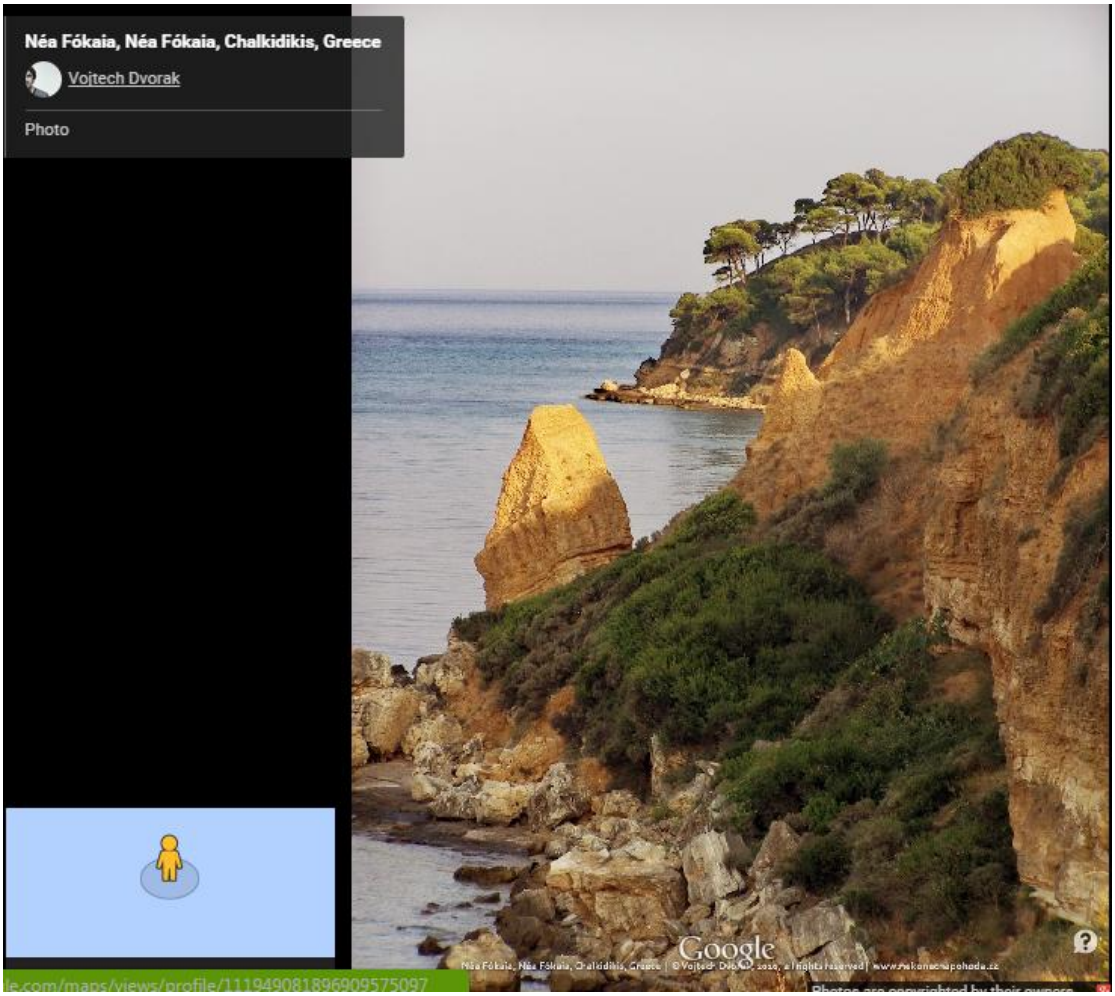

Figure 88 (https://www.google.gr/maps/@40.142925,23.40354,3a,75y,90t/data=!3m5!1e2!3m3!1s-x1AQIlb5uwU%2FUbdt6mERGGI%2FAAAAAAAAAFu4%2FyHrJQOrNX8A!2e4!3e12 **)**

Figure 89
(https://www.google.gr/maps/@40.128513,23.413455,3a,75y,90t/data=!3m5!1e2!3m3!1s95038247!2e1!3e10)

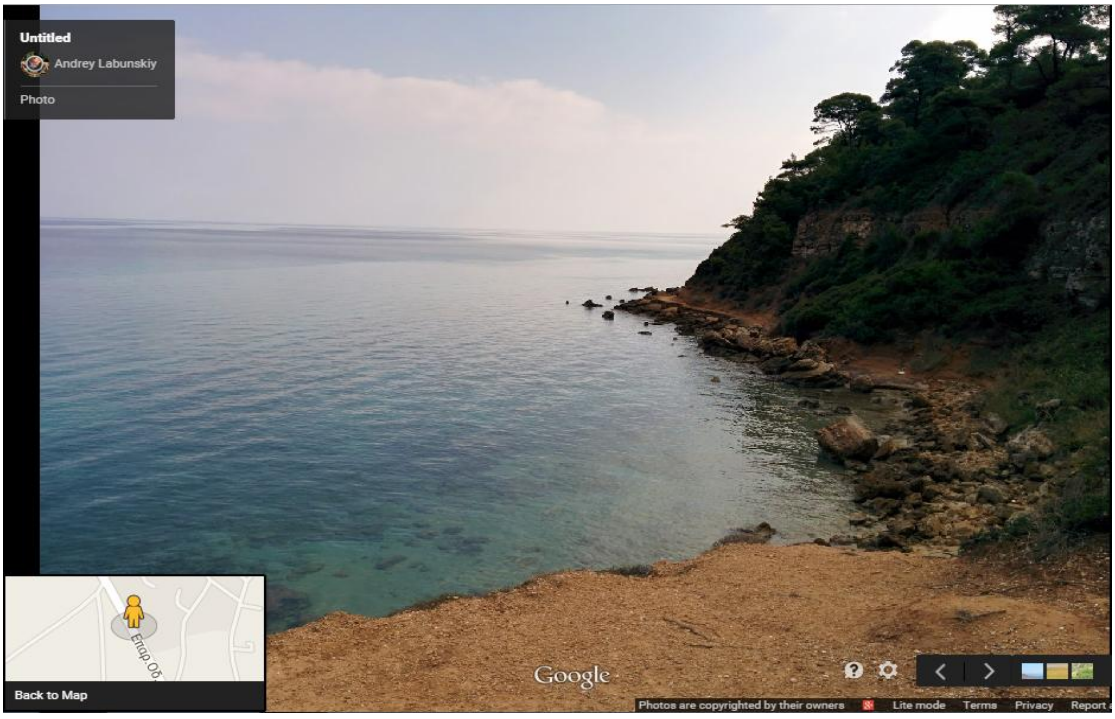

Figure 90
(https://www.google.gr/maps/@40.0946522,23.4353361,3a,75y,90t/data=!3m5!1e2!3m3!1s-x7WoIhiyzIk%2FVFuyBbMg7tI%2FAAAAAAAAATzg%2FxhJEzW4eysM!2e4!3e12)

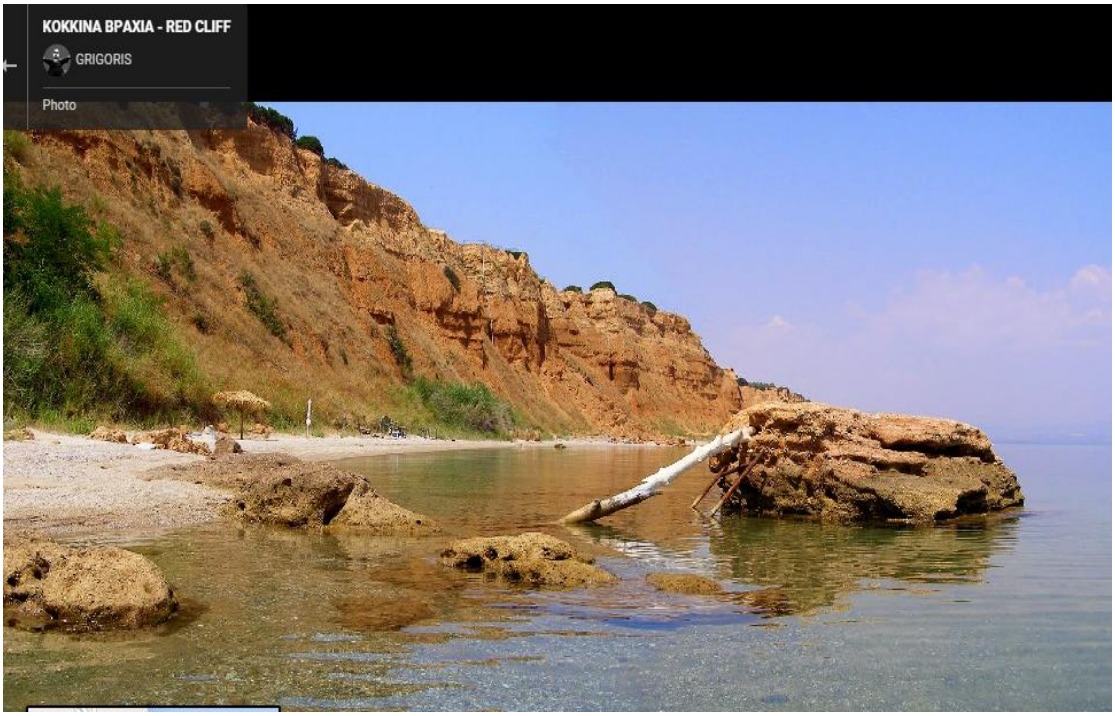

Figure 91
(https://www.google.gr/maps/@40.172586,23.348844,3a,75y,90t/data=!3m5!1e2!3m3!1s39681412!2e1!3e10)

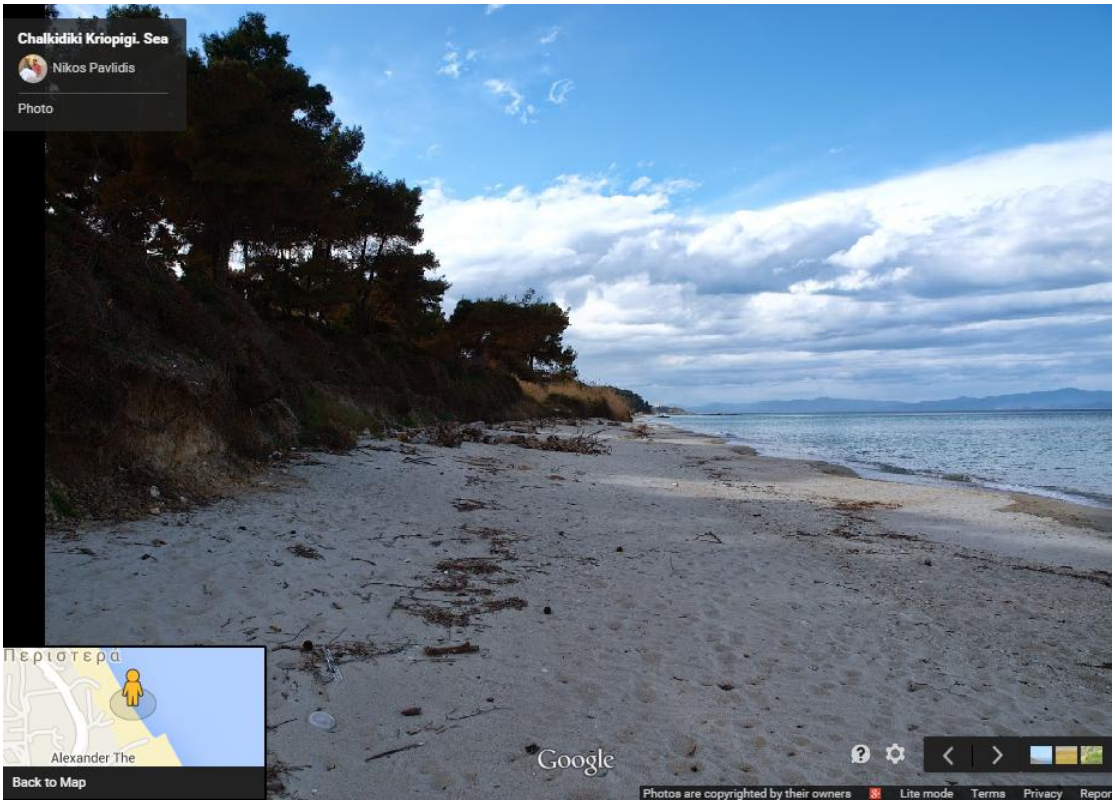

Figure 92
(https://www.google.gr/maps/@40.0540824,23.4680353,3a,75y,90t/data=!3m5!1e2!3m3!1s-SHWOpTV9TYU%2FU3MoaClLjZI%2FAAAAAAAAAFDk%2FZOfoUtpgIlU!2e4!3e12)

COASTS WITH DEPOSITION

(East part of the peninsula with direction from North to South.)

Figure 93 Beach of Nees Fokes with groynes and wavecrushers. (Google Earth)

APPENDIX III

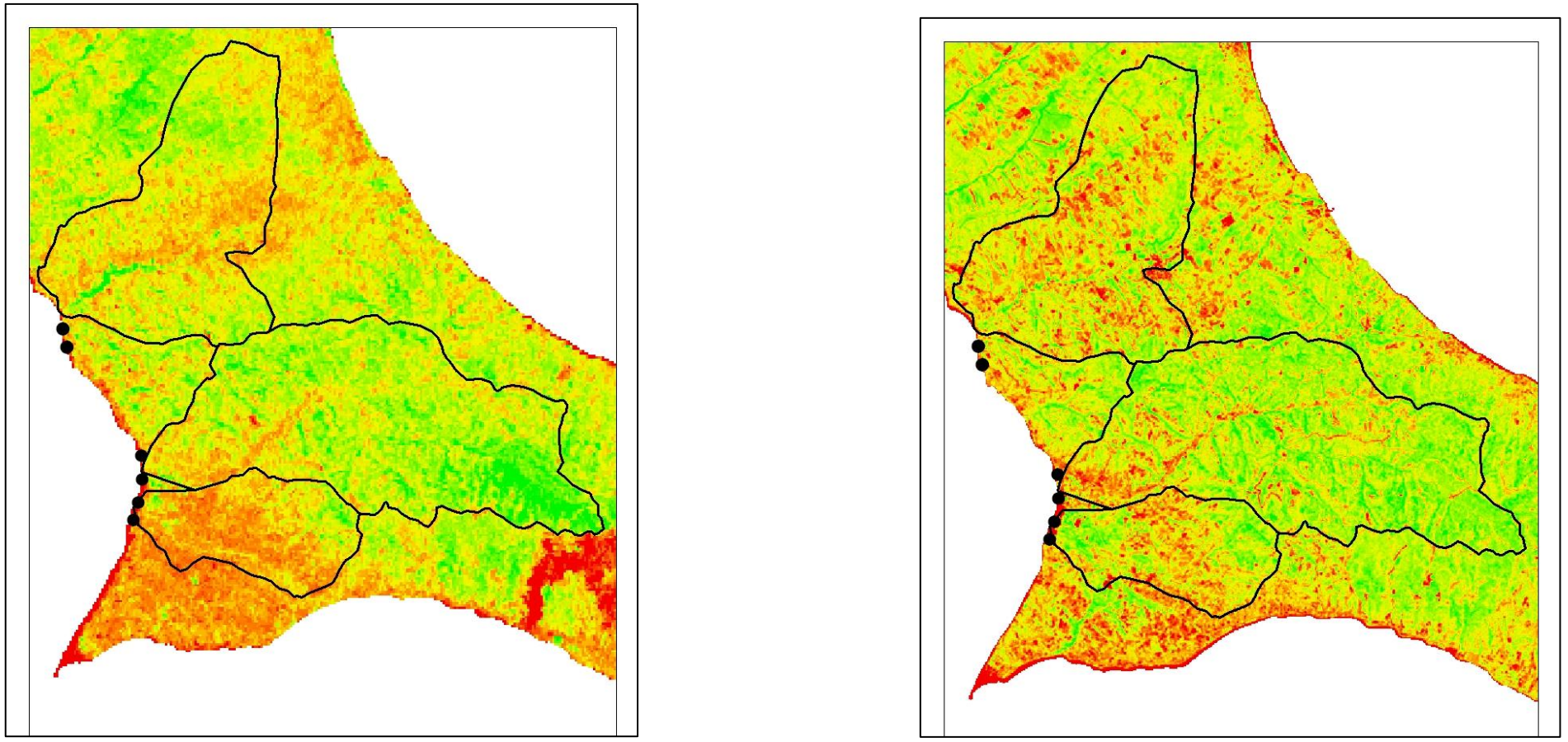

Figure 94 NDVI with 3 major basins of Kassandra for the year 1977 and 1985

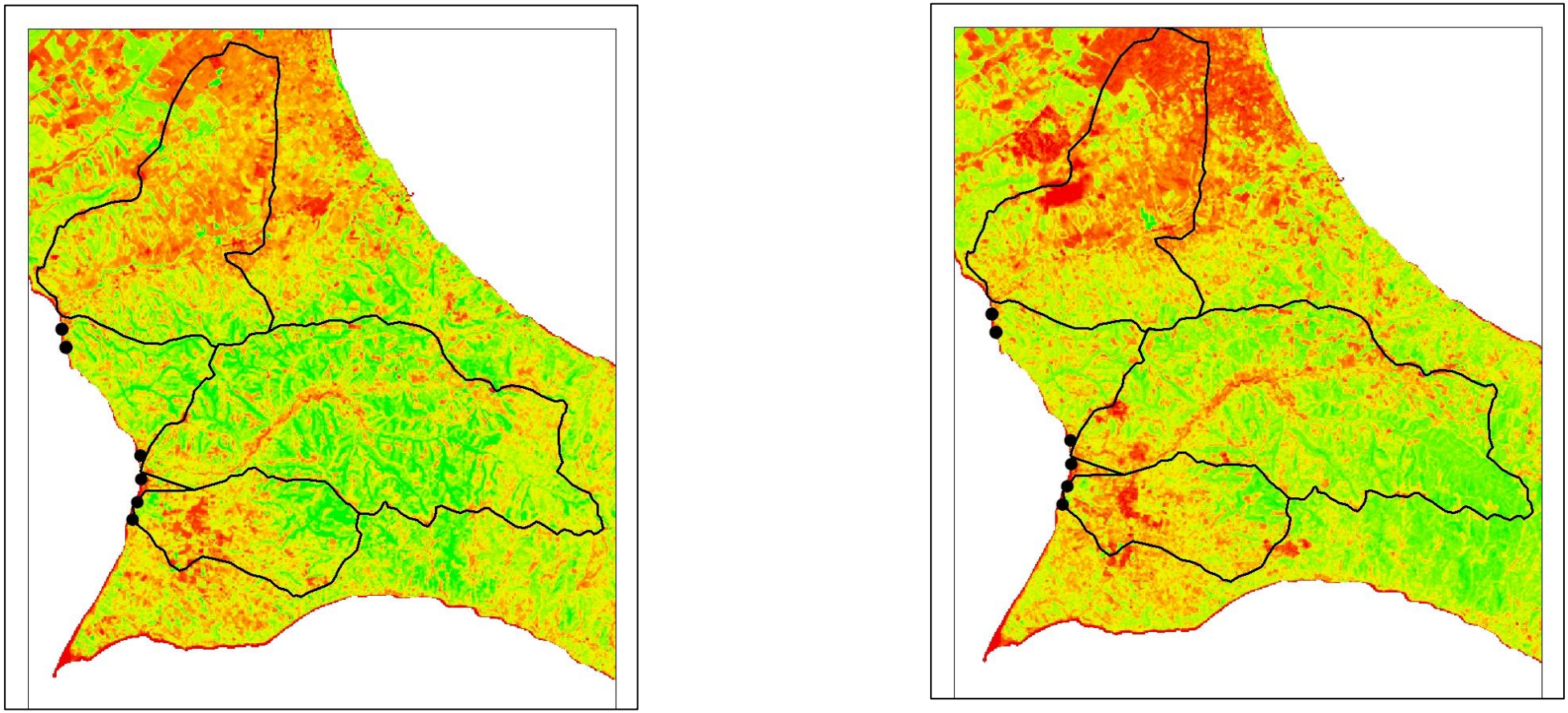

Figure 95 NDVI and 3 major basins of Kassandra for the years 2007 and 2011

REFERENCES

- Albanakis K., 2004. Research corrosion phenomena in the coastal zone of the Municipality of Michaniona Thessaloniki Prefecture and determination of their responses. Research Project 21 546 of the Aristotle University of Thessaloniki Research Committee.

- Alcantara A. I., Goudie S. A., 2010. Geomorphological Hazards and Disaster Prevention.. Published by Cambridge University Press.

- Alexakis, D., 2003: Continuous monitoring of Mount Camel and the wider region, with the help of Remote Sensing and Geographical Information Systems. An environmental approach, Thesis, Aristotle University of Thessaloniki, School of Geology, Thessaloniki. (In Greek)

- Alexander, D. (2002). Principles of Emergency planning and Management. Harpended: Terra publishing. ISBN 1-903544-10-6.

- Anders, F.J., and Byrnes, M.R., 1991, Accuracy of shoreline change rates as determined from maps and aerial photo-graphs: Shore and Beach, v. 59, pp. 17-26.

- Balafoutis C., 1977. Contribution to the study of the climate of Macedonia and Western Thrace. PhD thesis. Thessalonica

- Bankoff, G. Frerks, G. Hilhorst, D. (eds.) 2003. Mapping Vulnerability: Disasters, Development and People. ISBN 1-85383-964-7.

- Bantelas, AG, Savvaidis, PD, Ifadis, IM and Dukas, I.D., 1995: Geodesy: Geodetic instruments and methods of measurement and calculation. Publishing House Bros Kyriakidis, Thessaloniki, 501 p.

- Beven, K.J., Kirkby, M.J., 1979. A physically based variable contribution area model of basin hydrology. Hydrological Science Bulletin pp. 24, 43 – 69.

- Bird E (2008) Coastal Geomorphology: an Introduction, 2nd edn. Wiley, Chichester, UK

- Boardman J., Evans R., Ford J., 2003. Muddy floods on the South Downs, southern England: problem and responses. Environmental Change Institute, School of Geography and the Environment, University of Oxford,

- Brunsden, D., Doornkamp, J.C., Fookes, P.G., Jones, D.K.C., Kelly, J.M., 1975. Large-scale geomorphological mapping and highway engineering design. Q. J. Eng. Geol. 8, 227–253.

- Burt, T. P. and Butcher, D. P. (1985), Topographic controls of soil moisture distributions. Journal of Soil Science, 36: 469–486. doi: 10.1111/j.1365-2389.1985.tb00351.x

- Carter RG (1988) Coastal Environments. Academic Press, London, UK

- Chronis, G., 1986. The modern dynamic and recent Holocene sedimentation in the interior plateau of Thermaikos Gulf. Teaching. Thesis. University of Athens, Athens. pp. 227.

- (2004) GIS techniques and calculation for the coastal area management. Vulnerable zones determination in the northern hemi-delta of Ebro through the estimation of shoreline displacements in the Marquesa beach. In Territorio y

  (eds)). University of Murcia, Spain, pp. 111–125

- Crowell, M., Leatherman, S.P., and Buckley, M.K., 1991, Historical shoreline change— Error analysis and mapping accuracy: Journal of Coastal Research, v. 7, pp. 839-852.

- Dalezios, N. F., Environmental Remote Sensing, University Teaching, University of Thessaly, Volos, 2002. (In Greek)

- Demek, J., 1972: Manual of detailed geomorphological mapping. Academia, Prague, 344 p.

- Ding, H., Wang, R. C., Wu, J. P., Zhou, B., Shi, Z., & Ding, L. X., (2007)Quantifying land use change in Zhejiang coastal region, China using multi-temporal Landsat TM/ETM+ images,

- Directive 2007/60/EC of the European Parliament and of the council of 23 October 2007 on the assessment and management of flood risks.

- Dolan, R., Fenster, M.S., and Holme, S.J., 1991, Temporal analysis of shoreline recession and accretion: Journal of Coastal Research, v. 7, pp. 723-744.

- Domakinis, C., 2005: The use of Remote Sensing and GIS in mapping landslides in the coastal region Strymonikos - Kavala, Thesis, Aristotle University of Thessaloniki, School of Geology, Thessaloniki. (In Greek)

- Donati, L. and Turrini, M. C.: An objective method to rank the importance of the factors pre-20 disposing to landslides with the GIS methodology: application to an area of the Apennines (Valnerina; Perugia, Italy), Eng. Geol., 63, 277–289, 2002.

- e-EcoRisk, 2004. District business website support system and decision-making to address the environmental risk and disaster management of large-scale industrial waste ", funded by" European Commission-Research Directorate-General" (EVG1-2001 -00,087). (2004 / / Principal Investigator A. Filippides).Maidment, David R., Oscar Robayo, Watershed and Stream Network Delineation, Center for Research in Water Resources, University of Texas at Austin, September, 2002.

- Encyclopedia Britannica, 2008. Encyclopedia Britannica Online.

- Esmali A, Ahmadi H, 2003. Using GIS & RS in mass movements hazard zonation—a case study in Germichay Watershed, Ardebil, Iran. Map India Conference 2003. At http://www.gisdevelopment.net/application/natural_hazards/landslides/ma03004.htm [Accessed December 15, 2010]

- Fookes PG, Lee EM and Griffiths JS (2007) Engineering Geomorphology: Theory and Practice. Whittles Publishing, Caithness, UK

- Fourniadis, J., Economides, M. & Astaras, T., 2002: Identify areas susceptible to erosion, with the help of Geographic Information Systems (GIS) and Remote Sensing. An example of the drainage basin Anthemountas, Proceedings of the 6th Panhellenic Geographical Conference of Greek Geographical Society, Thessaloniki October 3-6, 2002, Volume II (In Greek).

- Genz, A.S., Fletcher, C.H., Dunn, R.A., Frazer, L.N., and Rooney, J.J., 2007, The predictive accuracy of shoreline change rate methods and alongshore beach variation on Maui, Hawaii: Journal of Coastal Research, v. 23, n. 1, pp. 87-105.

- Gupta, R.P., Joshi, B.C., 1989. Landslide hazard zoning using the GIS approach—a case study from the Ramganga Catchment, Himalayas. Eng. Geol. 28, 119–131.

- Green DR and King SD (eds), 2003. Coastal and Marine Geo information Systems: Applying the Technology to the Environment (Coastal Systems and Continental Margins),

- Haas, J., 2010. Soil moisture modelling using TWI and satellite imagery in the Stockholm region. KTH, School of Architecture and the Built Environment (ABE), Urban Planning and Environment, Geoinformatik och Geodesi.

- Hansen, A., 1984. Landslide hazard analysis. In: Brunsden, D., Prior, D.B. (Eds.), Slope Instability. Wiley, New York, pp. 523–602.

- Hanqiu, X.(2006) Modification of normalised difference water index (NDWI) to enhance open water features in remotely sensed imagery.

- Hapke, C.J., and Reid, D., 2007, National Assessment of Shoreline Change, part 4— Historical coastal cliff retreats along the California coast: U.S. Geological Survey Open-File Report 2007-1133. [http://pubs.usgs.gov/of/2007/1133]

- Hapke CJ, Reid D and Richmond B. 2009. Rates and trends of coastal change in California and the regional behavior of the beach and cliff system. Journal of Coastal Research 25(3): 603–615

- Hapke, C.J., Reid, D., Richmond, B.M., Ruggiero, P., and List, J. 2006, National Assessment of Shoreline Change part 3— Historical shoreline change and associated coastal land loss along sandy shorelines of the California coast: U.S. Geological Survey Open-File Report 2006-1219. [http://pubs.usgs.gov/of/2006/1219]

- Himmelstoss, E.A. 2009. "DSAS 4.0 Installation Instructions and User Guide".

- IGME Development in Geoenvironment, Waters - Geothermal - Minerals and quality of life in Central Macedonia, 2000. (In Greek).

- Jha AK, Bloch R, Lamond J., 2012. Cities and flooding : a guide to integrated urban flood risk management for the 21st century. The world bank, Washington, DC.

- Katafioti, M., 2008 Assessment of environmental conditions in Chalkidiki as regards heavy metals, Science Thesis, University / University of Patras, Department of Geosciences and Environment, Patras.

- Keller, E.,A., and Blodgett, R.H., 2006. Natural hazards – Earth's processes as hazards, disasters, and catastrophes: Upper Saddle River, New Jersey, Pearson Prentice Hall, 395 p.

- Kienholz, H., Hafner, H., Schneider, G., Tamrakar, R., 1983. Mountain hazards mapping in Nepal's middle mountains, maps of land use and geomorphic damages (Kathmandu–Kakani area). Mountain Res. Dev. 3 (3), 195–220.

- Kluwer, Vol. 4, Dordrecht, the Netherlands.

- Lekkas, E. L., 1996. Environmental Engineering I, Water Resources Management, University of the Aegean, Department of Environment, Mytilini, 1996.

- Lekkas, E.L., 2000: Physical and technological disasters, University of Athens, Athens, pp, 77-89.

- Marinos G., Sakellariou-Mane E., Sotiriadis L. & Sapountzidis E. 1970 – Sur la paleogeographie de L' Egéide de Nord dans la region de Kassandra (Chalkidiki-Macedoine-Grece) Annales Géologiques des Pays Helléniques, 22 : 1-27 (in Greek)

- Mc Feeters, S. K., 1996. The use of normalized difference water index (NDWI) in the delineation of open water features

- Moore, L.J., 2000, Shoreline mapping techniques: Journal of Coastal Research, v. 16, pp. 111-124.

- Morton, R.A., and Miller, T.L., 2005, National Assessment of Shoreline Change— part 2 Historical shoreline changes and associated coastal land loss along the U.S. southeast Atlantic coast: U.S. Geological Survey Open-file Report 2005-1401. [http://pubs.usgs.gov/of/2005/1401]

- Morton, R.A., Miller, T.L., and Moore, L.J., 2004, National Assessment of Shoreline Change— part 1 Historical shoreline changes and associated coastal land loss along the U.S. Gulf of Mexico: U.S. Geological Survey Open-File Report 2004-1043. [http://pubs.usgs.gov/of/2004/1043].

- Moudrakis, 1985. Geology of Greece (in Greek). Univ. Studio Press. Thessaloniki.

- Moyssiadou, P., 2010: Development of space-time predictive model of risk of natural hazards - implementation in areas of Halkidiki, Thesis, Aristotle University of Thessaloniki, Department of Civil Engineering, Thessaloniki. (In Greek)

- Nikolaidou, M., 2009: Use of Remote Sensing and GIS in the record flood of mountainous areas south of the lake bulbs. An environmental approach, Thesis, Aristotle University of Thessaloniki, School of Geology, Thessaloniki. (In Greek)

- Pappa M., 2012. Recording and Assessment of flood susceptibility using Remote Sensing and GIS .An example from N.E..Halkidiki.

- Paraschou, I., 2005: The geomorphological evolution of the valley of the river Inachus Fthiotida, a tributary of river Sperchios, Thesis, Aristotle University of Thessaloniki, School of Geology, Thessaloniki. (In Greek)

- Psilovikos A., Syrides G.& Chachamidou E., 1988. Coastal Phenomena in Kassandra peninsula, Chalkidiki. Bull. Geol. Soc. Greece, v. XX, 325-339, Athens (in Greek).

- Quinn, P. F., K. J. Beven, P. Chevallier, and Planchon O., 1991, The prediction of hillslope flowpaths for distributed modelling using digital terrain models, Hydrol. Processes, 5, 59 – 80.

- RISK – EOS Geo – information services for natural disasters. (www.riskeos.com)

- Rodhe, A. and Seibert, J., 1999, Wetland occurrence in relation to topography - a test of topographic indices as moisture indicators, Agricultural and Forest Meteorology 98-99: 325-340.

- Rogers J, Loran F and Astle G. 2008. National coastal erosion risk mapping the first national run. In Proceedings of the 31st International Conference on Coastal Engineering, (Smith JM ed.). World Scientific, Hamburg, Germany, pp. 4237–4249

- Rogers J, Hamer B, Brampton A., 2010. Beach Management Manual, 2nd edn, C685. CIRIA, London, UK

- Saaty, T.L., 1980: The Analytical Hierarchy Process, NY, McGraw Hill.

- Sabyasachi, M., & Amit, K. B., 2012. A three-unit-based approach in coastal-change studies using Landsat images.

- Samaras, A., Koutitas, C., 2009. The impact of catchment management on coastal morphology. The case of Fourka in Greece. Journal of Coastal Research, SI 56 (Proceedings of the 10th International Symposium), 1686-1690. Lisbon, Portugal, ISSN 0749-0258.

- Seibert, J., K. Bishop and L.Nyberg, 1997, A test of TOPMODEL's ability to predict spatially distributed groundwater levels, Hydrological Processes 11: 1131-1144.

- Syrides G. 1990. Lithostratigraphic, biostratigraphic and palaeogeographic study of the Neogene±Quaternary sedimentary deposits of Chalkidiki peninsula, Macedonia, Greece. PhD thesis, Scientific Annals, School of Geology Vol. 1, no. 11. Aristotle University of Thessaloniki. (In Greek).

- Sørensen, R. , Zinko, U. and Seibert, J., 2006. On the calculation of the topographic wetness index: evaluation of different methods based on field observations, Hydrology and Earth System Sciences, 10, 101-112.

- Soulakellis, P., 1994. Contribution to the analysis of satellite images Landsat-5/TM and GIS in Tectonic Geomorphology regions of Northern Greece, PhD Thesis, Department of Geology, Aristotle University of Thessaloniki. (In Greek)

- Soulios, G. Ch. 1996. General Hydrogeology, Aristotle University of Thessaloniki, University Studio Press, Thessaloniki. (In Greek)

- Syllaios, P., 2000. Introduction to Remote Sensing and Geographic Information Systems, Volume I, Introduction to Remote Sensing, Giachoudi-Giapouli, Thessaloniki. (In Greek)

- The American Heritage® Science Dictionary Copyright © 2002. Published by Houghton Mifflin.

- Thieler, E.R., Himmelstoss, E.A., Zichichi, J.L., and Ergul, Ayhan. 2009 Digital Shoreline Analysis System (DSAS) version 4.0 — An ArcGIS extension for calculating shoreline changes: U.S. Geological Survey Open-File Report 2008-1278. *updated for version 4.3. Available online at http://woodshole.er.usgs.gov/project-pages/DSAS/version4/index.html.

- Thorley, N., S. Clandillon, and P. De Fraipont, 1997. The contribution of spaceborne SAR and optical data in monitoring flood events: Examples in northern and southern France, Hydrological Processes, 11:1409-1413.

- Trenhaile AS, 1987. The Geomorphology of Rock Coasts. Clarendon Press, Oxford, UK.
- Trenhaile AS, 1997. Coastal Dynamics and Landforms. Oxford University Press, Oxford, UK

- Tsiros E., 2006. The Normalized Difference Vegetation Index (NDVI) and Other Indicators in Monitoring Hydrological Drought Thesis, University of Thessaly, Department of Agriculture Animal Production and Aquatic Environment, Volos.(In Greek)

- Tucker, J. C., Grant, D. M., & Dykstra, J. D., 2004. NASA's global ortho-rectified Landsat data set,

- U.S. Billion-Dollar Weather and Climate Disasters

- Veranis N., Geological structure and mineral resources in Municipality of Chalkidiki, IGME, Thessaloniki 1994. (In Greek)

- Wisner, B., Blaikie, P., Cannon, T and Davis, I., 2004. At Risk - Natural hazards, people's vulnerability and disasters. Wiltshire: Routledge. ISBN 0-415-25216-4.

- Wolman, M. G. (1971), Evaluating Alternative Techniques Floodplain Mapping , Water Resour. Woodroffe CD, 2003. Coasts: Form, Process and Evolution Cambridge University Press, Cambridge, UK. Res., 7(6), 1383–1392, doi:10.1029/WR007i006p01383.

- Zinko, U., Seibert, J., Dynesius, M., and Nilsson, C.: Plant species numberspredicted by a topography based groundwater-flow in-dex, Ecosystems, 8, 430-441, 2005.

URLS

- www.earthexplorer.usgs.gov
- http://woodshole.er.usgs.gov/project-pages/DSAS/
- http://penteli.meteo.gr/stations/kassandreia
- http://www.ypes.gr/ [Accessed January,29th, 2015]
- URL1: https://www.youtube.com/watch?v=2lvRZlVeju4 [Accessed July,16th, 2014]
- URL2: http://www.pestaola.gr/xalkidiki-rain-in-kassandra-and-sibiri/ [Accessed July,16th, 2014]
- URL3: https://www.youtube.com/watch?v=5Nx4vI00kWA[Accessed July,16th, 2014]
- URL4: http://www.tovima.gr/relatedarticles/article/?aid=212029[Accessed July,16th, 2014]
- URL5: http://www.motionteam.gr/photos/20316/363111/photo_594_400.jpg [Accessed July,16th, 2014]
- URL6: http://www.makthes.gr/news/reportage/5721/[Accessed July,16th, 2014]
- URL7: http://www.motionteam.gr/photos/20316/363041/photo_594_400.jpg [Accessed July,16th, 2014]